NASA TECHNICAL MEMORANDUM

NASA TM X-73314

TETHERED SUBSATELLITE STUDY

By William P. Baker, J. A. Dunkin, Zachary J. Galaboff, Kenneth D. Johnston, Ralph R. Kissel, Mario H. Rheinfurth, and Mathias P. L. Siebel

Science and Engineering

March 1976

NASA

George C. Marshall Space Flight Center
Marshall Space Flight Center, Alabama

TECHNICAL REPORT STANDARD TITLE PAGE

1. REPORT NO.	2. GOVERNMENT ACCESSION NO.	3. RECIPIENT'S CATALOG NO.
NASA TM X-73314		

4. TITLE AND SUBTITLE	5. REPORT DATE
Tethered Subsatellite Study	March 1976
	6. PERFORMING ORGANIZATION CODE

7. AUTHOR(S)	8. PERFORMING ORGANIZATION REPORT #
See Block 15	

9. PERFORMING ORGANIZATION NAME AND ADDRESS	10. WORK UNIT NO.
George C. Marshall Space Flight Center Marshall Space Flight Center, Alabama 35812	11. CONTRACT OR GRANT NO.
	13. TYPE OF REPORT & PERIOD COVERED
12. SPONSORING AGENCY NAME AND ADDRESS	Technical Memorandum
National Aeronautics and Space Administration Washington, D.C. 20546	14. SPONSORING AGENCY CODE

15. SUPPLEMENTARY NOTES
William P. Baker,* J. A. Dunkin,** Zachary J. Galaboff,*** Kenneth D. Johnston,***
Ralph R. Kissel,** Mario H. Rheinfurth,*** and Mathias P. L. Siebel†
Prepared by Space Sciences Laboratory, Science and Engineering

16. ABSTRACT

This report presents the results of studies performed relating to the feasibility of deploying a subsatellite from the Shuttle by means of a tether. The report addresses the dynamics, the control laws, the aerodynamics, the heating, and some communication considerations of the tethered subsatellite system. Nothing was found that prohibits the use of a subsatellite joined to the Shuttle by a long (100 km) tether. Further, more detailed studies directed at specific applications are recommended.

* Structures and Propulsion Laboratory
** Electronics and Control Laboratory
*** Systems Dynamics Laboratory
† Space Sciences Laboratory

17. KEY WORDS	18. DISTRIBUTION STATEMENT
	Unclassified — Unlimited

19. SECURITY CLASSIF. (of this report)	20. SECURITY CLASSIF. (of this page)	21. NO. OF PAGES	22. PRICE
Unclassified	Unclassified	144	NTIS

ACKNOWLEDGMENTS

The Tethered Subsatellite Study was performed by a group drawn from many disciplines at the Marshall Space Flight Center. The principal results of the study are presented by the authors in this report; many others, however, participated in defining the questions to be addressed and in bringing the study to a meaningful conclusion. Appreciation for their participation is extended to the following individuals:

J. C. Blair (ED11)

J. L. Burch (ES23)

F. Bugg (ED23)

C. R. Chappell (ES23)

A. V. Clark (EP34)

W. K. Dahm (ED31)

C. S. Jones (EC23)

I. T. Morgan (EC22)

D. L. Reasoner (ES23)

W. T. Roberts (PS01)

C. C. Rupp (PD12)

G. R. Swenson (ES44)

In addition, Mr. Rheinfurth gratefully acknowledges the helpful and stimulating discussions which he had with Dr. John Glaese on orbital tether dynamics during the conduct of this study.

TABLE OF CONTENTS

TABLE OF CONTENTS (Concluded)

LIST OF ILLUSTRATIONS

LIST OF ILLUSTRATIONS (Continued)

LIST OF ILLUSTRATIONS (Continued)

LIST OF ILLUSTRATIONS (Continued)

LIST OF ILLUSTRATIONS (Concluded)

LIST OF TABLES

LIST OF SYMBOLS

Symbol	Definition
A	Cross-sectional area of the subsatellite [L^2]
A_A	Axial cross-sectional area of the tether [L^2]
A_N	Normal cross-sectional area of the tether [L^2]
$C_A^{(m)}$	Tether axial force coefficient
$C_D^{(M)}$	Aerodynamic drag coefficient
$C_N^{(m)}$	Tether normal force coefficient
D	Subsatellite aerodynamic drag [MLT^{-2}]
D_A	Tether axial aerodynamic force [MLT^{-2}]
D_N	Tether normal aerodynamic force [MLT^{-2}]
E	Young's modulus of elasticity [$ML^{-1}T^{-2}$]
g_0	Gravitational constant [LT^{-2}]
I	Moment of inertia of subsatellite [ML^2]
i	Inclination angle of the main satellite orbit
L	Length of elongated tether [L]
ℓ	Length of unstretched tether [L]
ℓ_0	Constraint variable [L]
M	Mass of subsatellite [M]
m	Instantaneous mass of tether [M]

LIST OF SYMBOLS (Continued)

Symbol	Definition
Q_ℓ	Generalized force in the ℓ-generalized coordinate direction [MLT^{-2}]
Q_ϕ	Generalized force in the ϕ -generalized coordinate direction [$ML^2\ T^{-2}$]
Q_θ	Generalized force in the θ-generalized coordinate direction [$ML^2\ T^{-2}$]
Q_ζ	Generalized force in the ζ -generalized coordinate direction [MLT^{-2}]
R	Position of the main satellite in orbit [L]
R_E	Radius of the Earth [L]
R_0	Distance from the center of the Earth to main satellite [L]
T	Tension in the tether [MLT^{-2}]
t	Time [T]
V	Subsatellite relative wind velocity [LT^{-1}]
V_A	Axial relative wind velocity for the tether [LT^{-1}]
V_N	Normal relative wind velocity for the tether [LT^{-1}]
W	Work [$ML^2\ T^{-2}$]
α	Constant of exponential control law [T^{-1}]
β	Angle that defines the position of the main satellite relative to the intersection of the orbital and equatorial planes

LIST OF SYMBOLS (Concluded)

Symbol	Definition
$\dot{\gamma}$	Angular velocity of orbital reference frame [T^{-1}]
Ω_0	Angular velocity of the Earth [T^{-1}]
ω_0	By definition, $\omega_0 = g_0 R_E^2 / R^3$ [T^{-1}]
ζ	Length of tether elongation [L]

Note: Other symbols are defined in the text, as needed; symbols underscored represent vectors.

TECHNICAL MEMORANDUM X-73314

TETHERED SUBSATELLITE STUDY

I. INTRODUCTION

Mathias P. L. Siebel

Various concepts of using tethers in space have been studied previously; e.g., an early concept for Skylab had the solar observatory (Apollo Telescope Mount) tethered (rather than hard-docked) to the S-IVB stage, and other tether studies were performed in connection with astronaut rescue concepts. The present in-house study was performed to gain an understanding of a report received in September 1974 from the Smithsonian Astrophysical Observatory (SAO) entitled Shuttle-Borne "Skyhook": A New Tool for Low-Orbital-Altitude Research, by G. Colombo, E. M. Gaposchkin, M. D. Grossi, and G. C. Weiffenbach.

In their report SAO suggests a tether of approximately 100 km length deployed from the orbiter and carrying a subsatellite to an altitude of perhaps 100 km below the shuttle and 100 to 150 km above the Earth (Fig. I-1). The subsatellite would then be used as a platform on which various kinds of experimental apparatus would be carried for upper atmospheric measurements, high resolution gravity gradient measurements, and low frequency radio physics experiments in the lower magnetosphere where the tether wire itself is used as a dipole.

An in-house study performed by C. C. Rupp (see Bibliography) verified certain parameters and results of the SAO report. A further, more detailed in-house study was performed during the period from February 1975 to August 1975. The following are the principal aspects and the responsible investigators to the tether-subsatellite system that were considered:

Dynamic Analysis of a Tethered Subsatellite	Mario H. Rheinfurth and Zachary J. Galaboff
Investigation of a Tethered Subsatellite Control Law	Ralph R. Kissel
Aerodynamics	Kenneth D. Johnston

Thermal Studies	William P. Baker
Tethered Subsatellite Communications System Design	J. A. Dunkin

Reports on these individual efforts form the body of this report.

It will be seen that while many detailed questions remain unresolved, no fundamental effect has been discovered that makes the subsatellite concept unfeasible. More detailed systems and optimization studies are recommended. Further, it should be mentioned that in the course of the study, interest in using the tether was expressed by a number of members of the scientific and applications oriented communities. In addition to the applications originally suggested by SAO, other uses for the tether have been found both in the Atmospheric Magnetospheric Plasma in Space (AMPS) area (generation of Alfven waves and study of plasma wakes) and in more general areas. The more general applications proposed include cargo transfer, space station stabilization, the use of tethers as aids in the erection of large area space structures, satellite retrieval, power generation, and others.

It is recommended that further studies be performed to define common and specific application function features of tethered subsatellite systems. Such studies should culminate in an experiment on an early shuttle flight.

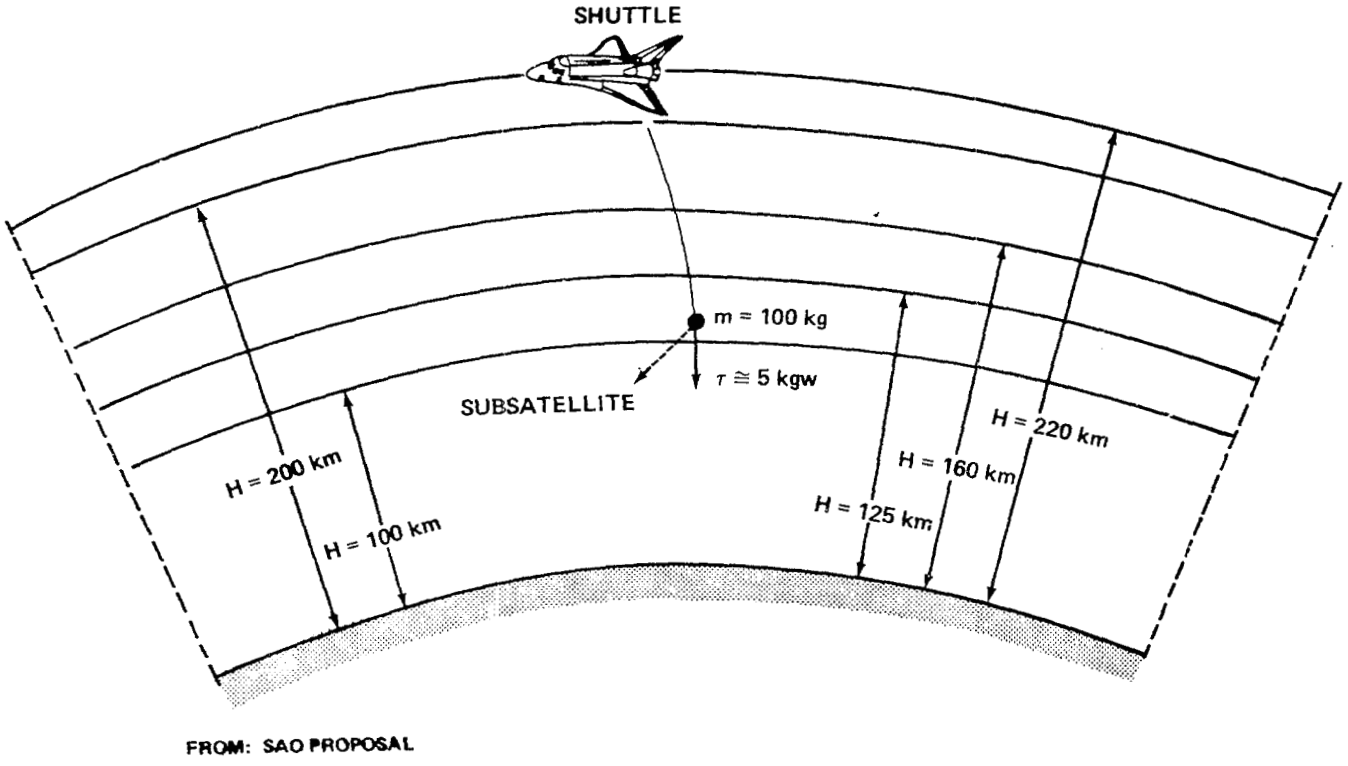

Figure I-1. Tethered subsatellite.

II. DYNAMICS ANALYSIS OF A TETHERED SUBSATELLITE

Mario H. Rheinfurth and Zachary J. Galaboff

A. Summary

A dynamic analysis was performed to study the feasibility of the tethered subsatellite concept with emphasis on its dynamic response and stability characteristics. The differential equations were derived that describe the three-dimensional motion of the subsatellite and the flexible tether that connects it with the main satellite. Because of limitations in manpower and resources, only a simplified model could be simulated on the computer. However, a serious effort was made to include the most significant factors in the analysis, factors that were deemed necessary to prove the dynamic feasibility of the concept. Analytical investigations and computer simulations performed thus far did not expose dynamic characteristics that would preclude a satisfactory deployment and stationkeeping of the tethered subsatellite. However, a serious dynamic problem was encountered during the attempt to retrieve the subsatellite. This problem occurs in the vicinity of the subsatellite and is characterized by a strong tendency of the subsatellite to sling around the main satellite. This phenomenon and the lateral tether flexibility, which was not included in the present analysis, are still critical issues and require further study.

B. Introduction

The objective of this study is to conduct a feasibility analysis of a subsatellite that is attached to an orbiting spacecraft by a tether. For this purpose, a computer program was developed that allows the prediction of the dynamic behavior of the tethered subsatellite during its deployment, stationkeeping, and retrieval. The dynamic analysis is kept sufficiently general to accommodate a rather wide variety of system parameters. Because the equations of motion are fairly complex for the general case of three-dimensional motion and tether flexibility, they are written in concise vector-dyadic and matrix form using Lagrangian mechanics. The derivation is carried to a point from which the interested reader can readily proceed towards a detailed scalar formulation. The computer simulation itself was performed under certain restrictive assumptions dictated by the nature of the study and by the limitations of manpower and resources. A detailed formulation of the corresponding simplified equations of motion is provided. In selecting the simplifying assumptions, particular

attention was given to the identification and deletion of dynamic effects that can be safely neglected. A point-by-point discussion of these effects is included. Consideration is also given to effects that should be included in a more refined analysis. The necessary extension and augmentations of the equations of motion can be obtained without difficulty from the vector-dyadic formulation presented in this section.

C. Lagrange's Equations

The dynamic analysis of complex systems is greatly facilitated by an approach attributed to Lagrange and generally referred to as analytical mechanics. This approach is general and systematic in nature and is readily adaptable to modifications and refinements of the mathematical model that is used to describe the dynamical system. It is obviously beyond the scope of this report to derive the equations of motion in an expository manner. A certain familiarity of the reader with the concepts of analytical mechanics will, therefore, be required for the understanding of this derivation. However, this familiarity is not necessary for the application of the equations of motion as they appear in their final form. On the other hand, the treatment is detailed enough that the cognizant reader should be able to supply potentially desirable addenda to the existing mathematical model without great difficulty.

In their classical form, Lagrange's equations are based on an inertial reference frame and employ generalized coordinates. Accordingly, they appear in the form of a matrix equation

$$\frac{d}{dt}\left(\frac{\partial T}{\partial \dot{\underline{q}}}\right) - \frac{\partial T}{\partial \underline{q}} + C^T \underline{\lambda} = \underline{Q} \qquad \text{(II-1)}$$

where $T = T(\underline{q}, \dot{\underline{q}})$ is the kinetic energy, expressed as a function of the generalized coordinate vector $\underline{q}$ and its time derivative $\dot{\underline{q}}$. The term $\underline{\lambda}$ represents the Lagrange multiplier vector, and C represents the constraint matrix appearing in the matrix equation for the constraints having the Pfaffian form:

$$\Phi = C\dot{\underline{q}} - \underline{b} = 0 \qquad \text{(II-2)}$$

The generalized force vector $\underline{Q}$ on the right side is determined via the principle of virtual work:

$$\delta W = \underline{Q}^T \delta \underline{q} \tag{II-3}$$

This states that the virtual work δW of the applied generalized forces $\underline{Q}$ is zero for virtual displacements $\delta \underline{q}$ which are consistent with the constraints imposed upon the system.

Equation (II-1) represents a set of second-order ordinary differential equations. The solution of these is necessary and sufficient to establish the complete dynamical behavior of the system as a function of time. However, it results that for more complex dynamic configurations, this form of the equations of motion is too complicated. A less complicated form of these equations is obtained by introducing one or more noninertial reference frames and expressing the kinetic energy in terms of nonholonomic velocities. These velocities are also referred to as derivatives of quasi-coordinates. The corresponding transformation from generalized velocities to nonholonomic velocities is given by Euler's kinematical equations

$$\underline{\Omega} = A(\underline{q})\, \dot{\underline{q}} \quad , \tag{II-4}$$

with $A(\underline{q})$ being the appropriate transformation matrix. The nonholonomic velocity vector $\underline{\Omega}$ is, in general, composed of both linear and angular velocity components. Introducing equation (II-4) into equation (II-1) yields Lagrange's equation in a quasi-coordinate form as

$$\frac{d}{dt}\left(\frac{\partial T}{\partial \underline{\Omega}}\right) + \left[\left(\dot{A} - J\right) A^{-1}\right]^T \frac{\partial T}{\partial \underline{\Omega}} - \left(A^{-1}\right)^T \frac{\partial T}{\partial \underline{q}} + B^T \underline{\lambda} = \left(A^{-1}\right)^T \underline{Q} \quad , \tag{II-5}$$

where $B = CA^{-1}$ and where J is the Jacobian matrix

$$J = \partial \underline{\Omega} / \partial \underline{q} \tag{II-6}$$

Judged by their outward appearance, the transformed equations (II-5) seem to be more complicated than their classical counterpart given in equation (II-1). However, th ir intrinsic simplicity will be obvious when the detailed steps of introducing the above-mentioned noninertial reference frames are carried out. Since these steps are rather lengthy — but straightforward — they will not be repeated at this point. They will produce the result that for each introduced noninertial reference frame, the equations of motion can be partitioned into three distinct sets. These sets can be physically interpreted as rigid-body translation, rigid-body rotation, and subsystem flexibility. Using vector-dyadic notation, this result can be stated in the following form:

Rigid-Body Translation

$$\frac{d}{dt}\left(\frac{\partial T}{\partial \underline{v}}\right) + \underline{\omega} \times \frac{\partial T}{\partial \underline{v}} + \Gamma_v \cdot \underline{\lambda} = \underline{F} \tag{II-7}$$

Rigid-Body Rotation

$$\frac{d}{dt}\left(\frac{\partial T}{\partial \underline{\omega}}\right) + \underline{\omega} \times \frac{T}{\partial \underline{\omega}} + \Gamma_\omega \cdot \underline{\lambda} = \underline{L} \tag{II-8}$$

Subsystem Flexibility

$$\frac{d}{dt}\left(\frac{\partial T}{\partial \dot{\underline{q}}}\right) - \frac{\partial T}{\partial \underline{q}} + \Gamma_q \cdot \underline{\lambda} = \underline{Q}_q \tag{II-9}$$

where Γ_v, Γ_ω, and Γ_q are the pertinent constraint dyadics as determined by the properly transformed constraint equation (II-2).

The elimination of the unknown Lagrange multipliers is usually performed by a separate computational routine. A frequently used one is outlined in the appendix.

D. Coordinate Systems

1. ORBITAL REFERENCE FRAME

The motion of the tethered subsatellite will be described relative to an orbital reference frame that is fixed in the main body. Since it is known in advance that the short-term dynamic effects of a tethered subsatellite on its main satellite are by engineering design extremely small, the dynamic analysis can be greatly simplified by assuming that the reference frame is traveling along a predetermined orbit. This orbit can be separately calculated by a trajectory analysis. Except for rather low orbits, this analysis requires only the consideration of gravitational forces. For a spherical gravitational field, the orbits will be Keplerian. The orbital reference frame is aligned such that the x_o-axis points in the direction of the inertial velocity vector, the z_o-axis toward the center of the Earth, and the y_o-axis completes the right-hand triad. It is a noninertial coordinate system. In the particular case of a circular orbit, the x_o-axis will be parallel to the inertial velocity vector. The long-term dynamic effects of the tethered subsatellite on its main satellite can be calculated with sufficient accuracy in a separate analysis after the completion of the dynamic analysis described herein.

2. QUASI-COORDINATE REFERENCE FRAME

To derive the equations of motion using the quasi-coordinate formulation of Lagrange's equations, a noninertial quasi-coordinate reference frame is introduced. The axes of this second reference frame will be labeled x, y, z. Its origin is chosen to coincide with the orbital reference frame. It is advantageous to align the axes of the quasi-coordinate frame parallel to the principal axes of the undeformed tether/subsatellite body. The orientation of the quasi-coordinate reference frame relative to the orbital reference frame can be defined by three Euler angles. Initially, the two frames are coincident. A series of three rotations in the proper sequence defines the relative orientation. The three rotations are:

a. A positive rotation ψ about the z-axis.

b. A positive rotation θ about the y-axis.

c. A positive rotation ϕ about the x-axis.

Frequently, these Euler angles are given the following names: the yaw (heading) angle ψ, the pitch (attitude) angle θ, and the roll (bank) angle ϕ. Figure II-1

illustrates the relationship between the two reference frames. For the sake of visibility, only the last two angles are shown in the figure. The angular velocity $\underline{\omega}$ of the quasi-coordinate frame relative to the orbital reference frame can be expressed in terms of the time derivatives of these Euler angles through the well-known Euler kinematical equations. This relationship is given as:

$$\omega_x = \dot{\phi} - \dot{\psi} \sin\theta$$

$$\omega_y = \dot{\theta} \cos\phi + \dot{\psi} \cos\theta \sin\phi \qquad \text{(II-10)}$$

$$\omega_z = \dot{\psi} \cos\theta \cos\phi - \dot{\theta} \sin\phi$$

The Eulerian angles define the orientation of a body by the minimum number of independent coordinates. Their primary attractiveness stems from the fact that they permit a simple geometrical interpretation of the attitude motion of a body. However, they suffer from an intrinsic singularity condition. Another computational drawback of the Euler angle method is the nonlinearity of the differential equation (II-10) which has to be solved to obtain the Euler angles. Both of these computational disadvantages can be avoided by defining the orientation of a body in terms of direction cosines or quaternions. Since one of the primary purposes of this study was to gain physical insight into the dynamic characteristics of the tethered subsatellite, the equations of motion were, nevertheless, derived in terms of Euler angles.

E. Kinetic Energy

The kinetic energy of the dynamical system relative to inertial space is defined as

$$T = \frac{1}{2} \int [\underline{V}_0 + (\underline{\Omega} \times \underline{R}) + \dot{\underline{R}}]^2 \, dm \qquad \text{(II-11)}$$

where

$\underline{V}_0$ = inertial velocity of the origin of the quasi-coordinate frame

$\underline{\Omega}$ = angular velocity of the quasi-coordinate frame relative to inertial space

$\underline{R}$ = position vector from the origin to a mass particle

$\dot{\underline{R}}$ = velocity of a mass particle relative to the quasi-coordinate frame.

The integration extends over the total tethered subsatellite system.

Because the origin of the orbital reference frame is assumed to be in a state of free-fall, its velocity can be set equal to zero ($\underline{V}_0 = 0$). A formal proof of this statement will not be presented. The angular velocity $\underline{\Omega}$ of the quasi-coordinate frame can be expressed as

$$\underline{\Omega} = \dot{\underline{\gamma}} + \underline{\omega} \quad , \tag{II-12}$$

where

$\dot{\underline{\gamma}}$ = angular velocity of orbital reference frame relative to inertial space

$\underline{\omega}$ = angular velocity of quasi-coordinate frame relative to orbital reference frame.

The position vector $\underline{R}$ can be expressed in three components as

$$\underline{R} = \underline{\ell}_0 + \underline{r} + \underline{w} \tag{II-13}$$

where

$\underline{r}$ = position vector of a mass particle originating from $\underline{\ell}_0$

$\underline{w}$ = elastic displacement vector of a mass particle from undeformed state.

The generic vector $\underline{\ell}_0$ is introduced as an extraneous coordinate for the purpose of determining internal reaction forces at points of interest. The elastic displacement vector will be described in terms of the normal modes (eigenfunctions) of the dynamical system; i.e.,

$$\underline{w}(\underline{r},t) = \sum \underline{\Phi}_n (r)\, q_n(t) \quad , \tag{II-14}$$

where $\underline{\Phi}_n(r)$ represents a three-dimensional normal mode and $q_n(t)$ represents its associated generalized coordinate. The normal modes are calculated by a separate structural analysis. Using normal mode information greatly facilitates the formulation and solution of the equations of motion. Although it is realized that such a modal analysis is theoretically only applicable to linear time-invariant structures, past experience has demonstrated that it can also be used for systems whose parameters change only slowly with time. The tethered subsatellite system falls into this category because the deployment and retrieval velocities have to be kept sufficiently small to prevent undesirable nonlinear response phenomena and dynamic instability of the tether because of excessive Coriolis effects.

F. Equations of Motion

Since the objective of this study was to explore the feasibility of the tethered subsatellite concept, the analysis was based on a rather simplified dynamic model of the system. However, some of the simplifications had to be introduced because of limitations in time and resources. The most significant simplifications in this latter category were the omission of lateral tether dynamics and the use of only one normal mode for the elastic expansion of the tether. Torsional rigidity of the tether was also neglected. However, its effect will be very small.

In general, the elastic deformation vector of the tether can be expressed in modal form as follows:

$$w(\underline{r},t) = [\Sigma X_i(x,y,z)\ \xi_i(t)]\ \underline{e}_1 + [\Sigma Y_j(x,y,z)\ \eta_j(t)]\ \underline{e}_2$$

$$+ [\Sigma Z_k(x,y,z)\ \zeta_k(t)]\underline{e}_3 \quad , \tag{II-15}$$

where $\underline{e}_1$, $\underline{e}_2$, and $\underline{e}_3$ are unit vectors along the axes of the quasi-coordinate reference frame. The terms $X_i(x,y,z)$ and $Y_i(x,y,z)$ represent the lateral normal tether modes with $\xi_i(t)$ and $\eta_j(t)$ being their corresponding generalized coordinates. The term $Z_k(x,y,z)$ represents the longitudinal normal tether modes and $\zeta_k(t)$ their corresponding generalized coordinates. With the above-mentioned simplifications, the deformation vector reduces to

$$\underline{w}(\underline{r},t) = Z_1(z)\ \zeta_1(t)\ \underline{e}_3 \tag{II-16}$$

The first longitudinal mode was approximated by

$$Z_1(z) \approx \frac{z}{\ell} \tag{II-17}$$

This approximation was considered sufficiently accurate for the feasibility study of the tethered subsatellite concept.

The tether itself was assumed to have a constant diameter and uniform mass distribution per unit length. For simplicity, the subsatellite was given a spherical shape and mass distribution. Because tether torsion was not taken into consideration, the rotational motion of the subsatellite about the tether axis was set equal to zero. Therefore, the motion of the subsatellite can be described in terms of only two of the three Euler angles. The two Euler angles chosen were the pitch angle θ, which describes the in-plane motion of the subsatellite, and the roll angle ϕ, which describes its out-of-plane motion. The equations of motion can then be expressed in the following form:

In-Plane Motion

$$\left[\left(M+\frac{m}{3}\right)L^2\cos^2\phi+I\right]\ddot{\theta}+2\left[\left(M+\frac{m}{2}\right)\dot{\ell}+\frac{m}{3}\dot{\zeta}\right]L(\dot{\theta}-\dot{\gamma})\cos^2\phi$$

$$+2\left(M+\frac{m}{3}\right)L^2(\dot{\gamma}-\dot{\theta})\dot{\phi}\sin\phi\cos\phi=Q_\theta \quad . \tag{II-18}$$

Out-of-Plane Motion

$$\left[\left(M+\frac{m}{3}\right)L^2+I\right]\ddot{\phi}+2\left[\left(M+\frac{m}{2}\right)\dot{\ell}+\frac{m}{3}\dot{\zeta}\right]L\dot{\phi}$$

$$+\left(M+\frac{m}{3}\right)L^2(\dot{\gamma}-\dot{\theta})^2\cos\phi\sin\phi=Q_\phi \tag{II-19}$$

Stretch Equation

$$\left(M+\frac{m}{3}\right)\ddot{\zeta}+\left(M+\frac{m}{2}\right)\ddot{\ell}-\left(M+\frac{m}{3}\right)L\left[\dot{\phi}^2+(\dot{\gamma}-\dot{\theta})^2\cos^2\phi\right]=Q_\zeta \tag{II-20}$$

The equation for the tension in the tether is obtained by differentiating the Lagrange equation (II-9) with respect to the extraneous variable $\underline{\ell}_0$. For the design of the tether control system, it is necessary to know the tether tension at the deployment reel/tether interface. This is obtained by setting the extraneous variable

$$\underline{\ell}_0=\ell_0\,\underline{e}_3 \tag{II-21}$$

and the corresponding constraint condition to

$$\ell_0=\ell_c(t) \tag{II-22}$$

where $\ell_c(t)$ represents a prespecified time function that is determined by the particular tether control law. The Lagrange multiplier $\underline{\lambda}$ appearing in equation (II-9) yields the tension in the tether directly. After all necessary differentiation steps are performed, the tension equation is obtained by setting $\ell_0 = 0$, $\dot{\ell}_0 = \dot{\ell}$, and $\ddot{\ell}_0 = \ddot{\ell}$. This yields

$$(M + m)\ddot{\ell} + \left(M + \frac{m}{2}\right)\ddot{\zeta} - \left(M + \frac{m}{2}\right)L[\dot{\phi}^2 + (\dot{\gamma} - \dot{\theta})^2 \cos^2\phi] + T = Q_\ell \tag{II-23}$$

where T is the tether tension.

G. Generalized Forces

The generalized forces arise from several different sources. The most significant of these will be discussed in this subsection. Others can be added later if needed. As previously mentioned, the generalized forces are calculated by the virtual work done by the external forces through virtual displacements. The virtual work can be conveniently expressed in terms of the coordinates (x_0, y_0, z_0) of the orbital reference frame and the corresponding components of the external forces. The desired generalized forces are then obtained by a subsequent transformation to the generalized coordinates. Thus, the virtual work is

$$\delta W = F_{x_0}\,\delta x_0 + F_{y_0}\,\delta y_0 + F_{z_0}\,\delta z_0 \quad , \tag{II-24}$$

The position of a mass particle of the tether can be defined in terms of the generalized coordinates of the dynamical system as

$$\begin{aligned} x_0 &= [\ell_0 + z + \Phi(z)\,\zeta]\ \sin\theta\cos\phi \\ y_0 &= -[\ell_0 + z + \Phi(z)\,\zeta]\ \sin\phi \\ z_0 &= [\ell_0 + z + \Phi(z)\,\zeta]\ \cos\theta\cos\phi \quad , \end{aligned} \tag{II-25}$$

where $\Phi(z)$ is the approximation used for the first longitudinal mode of the tether. For the calculation of the generalized forces due to a virtual displacement of the subsatellite, equation (II-25) is used setting $z = \ell$ and $\Phi(\ell) = 1$.

The virtual displacements can be expressed in terms of the generalized coordinates by using the following differential relationships:

$$\delta_{x_0} = [\ell_0 + z + \Phi(z)\zeta] \cos\theta \cos\phi\delta\theta - [\ell_0 + z + \Phi(z)\zeta] \sin\theta \sin\phi\,\delta\phi + \sin\theta \cos\phi\delta\ell_0 + \Phi(z) \sin\theta \cos\phi\,\delta\zeta$$

$$\delta_{y_0} = -[\ell_0 + z + \Phi(z)\zeta] \cos\phi\,\delta\phi - \sin\phi\,\delta\ell_0 - \Phi(z) \sin\phi\,\delta\zeta \qquad \text{(II-26)}$$

$$\delta_{z_0} = -[\ell_0 + z + \Phi(z)\zeta] \sin\theta \cos\phi\,\delta\theta - [\ell_0 + z + \Phi(z)\zeta] \cos\theta \sin\phi\,\delta\phi + \cos\theta \cos\phi\,\delta\ell_0 + \Phi(z) \cos\theta \cos\phi\,\delta\zeta$$

Inserting equation (II-26) into equation (II-24) and collecting the appropriate terms yields the virtual work as

$$\delta W = Q_\theta\,\delta\theta + Q_\phi\,\delta\phi + Q_\zeta\,\delta\zeta + Q_{\ell_0}\,\delta\ell_0 \quad . \qquad \text{(II-27)}$$

1. FIRST-ORDER GRAVITY GRADIENT FIELD

Since the origin of the orbital reference frame moves along a free-fall trajectory, the only gravitational forces acting on the tethered subsatellite arise from the gravity gradient field. The gravity gradient force terms are obtained by a Taylor-series expansion of the gravity field about the free-fall trajectory. The first-order terms of this series are well known. Applying these terms to a mass particle of size dm results in the following:

$$dF_{x_0}^{(1)} = -\omega_0^2 x_0 \, dm$$

$$dF_{y_0}^{(1)} = -\omega_0^2 y_0 \, dm$$

$$dF_{z_0}^{(1)} = 2\omega_0^2 z_0 \, dm \qquad \text{(II-28)}$$

where

$$\omega_0^2 = \frac{g_0 R_E^2}{R^3}$$

It should be noted that these expressions are not restricted to circular orbits, but are valid for general orbits followed by the orbital reference frame. Summing up the forces over all mass particles of the dynamical system yields the first-order gravity gradient terms as:

$$Q_\theta^{(G1)} = -3\left(M + \frac{m}{3}\right) \omega_0^2 L^2 \sin\theta \cos\theta \cos^2\phi$$

$$Q_\phi^{(G1)} = -3\left(M + \frac{m}{3}\right) \omega_0^2 L^2 \cos^2\theta \sin\phi \cos\phi \qquad \text{(II-29)}$$

$$Q_\zeta^{(G1)} = \left(M + \frac{m}{3}\right) \omega_0^2 L(3\cos^2\theta \cos^2\phi - 1)$$

$$Q_{\ell_0}^{(G1)} = \left(M + \frac{m}{2}\right) \omega_0^2 L(3\cos^2\theta \cos^2\phi - 1)$$

2. SECOND-ORDER GRAVITY GRADIENT FIELD

The accuracy of the dynamic model can be improved by including higher order terms of the gravity gradient field in the analysis. For most practical space structures, however, it will not be necessary to go beyond second-order terms. These are less known than the first-order terms, but their derivation is straightforward. Applying these second-order terms to a mass particle of size dm yields the following forces:

$$dF_{x_0}^{(2)} = -3\,\omega_0^2\,\frac{x_0\,z_0}{R_0}\,dm$$

$$dF_{y_0}^{(2)} = -3\,\omega_0^2\,\frac{y_0\,z_0}{R_0}\,dm \qquad \text{(II-30)}$$

$$dF_{z_0}^{(2)} = \omega_0^2\left[-\frac{3}{2}\left(\frac{x_0^2 + y_0^2}{R_0}\right) + \frac{3z_0^2}{R_0}\right]$$

In comparison with the first-order gravity gradient terms, it is seen that they are very small. Even for distances up to 100 km from the origin of the orbital reference frame, their contribution is on the order of a few percent. They were, therefore, not considered in the analysis.

The generalized forces associated with these forces can again be obtained by summing over the whole dynamical system and applying equations (II-25) and (II-26).

3. ROTATING ATMOSPHERE

For tethered subsatellites moving in orbits of extremely low altitudes (100 to 200 km), the aerodynamic disturbances arising from the atmosphere of the Earth dominate those arising from the gravity gradient field and decisively influence the dynamic response of the system. To limit the size of the computer program, the variation of the atmospheric density with altitude was assumed to be exponential. A least-square curve fit for such an "exponential" atmosphere is shown in Figure II-2. For the analysis, it was of some advantage to define the exponential density variation in the form

$$\rho = \rho_0 e^{bh} = \rho_0 e^{h/H} \tag{II-31}$$

where

ρ_0 = reference density

$H = \frac{1}{b}$ = reference height

h = distance from main satellite vertically down.

The data are based on the 1962 U.S. Standard Atmosphere. Only a single scale height H was used in the analysis, which corresponded to an altitude range of $80 < h < 100$ km. This was considered the range of major concern. As a consequence, the atmospheric density in the vicinity of the main satellite was much smaller than the actual one. Therefore, the dynamic response of the tethered subsatellite during its initial deployment phase was not accurately modeled. However, this was not considered to be critical, because it was found that the initial dynamic transients damp out rather quickly during the deployment phase. In fact, an increase in drag on the subsatellite will benefit the deployment initiation. For the tether, the aerodynamic forces were defined as:

a. Normal Force

$$\underline{D}_N = \frac{1}{2} \rho C_N A_N V_N \underline{V}_N \tag{II-32}$$

b. Axial Force

$$\underline{D}_A = \frac{1}{2} \rho C_A A_A V_A \underline{V}_A \tag{II-33}$$

where $\underline{V}_N$ and $\underline{V}_A$ represent the normal and axial relative wind velocities. The normal and axial force coefficients C_N and C_A are usually given as functions of angle of attack and other aerodynamic parameters. In the present analysis, they were assumed to be constant.

For the spherical subsatellite, the aerodynamic force was defined as

$$\underline{D} = \frac{1}{2} \rho C_D A V \underline{V} \tag{II-34}$$

with $\underline{V}$ being the relative wind velocity and C_D the aerodynamic drag coefficient. The latter was assumed to be constant.

The relative wind velocity was determined with the assumption that the atmosphere rotates with the Earth. Resolving the relative wind vector in components along the axes of the orbital reference frame yields the following results:

$$\begin{aligned} V_{x_0} &= - R_0 (\omega_0 - \Omega_0 \cos i) \\ V_{y_0} &= R_0 (\Omega_0 \sin i \cos \beta) \end{aligned} \tag{II-35}$$

It can be easily verified that the motion of the tethered subsatellite relative to the orbital reference frame is negligible when compared to the total relative wind velocity. Therefore, the velocity terms in equations (II-32), (II-33), and (II-34) can be directly calculated from equation (II-35). The detailed steps of this calculation will not be given. Likewise, the calculation of the generalized aerodynamic forces acting on the system via the principle of virtual work will not be presented. The final result gives the generalized aerodynamic forces as

$$\begin{aligned} Q_\theta^{(A)} &= \rho e^{bh_0} \left[C_D^{(M)} AL \mu_0 V^{(M)} + C_N^{(m)} \eta\mu_2 V_N^{(m)} \right] V_x \cos \phi \\ Q_\phi^{(A)} &= - \rho e^{bh_0} \left[C_D^{(M)} AL \mu_0 V^{(M)} + C_N^{(m)} \eta\mu_2 V_N^{(m)} \right] V_y \end{aligned} \tag{II-36}$$

$$Q_{\zeta}^{(A)} = \rho\, e^{bh_0} \left[C_D^{(M)}\, A\, \mu_0\, V^{(M)} + C_A^{(m)}\, \frac{r}{L}\, \mu_2\, V_A^{(m)} \right] V_z$$

$$Q_{\ell_0}^{(A)} = \rho\, e^{bh_0} \left[C_D^{(M)}\, A\, \mu_0\, V^{(M)} + C_A^{(m)}\, r\, \mu_1\, V_A^{(m)} \right] V_z \quad ,$$

(II-36)
(Concluded)

with the following definitions:

$$V_x = V_{x_0} \cos\theta$$

$$V_y = V_{x_0} \sin\theta \sin\phi + V_{y_0} \cos\phi$$

$$V_z = V_{x_0} \sin\theta \cos\phi - V_{y_0} \sin\phi$$

and

$$V^{(M)} = \sqrt{V_{x_0}^2 + V_{y_0}^2}$$

$$V_N^{(m)} = \sqrt{V_x^2 + V_y^2}$$

$$V_A^{(m)} = V_z$$

Also,

$$\mu_0 = \frac{1}{2}\, e^{bL \cos\theta \cos\phi}$$

$$\mu_1 = \frac{e^{bL \cos\theta \cos\phi} - 1}{b \cos\theta \cos\phi}$$

$$\mu_2 = \frac{e^{bL \cos\theta \cos\phi} (bL \cos\theta \cos\phi - 1) + 1}{(b \cos\theta \cos\phi)^2}$$

$$h_0 = \frac{h_e}{2} [1 - \cos(\gamma + \gamma_0)]$$

The last of these definitions is to be used for elliptical orbits of the main satellite where h_e represents the altitude variation because of the eccentricity of the orbit. The angle γ represents the true anomaly of the main satellite, and the angle γ_0 provides a convenient definition for initiating various maneuvers of the tethered subsatellite.

The numerical values for the aerodynamic coefficients were assumed to be constant at the following levels:

$$\text{Subsatellite} - C_D^{(M)} = 1.0$$

$$\text{Tether} - C_N^{(m)} = 2.2$$

$$C_A^{(m)} = 0.2$$

4. ORBITAL ECCENTRICITY

The effect of orbital eccentricity on the dynamic response of a tethered subsatellite is twofold; one is a geometric effect, and the other is a dynamical effect. The geometric effect is due to the altitude variation of the tethered subsatellite which is caused by the eccentric orbit of the main satellite. As a consequence, the tether/subsatellite system is subject to unsteady aerodynamic disturbances. To incorporate this effect into the analysis, it was assumed that the main satellite moves in a Keplerian orbit whose geometry is defined as

$$R = \frac{R_p(1+\epsilon)}{1+\epsilon\cos\gamma} \quad , \tag{II-37}$$

where R_p is the perigee distant, ϵ is the eccentricity of the orbit, and γ is the true anomaly.

Since the eccentricity ϵ will be small ($\epsilon << 1$) for all orbits of practical interest, it is possible to expand equation (II-37) in a Taylor series as follows:

$$R = R_p(1+\epsilon)\,(1 - \epsilon\cos\gamma + \epsilon^2\cos^2\gamma - \ldots) \quad . \tag{II-38}$$

Taking only the first-order term in ϵ, the altitude variation becomes then

$$\Delta h = R - R_p = \epsilon R_p(1 - \cos\gamma) \tag{II-39}$$

From this it follows that, for small eccentricities, the altitude variation of the tethered subsatellite is approximately sinusoidal. The relationship between the maximum altitude change and the orbital eccentricity can be readily obtained from equation (II-39) as

$$\epsilon = \frac{h_e}{2R_p} \tag{II-40}$$

It is instructive to consider a numerical example. Assuming an altitude of 200 km for the main satellite (R_p = 6570 km) and a maximum altitude variation (h_e = 20 km) of the subsatellite leads to an orbital eccentricity of $\epsilon = 1.5 \times 10^{-3}$. This result confirms the validity of the above Taylor-series expansion.

Having demonstrated the smallness of the eccentricity, it is now possible to assess the dynamic effect of the eccentricity using a series expansion expressing the true anomaly γ in terms of the eccentricity ϵ and the mean anomaly M. This relationship is given by

$$\gamma = M + \left(2\epsilon - \frac{1}{4}\epsilon^3\right)\sin M + \left(\frac{5}{4}\epsilon^2 - \frac{11}{24}\epsilon^4\right)\sin 2M + \ldots \quad , \quad \text{(II-41)}$$

where

$$M = \sqrt{\frac{g_0 R_E^2}{a^3}}\, t = nt$$

and

$$n = 2\pi/T$$

with a representing the semimajor axis and T the orbital period. Neglecting terms higher than first order in equation (II-41) yields the angular velocity of the main satellite in its orbit as:

$$\dot{\gamma} = n(1 + 2\epsilon \cos nt) \qquad \text{(II-42)}$$

From this it follows that the angular velocity of an eccentric orbit is sinusoidal for small values of its eccentricity. However, it is seen that the sinusoidal fluctuations are extremely small. For most practical orbits, these fluctuations are less than 1 percent of the mean angular velocity. It is, therefore, permissible to replace the time-varying angular velocity $\dot{\gamma}$ by its mean angular velocity n in the equations of motion.

The angular acceleration of the eccentric orbit is obtained by differentiating equation (II-42) with respect to time. This yields

$$\ddot{\gamma} = -2\epsilon n^2 \sin nt \quad . \qquad \text{(II-43)}$$

The inertial forces arising from this angular acceleration are, therefore, proportional to ϵn^2. Their magnitude can be estimated by comparing them with the gravity gradient forces of equation (II-28). These are seen to be proportional to the square of the term ω_0. This term, however, is very nearly equal to the mean angular velocity n. As a consequence, the inertial forces arising from the orbital angular acceleration are by a factor ϵ smaller than the gravity gradient forces. Because of the extreme smallness of the eccentricity, they can be rightfully neglected and were not included in the equations of motion.

5. OBLATENESS OF EARTH

The effects of the oblateness of the Earth on the dynamic response of a tethered subsatellite are threefold; two aspects are geometrical in nature, while the third is dynamical. The first geometrical effect, the flattening of the Earth at its poles, brings about variations in orbital altitude of approximately 20 km. It has its greatest effect on satellites in polar orbits. The second geometric effect results because the orbits of the main satellite are no longer circular. In fact, they are not even closed but precess in a westerly direction. The rate of precession will depend upon the inclination of the orbit and, to a somewhat smaller extent, on its altitude. However, the orbit regression amounts to only a few degrees per day and will not induce any discernible dynamic effects on the tethered subsatellite. The altitude variations resulting from these non-circular orbits range from 5 to 10 km, depending on the inclination of the orbit.

Like the geometric effect of the orbital eccentricity, the geometric effects of the Earth's oblateness will result in a constantly changing aerodynamic disturbance force. A detailed simulation of this condition was not attempted. It is expected that the influence of these effects on the dynamic behavior of the tethered subsatellite is very similar to that observed for the orbital eccentricity.

The dynamical effect of the oblateness of the Earth is due to the deviation of the gravitational field from its spherical symmetry. To determine this effect, we begin with the oblateness force exerted on a particle of mass m. Resolved in components relative to the orbital reference frame, they are

$$
\begin{aligned}
F_{x_0} &= -2m\,J\,g\left(\frac{R_E}{R}\right)^4 \sin^2 i \sin\beta\cos\beta \\
F_{y_0} &= 2m\,J\,g\left(\frac{R_E}{R}\right)^4 \sin i\cos i\sin\beta \qquad \text{(II-44)} \\
F_{z_0} &= 3m\,J\,g\left(\frac{R_E}{R}\right)^4 \left(\frac{1}{3} - \sin^2 i \sin\beta\right) ,
\end{aligned}
$$

where the oblateness term $J = 1.637 \times 10^{-3}$. The angle β defines the position of the main satellite relative to the intersection of the orbital and equatorial planes. The position of any mass element dm of the tethered subsatellite in terms of (R_0, β_0) can be approximately expressed as

$$\beta_0 = \beta + \frac{x}{R} \tag{II-45}$$

and

$$\frac{1}{R_0^4} = \frac{1}{R^4}\left(1 + \frac{4z}{R}\right) \tag{II-46}$$

Analogous to the gravity forces, only the gradient effects of the oblateness forces are of interest. These are obtained by inserting equation (II-45) and equation (II-46) into equation (II-44) and subtracting the zeroth oblateness contributions. Retaining only linear terms then yields the first-order oblateness gradient forces as

$$\begin{aligned}
dF_{x_0}^{(0)} &= -2\omega_0^2 J\left(\frac{R_E}{R}\right)^2 \sin^2 i(x\cos 2\beta + 2z\sin^2\beta)\, dm \\
dF_{y_0}^{(0)} &= 2\omega_0^2 J\left(\frac{R_E}{R}\right)^2 \sin i\cos i\,(x\cos\beta + 4z\sin\beta)\, dm \\
dF_{z_0}^{(0)} &= 3\omega_0^2 J\left(\frac{R_E}{R}\right)^2 \left[4z\left(\frac{1}{3} - \sin^2 i\sin^2\beta\right) + x\sin^2 i\sin^2\beta\right] dm
\end{aligned} \tag{II-47}$$

A comparison of these terms with the corresponding gravity gradient terms of equation (II-3) will readily reveal that they are several orders of magnitude smaller. Therefore, the dynamical effect of the oblateness of the Earth can be safely disregarded.

6. VISCOELASTIC TETHER FORCE

The viscoelastic properties of the tether were modeled by very idealized elements. Accordingly, the elasticity was represented by a linear spring whose spring constant k is

$$k = \left(\frac{\pi d^2}{4}\right) \frac{E}{\ell} \tag{II-48}$$

where d is the diameter of the tether and E is Young's modulus. Likewise, the damping, which is a rather complex phenomenon, was represented by an equivalent viscous damper with a damping force proportional to the velocity of the generalized modal coordinate (modal damping). Consequently, the generalized force due to the elasticity and damping of the tether can be directly obtained as

$$Q_\zeta = -k\zeta - C_2\dot{\zeta} \tag{II-49}$$

where C_2 is the coefficient of viscous damping. It is important to note that the energy dissipation due to frictional losses in the tether material is, in general, too small to aid in damping out transient responses of the tethered subsatellite. As is pointed out in other sections of this report the removal of these transients requires the employment of an active tether control law.

H. Tether Control Laws

The deployment, retrieval, and quite probably the stationkeeping phase of a tethered subsatellite require an active tether control system to guarantee adequate dynamic systems performance. In accordance with the principles of control system design, the tether control law will incorporate information about the dynamic state of the system in a closed-loop mode. This can be implemented in various ways depending on whether the design is based upon classical or optimal control theory. In subsequent chapters, a tether control law is analyzed which generates a tether tension, T, through a linear feedback law of the form:

$$T = k_1 \ell + c_1 \dot{\ell} + k_2 \ell_c \quad , \tag{II-50}$$

in which the gain values k_1, c_1, and k_2 are properly chosen. Implementation of this control law requires the measurement of the tether tension, the rate of tether deployment, and the length of the tether itself. The present discussion examines the possibility of employing a control law that does not require the measurement of the tether tension. Besides being simple, this control law is useful for exposing some distinctive features of the dynamic behavior of the tethered subsatellite during its deployment. In this discussion, some facts will also be presented on the problems associated with the retrieval of a tethered subsatellite. The tether control law to be analyzed consists of the following three phases:

1. Exponential Increase of Deployment Rate

$$\dot{\ell} = \alpha \ell \qquad \text{for} \qquad \ell_0 < \ell \leq \ell_1 \tag{II-51a}$$

2. Constant Deployment Rate

$$\dot{\ell} = c \qquad \text{for} \qquad \ell_1 < \ell \leq \ell_2 \tag{II-51b}$$

3. Exponential Decrease of Deployment Rate

$$\dot{\ell} = \alpha(\ell_c + \ell_0 - \ell) \qquad \text{for} \qquad \ell_2 < \ell \leq \ell_c \tag{II-51c}$$

Numerical values used for the dynamic analysis are:

$\ell_0 = 10$ m $\qquad\qquad$ $\ell_1 = 10^4$ m

$\ell_2 = 9 \times 10^4$ m $\qquad\qquad$ $\ell_c = 9.999 \times 10^4$ m

$c = 5$ m/s $\qquad\qquad$ $\alpha = 5 \times 10^{-4}$ s^{-1}

Time histories of the tether length and its deployment rates based upon this so-called exponential control law are given in Figures II-3 and II-4. To gain physical insight into the dynamic behavior of the system, the attitude equations

were examined for both the in-plane and out-of-plane motion in the absence of aerodynamic disturbances. Furthermore, the tether mass was assumed to be negligible and the orbit of the main satellite to be circular. For this special case, the in-plane motion is decoupled from the out-of-plane motion and is described by

$$\ddot{\theta} + 2\left(\frac{\dot{\ell}}{\ell}\right)\dot{\theta} + \frac{3}{2}\omega_0^2 \sin 2\theta = 2\left(\frac{\dot{\ell}}{\ell}\right)\omega_0 \quad . \tag{II-52}$$

The out-of-plane motion only decouples from the in-plane motion for small pitch angles θ. With this assumption, the out-of-plane motion is described by

$$\ddot{\phi} + 2\left(\frac{\dot{\ell}}{\ell}\right)\dot{\phi} + 4\omega_0^2\phi = 0 \quad . \tag{II-53}$$

At first the dynamic behavior of the system is examined for constant tether length ($\dot{\ell} = 0$). For this case, both the in-plane and out-of-plane motion are analogous to a simple pendulum motion with stable equilibria at $\theta = 0°$ and $\theta = 180°$. However, the in-plane oscillation has a different period than the out-of-plane oscillation, even for small attitude angles. They are given as

Out-of-Plane Period

$$T_0 = \frac{\pi}{\omega_0} \tag{II-54}$$

In-Plane Period

$$T_I = \frac{2}{\sqrt{3}}\frac{\pi}{\omega_0} = 1.15\, T_0$$

The in-plane period is seen to be somewhat larger than the out-of-plane period. It is important to notice that the periods of both oscillations are independent of the tether length.

For large attitude angles, the in-plane and out-of-plane motions are no longer decoupled. As a consequence, the tethered subsatellite will, in general, exhibit a rather complex motion. Because the frequencies of the two oscillations are incommensurable, the resulting pattern of the motion will somewhat resemble the so-called Lissajous figures encountered in celestial mechanics.

During the deployment and retrieval maneuvers, the tether length is no longer constant. Examination of the preceding equations of motion reveals that the dynamic behavior of the tethered subsatellite becomes distinctively different for these two maneuvers. For deployment, the tether length ℓ is increasing ($\dot{\ell} > 0$) and the second terms of equations (II-52) and (II-53) containing the derivative of the tether length take the place of an equivalent damping. In such a case, existing oscillations will have a tendency to die. For retrieval, the tether length is decreasing ($\dot{\ell} < 0$) and the second term introduces negative damping. In this case, existing oscillations will tend to build up. It has been found by simulation that this pattern is very pronounced in the out-of-plane motion. Because of the presence of the term of the right side of equation (II-52), however, the in-plane motion does not build up rapidly. It is expected that this accumulation of kinetic energy during the retrieval phase can be held within acceptable limits by a proper design of the tether control law. Such a control law will, by necessity, lead to a "yo-yo" type of retrieval motion. This motion will be characterized by fast retrieval rates in the neighborhood of the maximum attitude excursions of the subsatellite and slow or even negative retrieval rates (i.e., $\dot{\ell} > 0$) in the vicinity of the equilibrium points. Because of this yo-yo effect, the retrieval time of a tethered subsatellite will, *ceteris paribus*, be longer than the time for its deployment. Some preliminary studies concentrating on the problems associated with the retrieval of a tethered subsatellite are presented in a subsequent section. One can conceivably also use this yo-yo effect for the removal of residual kinetic energy from a tethered subsatellite during its stationkeeping mode. An optimal bang-bang type, yo-yo control law for this purpose is illustrated in Figure II-5. Each time the subsatellite passes through its equilibrium position the tether length is suddenly decreased by a small amount δ and then increased by the same amount when the subsatellite reaches its extreme position. The dissipation of kinetic energy per cycle resulting from this maneuver can be related to an equivalent viscous damping effect. For small oscillations of the in-plane motion, the corresponding critical damping ratio becomes

$$\zeta_{e_J} = \frac{2\sqrt{3}}{\pi}\left(\frac{\delta}{\theta_0\,\ell}\right) \qquad \text{(II-55)}$$

where θ_0 is the amplitude of the in-plane oscillation. It is seen that the damping effect increases with decreasing amplitude, indicating that yo-yo control of the in-plane motion could be very effective. The corresponding damping effect for the out-of-plane motion can be calculated as

$$\zeta_{e_0} = \frac{1}{\pi}\left(\frac{\delta}{\ell}\right) \tag{II-56}$$

This damping effect is independent of the amplitude, indicating that a yo-yo control of the out-of-plane motion could be very ineffective. In fact, a yo-yo motion amounting to a 3 percent change in tether length induces only a 1 percent damping ratio.

A schematic presentation of this yo-yo control law is shown in Figure II-5. It should be realized that the bang-bang type operation of this optimal yo-yo control law prevents its direct hardware implementation. It was only discussed for demonstrating the dynamic principle involved in removing kinetic energy from a system without the expulsion of mass by reaction jets.

Inspection of the in-plane motion, equation (II-52), also uncovered an interesting and important dynamic peculiarity associated with the deployment and retrieval phase of the tethered subsatellite. It is seen that the subsatellite can assume a steady-state attitude angle θ if the deployment velocity increases exponentially as in equation (II-51a). However, stability of the motion can only be maintained as long as the attitude angle stays below 45°. Obviously, this limits the deployment rate α, which, in turn, establishes a lower bound for the deployment time of the subsatellite. For negligible tether mass, the upper limit of the deployment rate, α_u, is constant with time. If the tether mass is taken into account, the system reaches only a quasi-steady state and the upper limit of the deployment rate changes with time according to the relationship

$$\alpha_u = \frac{3}{4}\left(\frac{M + \frac{m}{3}}{M + \frac{m}{2}}\right)\omega_0 \tag{II-57}$$

where $m = m(t)$ is the instantaneous tether mass. To verify this result, computer simulations were made with the deployment rate α as a parameter. The dynamic behavior of the subsatellite during the exponential buildup phase of the deployment velocity is shown in Figure II-6. The critical deployment rate was determined by iteration to be approximately $\alpha_c \approx 9.5 \times 10^{-4}\ s^{-1}$. This value agrees rather well with the quasi-steady value of equation (II-56). Physically, the onset of the instability is caused by the loss of tension in the tether. From this time point on, the subsatellite becomes a free-flying object until the tension is regained. For all practical purposes, however, loss of tension in the tether also signals loss of control over the subsatellite. The same dynamic peculiarity also exists, of course, for the retrieval phase with the proper sign reversal of the attitude angle θ. Instead of trying to stay "in front" of the main satellite as during its deployment, the tethered subsatellite will now stay "behind" the main satellite ($\theta < 0$). As was discussed previously, the retrieval phase is, however, dominated by the second term of equations (II-52) and (II-53), especially for the out-of-plane motion. The negative damping effect caused by this term becomes very noticeable in the vicinity of the main satellite where the tether length is small. There the tethered subsatellite acquires a spectacular tendency to wrap around the main satellite, unless the retrieval rate is reduced to an extremely small level. It should be pointed out that these dynamic characteristics of a tethered subsatellite during its deployment and retrieval are intrinsic in nature and therefore independent of the particular tether control law chosen for these maneuvers.

I. Results of Computer Simulations

To gain a conclusive engineering understanding of the dynamic behavior of the tethered subsatellite system, the analytical investigations were supplemented by detailed computer simulations. These were based on design specifications proposed by the Smithsonian Astrophysical Observatory. Accordingly, the following system parameters were used:

Main Satellite

Orbital Altitude	$H = 200$ km

Subsatellite

Spherical Mass	$M = 170$ kg
Cross Section	$A = 1\ m^2$
Drag Coefficient	$C_D = 1.0$

Tether

Deployed Length	$\ell = 100$ km
Radius	$r = 0.183 \times 10^{-3}$ m
Density	$\rho = 7.93 \times 10^{3}$ kg m^{-3}
Total Mass	$m = 83.4$ kg
Normal Force Coefficient	$C_N = 2.2$
Axial Force Coefficient	$C_A = 0.2$

The sensitivity of the dynamic response characteristics was investigated with respect to variations of both system parameters and initial conditions. This revealed a number of interesting and important aspects of the system. First, it was noticed that the system is relatively insensitive with respect to variations of the initial deployment conditions. Dynamic transients arising from these do not build up but stay within acceptable limits. The initial alignment of the subsatellite and its actual release mechanism should, therefore, not be a critical item. Likewise, it was found that the dynamic response characteristics were not very sensitive to changes in payload and tether mass. The design of the tethered subsatellite system can, therefore, accommodate a rather wide range of these parameters. On the other hand, the effect of orbital eccentricity was very pronounced because of the drastic atmospheric density variations induced by the altitude changes of the subsatellite. Care has to be taken, therefore, to maintain a nearly circular orbit of the main satellite during the operation of the tethered subsatellite. For a subsatellite altitude of 100 km, it seems advisable to limit the altitude variations due to orbital eccentricity to 10 km or less. This requirement becomes, of course, less stringent for higher subsatellite altitudes because of the decreasing effect of the atmospheric disturbances.

To illustrate the dynamic behavior of the tethered subsatellite, only a few typical cases were selected, and these are shown in Figures II-7 through II-20. The plots are arranged in the following order:

1. Pitch Angle θ
2. Roll Angle ϕ

3. In-Plane Motion (x - z Plot)

4. Out-of-Plane Motion (y-z Plot)

5. Equatorial Motion (x-y Plot)

6. Tether Elongation ζ

7. Tether Tension T

Initial conditions for all cases are $\theta_0 = \phi_0 = 3°$ and $\dot{\theta}_0 = 0$, $\dot{\phi}_0 = \omega_0$. They reflect initial misalignments and a small out-of-plane release impulse of the subsatellite. Each figure contains two plots: one for a circular orbit (Case A) and one for an eccentric orbit with ΔH = 10 km (Case B). Figures II-7 through II-13 present equatorial orbits and Figures II-14 through II-20 present polar orbits. Cases of intermediate orbital inclinations were not included because the general nature of their dynamic response characteristics can be easily visualized by proper interpolation between the cases shown. The time histories of the state variables presented are essentially self-explanatory. However, a few remarks seem to be in order. For equatorial orbits, the out-of-plane motion (y-z plot) is essentially dictated by the initial conditions. Since the exponential deployment does not provide damping, the responses are very nearly constant. The equatorial motion (x-y plot) shows the typical Lissajou characteristics, especially for the fully deployed condition. Eccentricity of the orbit introduces substantial excursions of the in-plane motion (x-z plot) with dynamic transients of several thousand meters over and above the steady-state response. For polar orbits the effect of the rotating atmosphere is clearly visible. It leads to out-of-plane transients of 2000 to 5000 m. However, there are no indications of resonance. The tensile forces in the tether never exceed 100 N. They should not present problems relative to the material properties of the tether. The same holds true for the elastic expansion of the tether which stays below 400 m or 0.4 percent of the total tether length.

J. Steady-State Lateral Tether Deflection

Because of limitations in manpower and resources, only a cursory examination could be made of the effect of lateral tether dynamics. The following analysis makes use of the Rayleigh-Ritz method, which is based on the premise that the exact deflection of an elastic system can be approximated by the superposition of suitably chosen mode functions. The success of the Rayleigh-Ritz method depends very much on the choice of these mode functions.

They are usually selected from the natural mode shapes (eigenfunctions) of the dynamical system under investigation or of one which is very similar to it. For the tethered subsatellite system, it would be natural to use the eigenfunction of a string vibrating under nonuniform tension. This would be determined by the gravity gradient force field. The string would be suspended at one end and have a mass attached to the other end. Since a computer program was not readily available to compute these eigenfunctions, the analysis was based on eigenfunctions of a string under uniform tension. The string was assumed to have an infinite end mass. To provide for maximum tether flexibility, the tension was set equal to the smallest value of the tension in the tether. This occurs at the attach point of the subsatellite. For this condition, the eigenfunctions, ψ_n, are simply given by

$$\psi_n(z) = \sin \frac{n \pi z}{\ell} \qquad n = 1, 2, \ldots \tag{II-58}$$

The associated eigenvalues (natural frequencies) of the system are

$$\omega_n = \frac{n \pi}{\ell} \sqrt{\frac{T}{\rho A}} \tag{II-59}$$

In accordance with the Rayleigh-Ritz method, the modal response of the system is obtained from the equation

$$\ddot{\eta}_n + \omega_n^2 \eta_n = \frac{\int_0^{\ell} \psi_n(\xi)\, f(\xi,t)\, d\xi}{M_n} \tag{II-60}$$

where $f(\xi,t)$ represents the aerodynamic force per unit length of the tether η_n the generalized coordinate, and M_n the generalized mass of the nth mode shape. The total response of the tether over and above the rigid tether response is then obtained by superposition of the individual modal responses as

$$u(z,t) = \Sigma\, \psi_i(z)\, \eta_i(t) \qquad i = 1, 2, \ldots N \quad , \tag{II-61}$$

where N is the total number of mode shapes used in the Rayleigh-Ritz approximation. For the present feasibility study, the response of the fully deployed tether was only determined for a steady-state aerodynamic excitation force. This very closely corresponds to a tethered subsatellite moving in a circular equatorial orbit. For eccentric or inclined orbits, the aerodynamic forcing function contains a component that has an approximate sinusoidal variation with time and a period close to the orbital period of the orbiter. However, it should be remarked that the period of the first few tether mode shapes is very much smaller than the orbital period. Therefore, no serious resonance phenomena are expected to occur for these orbits, at least not for the fully deployed condition.

The total number N that has to be used to obtain a satisfactory approximation to the actual deflection of a dynamic system depends strongly on the forcing function itself. Because of the drastic exponential increase of the atmospheric density with decreasing altitude, the aerodynamic excitation is concentrated at the lower end of the tether. As a consequence of this strong nonuniform force distribution, it takes a relatively large number of mode shapes for convergence. This fact is illustrated in Figures II-21 through II-25. It is seen that satisfactory convergence requires the inclusion of 8 to 10 mode shapes. The maximum deflection of the tether is about 6 km, i.e., about 6 percent of its total length.

A more accurate analysis of the lateral tether flexibility would have to be based on Lagrange's equation (II-9) using the previously mentioned refined mode shapes.

K. Conclusions and Recommendations

The feasibility study conducted thus far did not expose any hazardous or adverse dynamic response characteristics of the tethered subsatellite during its deployment and stationkeeping phase. In fact, its dynamic behavior was unexpectedly favorable. Part of this can, of course, be attributed to the fact that a rather long duration was allowed for the deployment maneuver whose initial velocities were kept at a few millimeters per second. In practice, this would lead to deployment times of 8 to 12 h. However, there seemed to be no objection to allotting this amount of time to the total deployment phase. The dynamic transients and steady-state excursions during the stationkeeping phase appeared to be acceptable for the proposed satellite-borne experiments. Besides, there seems to be the possibility of reducing these dynamic responses by a properly

chosen yo-yo tether control law. This could obviate the potential necessity of having an active reaction-jet control system on board the subsatellite. Tensile forces in the tether were well within the strength limits of the proposed tether materials and gauges. No dynamic resonance phenomena were observed as a result of aerodynamic disturbances for inclined or eccentric orbits. Although diurnal fluctuations of the atmospheric density were not simulated, they will probably not introduce serious dynamic response problems. They will, however, slightly increase the steady-state excursions of the subsatellite. Whereas the dynamical effects of the Earth's oblateness were found to be negligible, its geometric effects are significant. A satisfactory assessment of these would have to be based on a more accurate definition of the atmospheric density variations above the surface of the Earth including diurnal effects. It did not come as a surprise that a serious dynamic problem arose during the attempt to retrieve the subsatellite. This problem is characterized by a spectacular wrap-around phenomenon during the last phase of the retrieval maneuver, when the subsatellites come into the close vicinity of the main satellite. A similar behavior had already been observed in earlier dynamic studies that were performed to prove the feasibility of rescuing a disabled astronaut by tether retrieval. Since this problem and its potential solution will be discussed in a later section of this report, it will not be pursued further here. It seems appropriate to mention, however, that an earlier planar analysis of the retrieval phase did not reveal this phenomenon because the tether control law could provide sufficient damping for the in-plane motion. Therefore, it is recommended that future analyses be performed using a three-dimensional dynamical model of the tethered subsatellite.

Based on the physical insight gained in the present dynamic analysis, it is further recommended that the dynamic analysis be expanded by including lateral tether mode shapes in both pitch plane and yaw plane. In addition, the effect of the tethered subsatellite on the main satellite should be assessed, in order to estimate the propellant consumption for maintaining proper attitude and orbital position of the main satellite. This can be done in a separate analysis. Some effort should be devoted to analyze the effect of the ionospheric plasma and the Earth's magnetic field on the tether. Both of these effects are expected to be small.

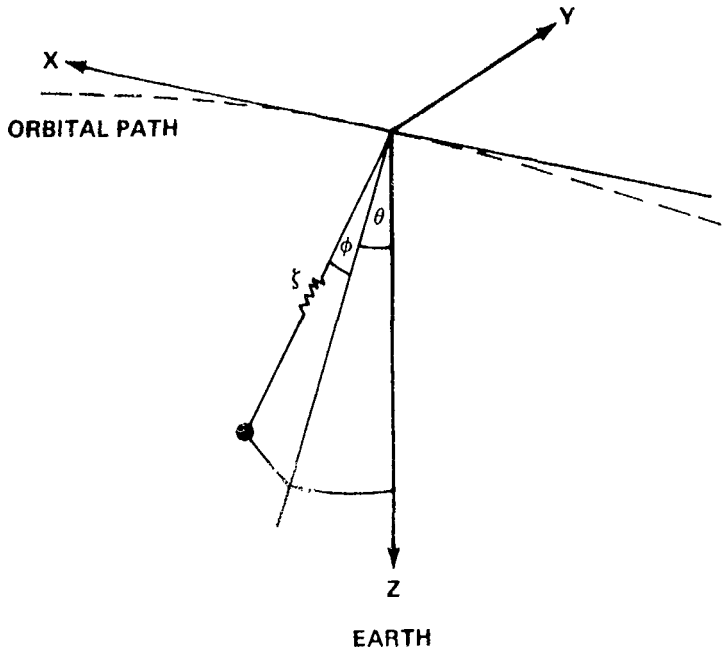

Figure II-1. Coordinate system.

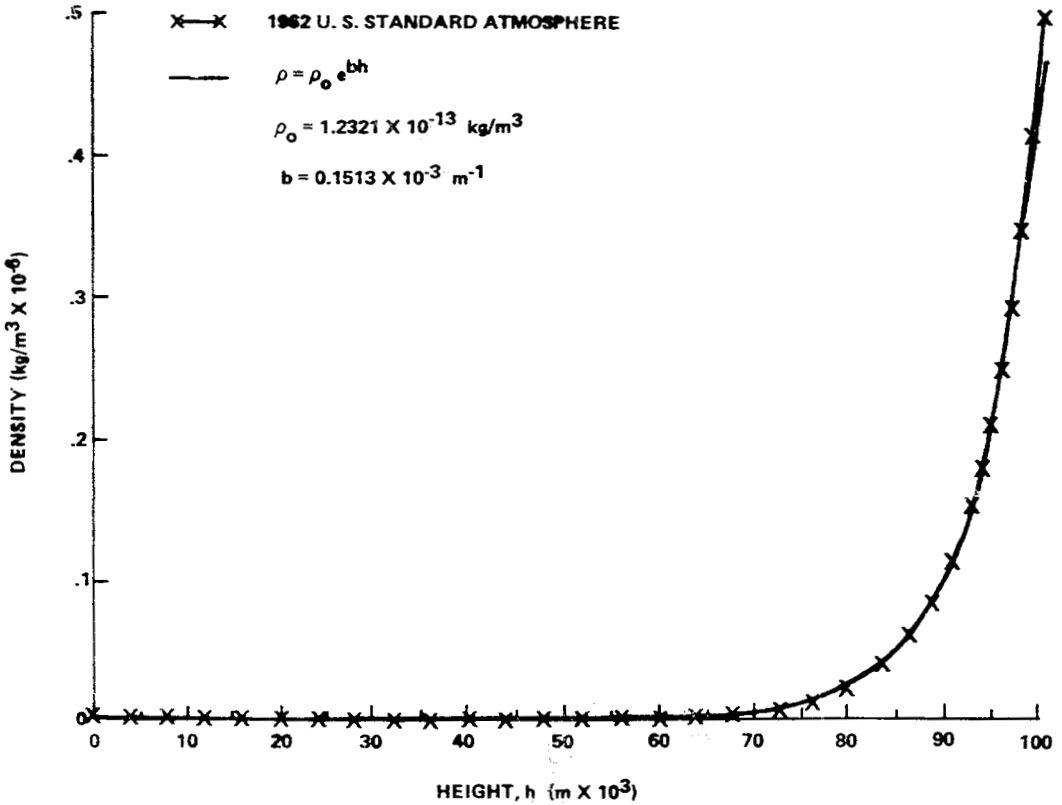

Figure II-2. Exponential atmosphere model.

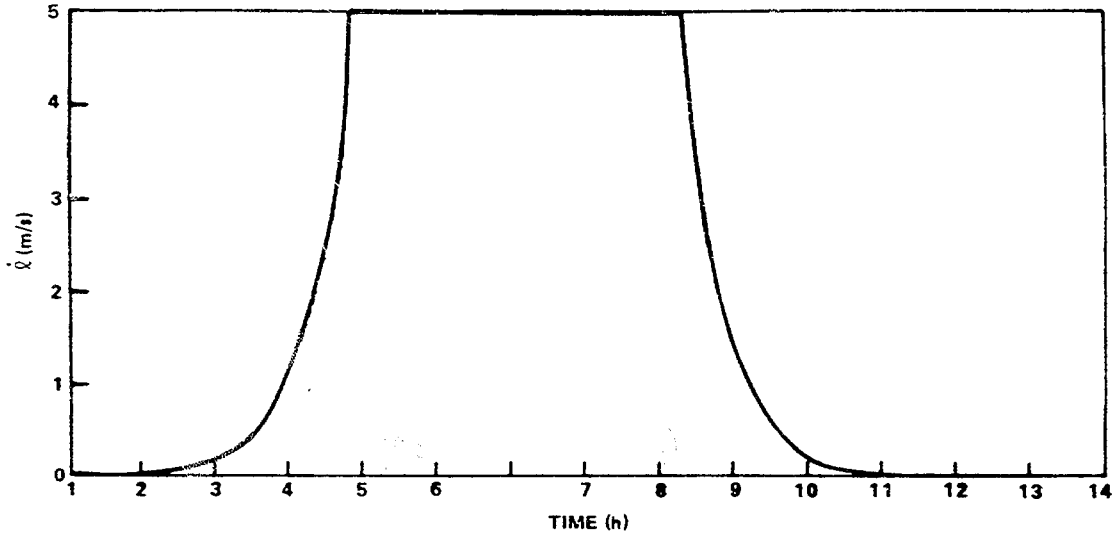

$\dot{\ell} = \alpha \ell$ FOR $\ell_0 < \ell \leq \ell_1$ $\ell_0 = 10$ m

$\dot{\ell} = c$ = CONSTANT FOR $\ell_1 < \ell \leq \ell_2$ $\ell_1 = 10$ km

$\dot{\ell} = \alpha (\ell_c + \ell_0 - \ell)$ FOR $\ell_2 < \ell \leq \ell_c$ $\ell_2 = 90$ km

$\alpha = 5 \times 10^{-4}\ s^{-1}$ $\ell_c = 99.99$ km

Figure II-3. Exponential deployment law — rate of tether deployment versus time.

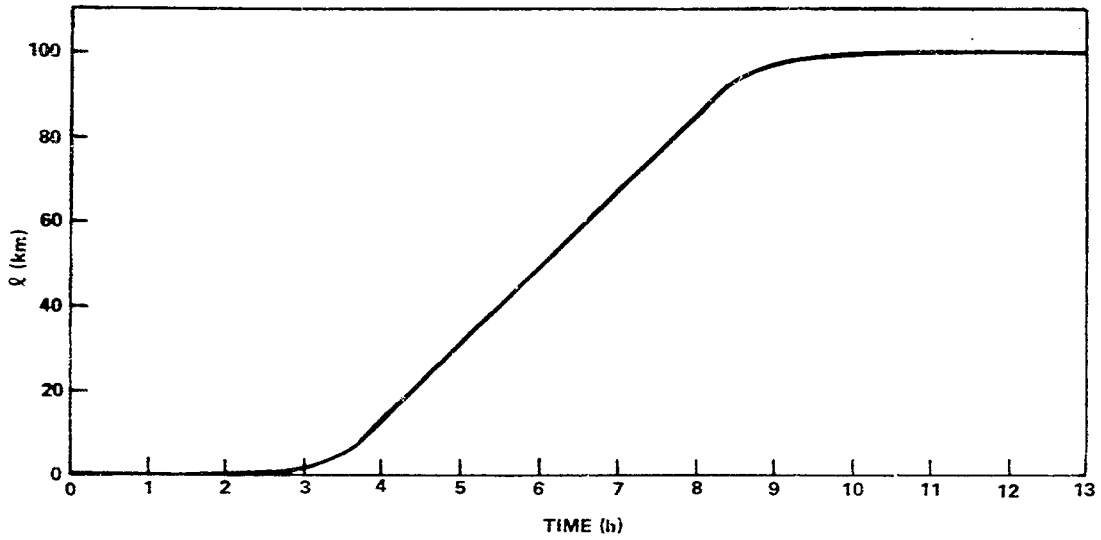

Figure II-4. Exponential deployment law — tether length versus time.

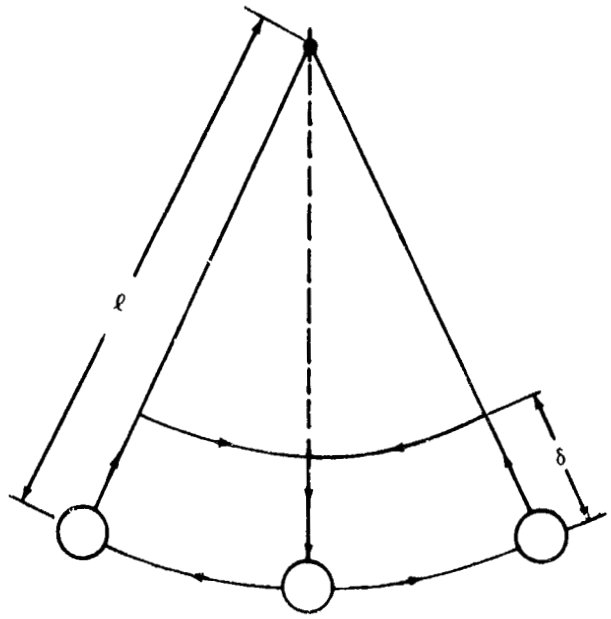

$$\zeta_\theta = \frac{1}{\pi}\left(\frac{\delta}{\ell}\right)$$

Figure II-5. Optimal yo-yo control (out-of-plane motion).

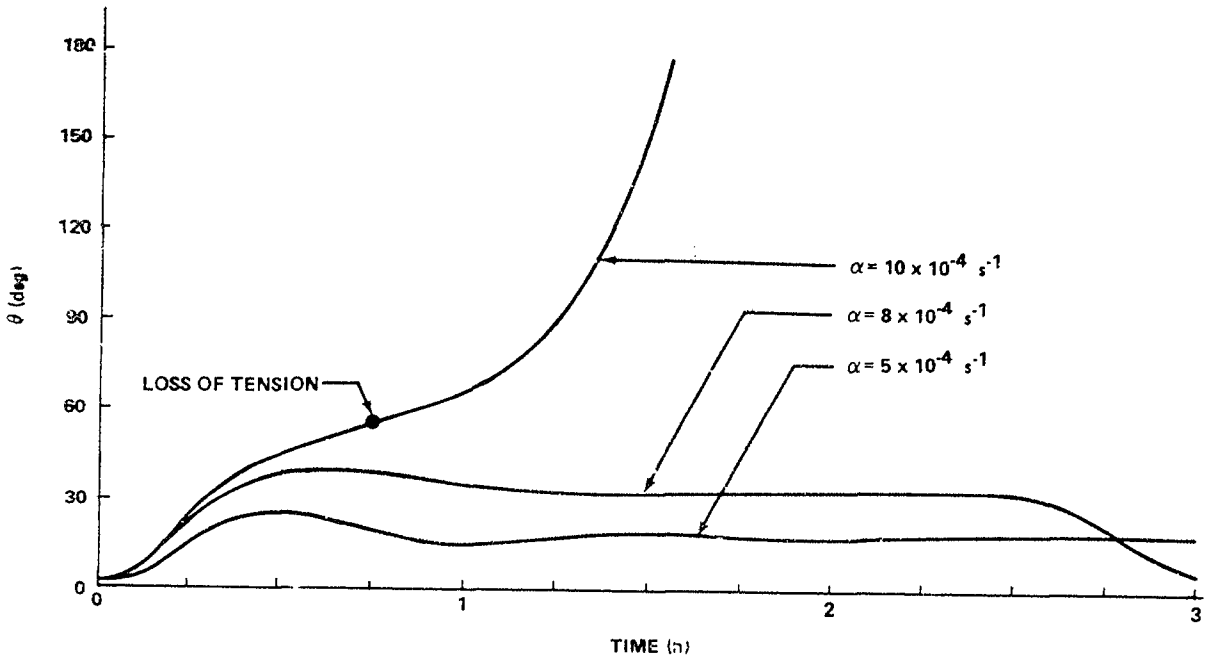

STABILITY CONDITION: $\alpha < 3/4 \left(\frac{M + m/3}{M + m/2} \right) \omega_o$

CRITICAL DEPLOYMENT RATE: $\alpha_c \approx 9.5 \times 10^{-4}\ s^{-1}$

Figure II-6. Deployment dynamic stability behavior.

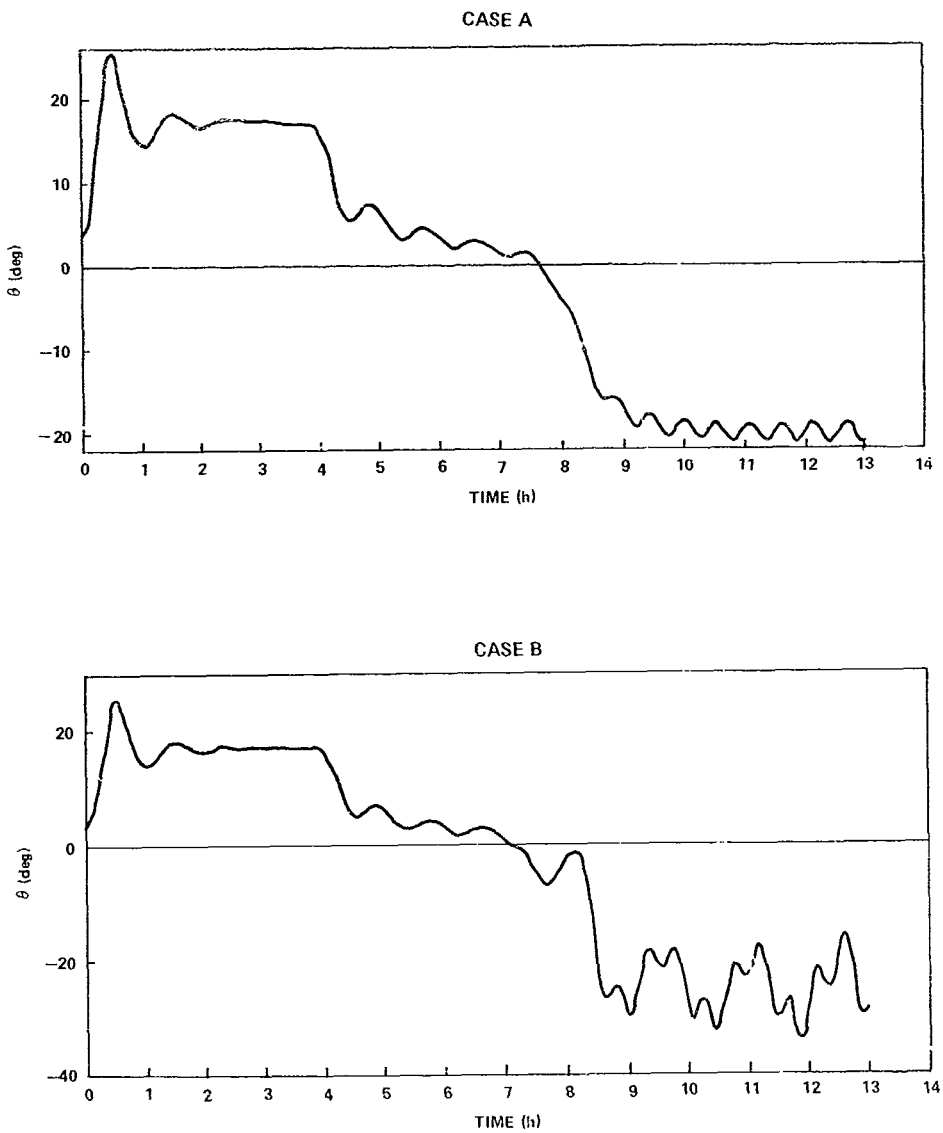

Figure II-7. Pitch angle versus time — equatorial orbit.

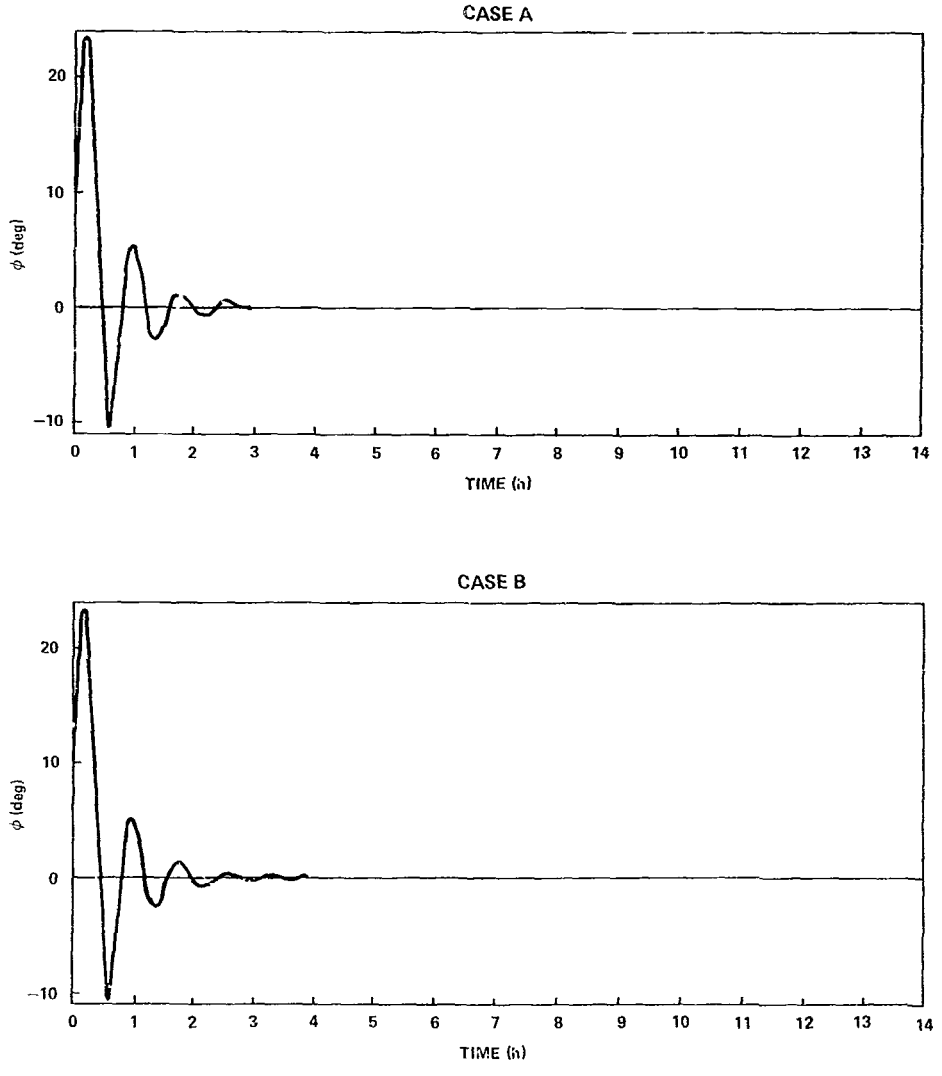

Figure II-8. Roll angle versus time — equatorial orbit.

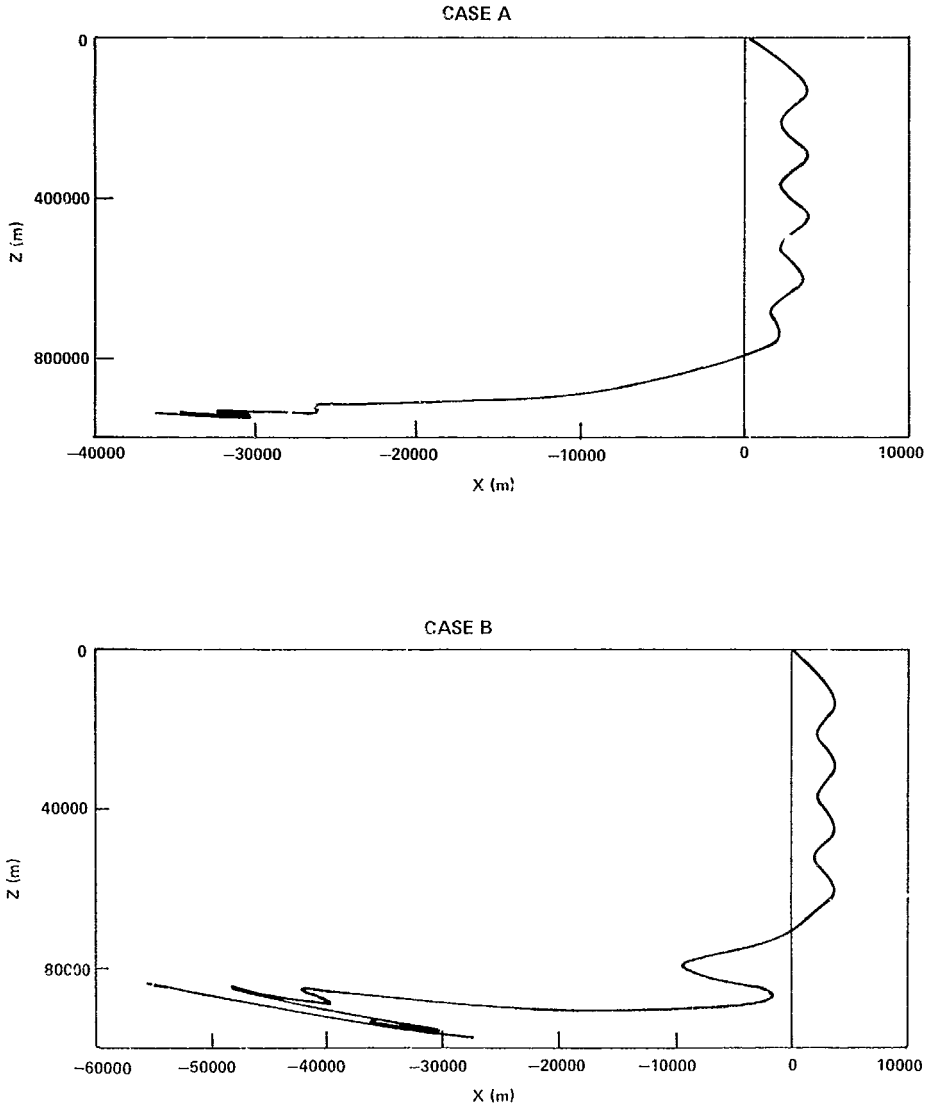

Figure II-9. In-plane motion (x-z plot) — equatorial orbit.

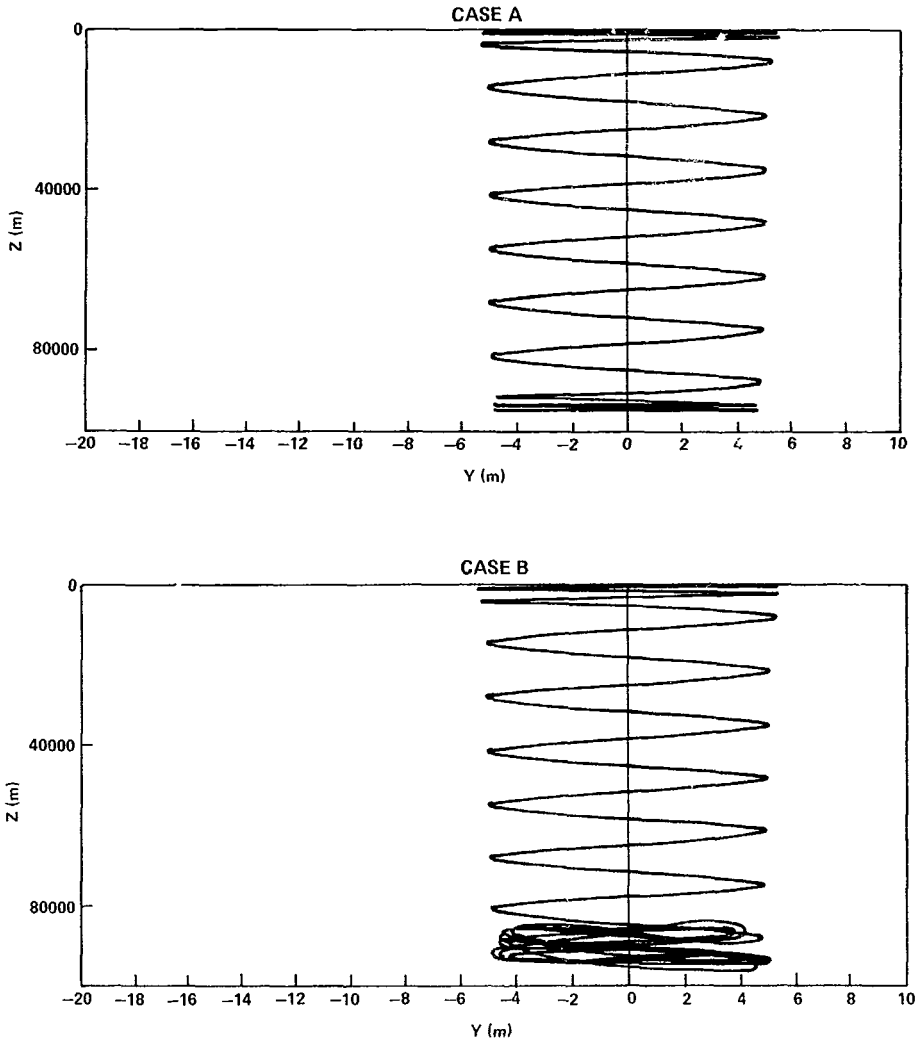

Figure II-10. Out-of-plane motion (y-z plot) — equatorial orbit.

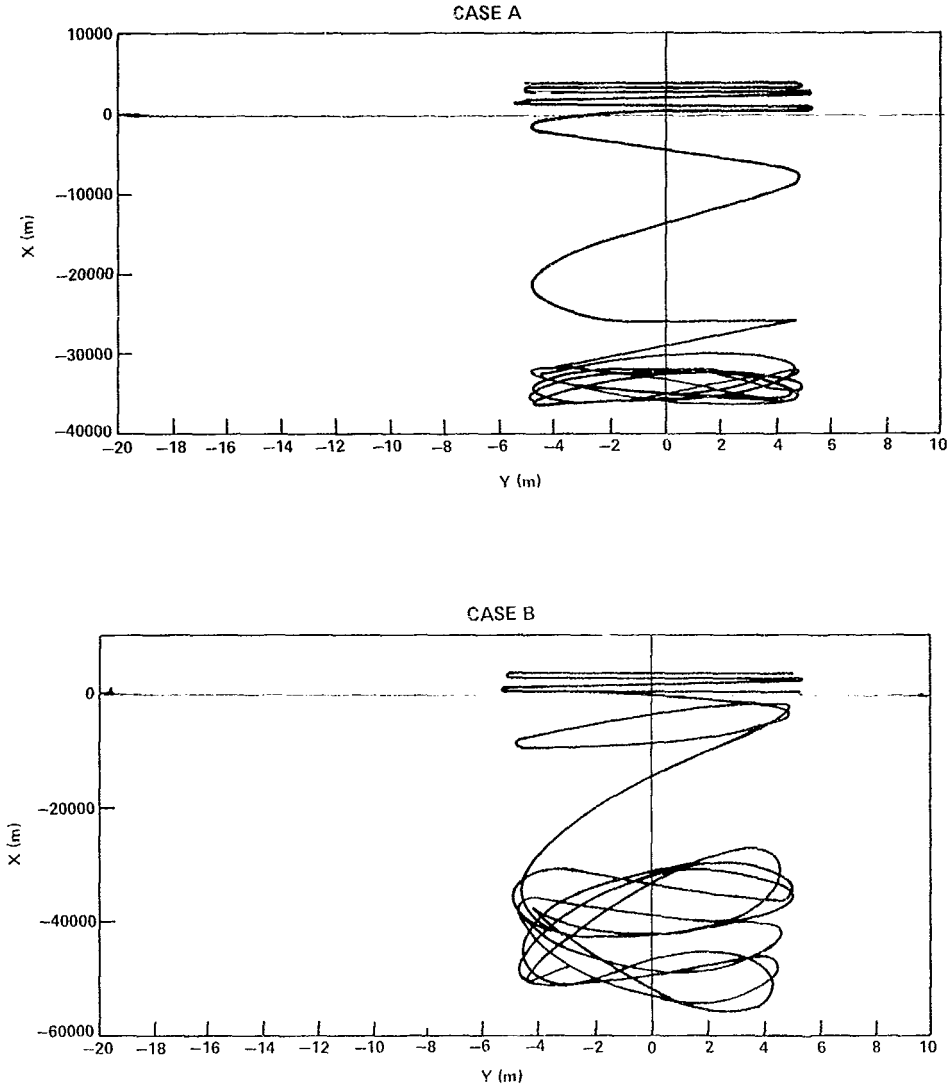

Figure II-11. Equatorial motion (x-y plot) — equatorial orbit.

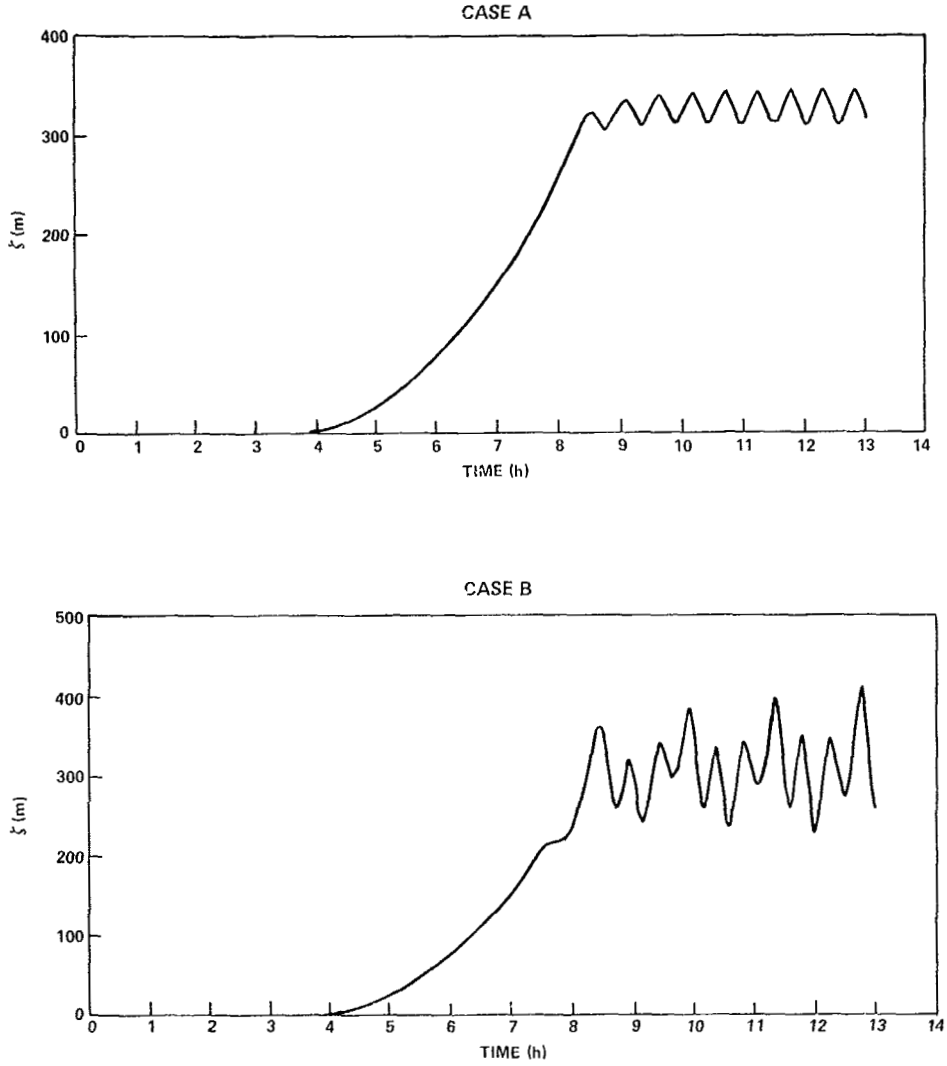

Figure II-12. Tether elongation versus time — equatorial orbit.

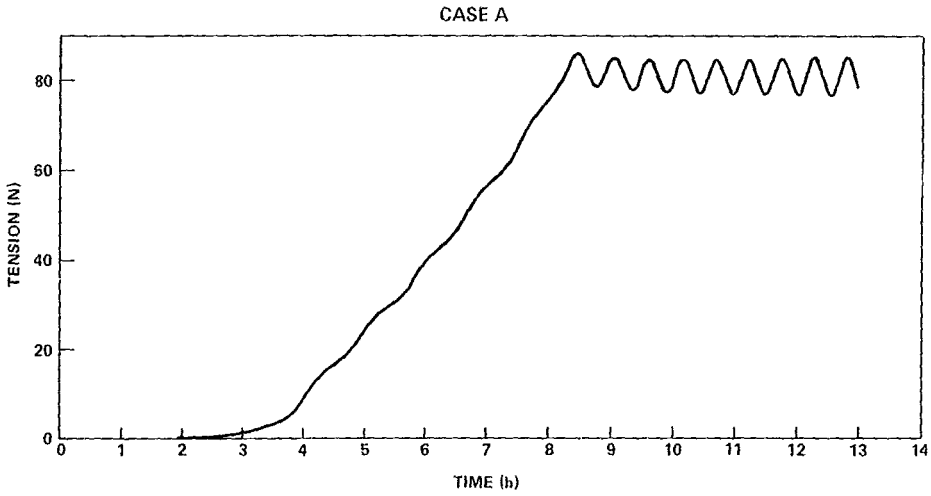

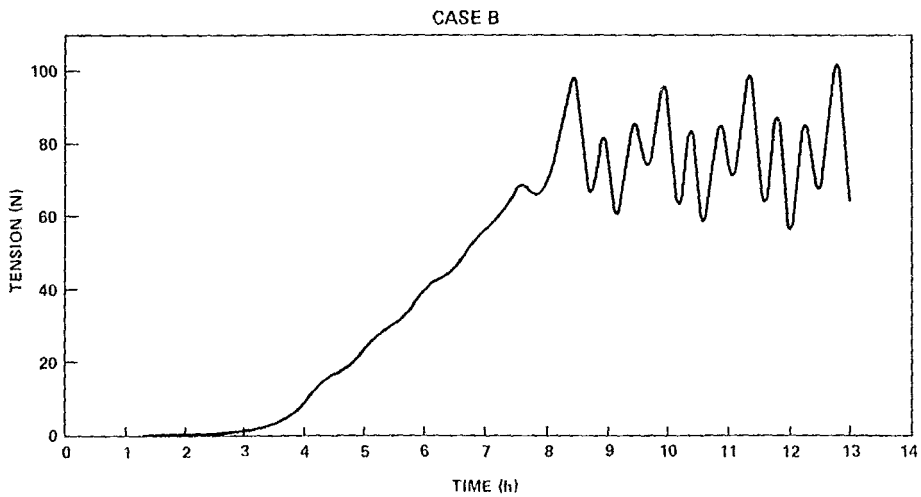

Figure II-13. Tether tension versus time — equatorial orbit.

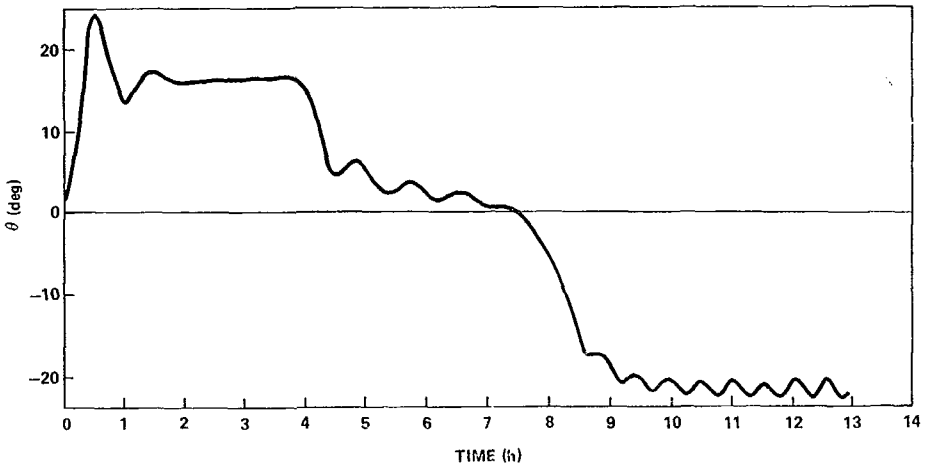

CASE B

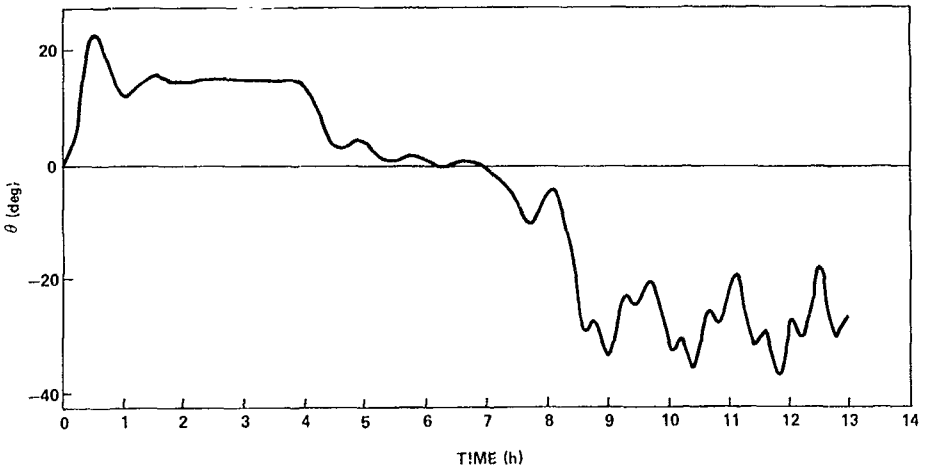

Figure II-14. Pitch angle versus time — polar orbit.

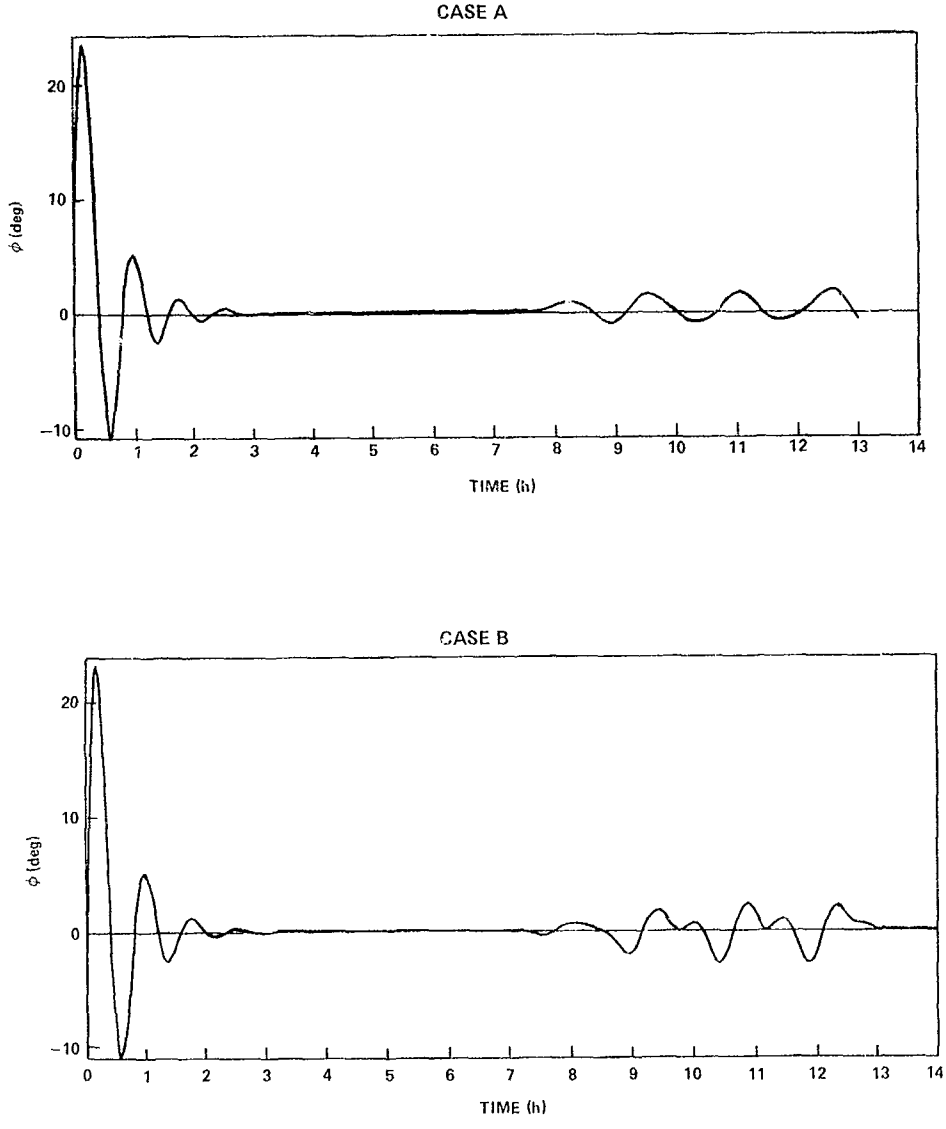

Figure II-15. Roll angle versus time — polar orbit.

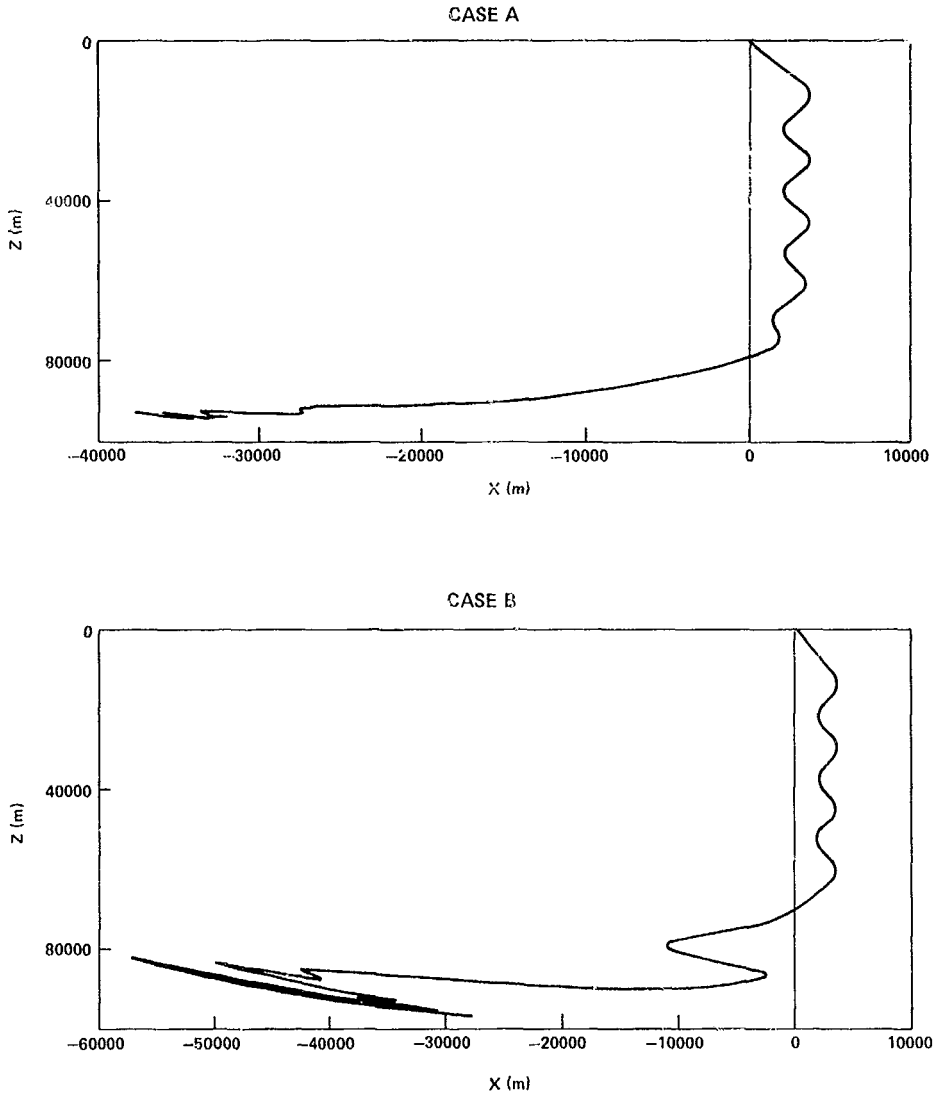

Figure II-16. In-plane motion (x-z plot) — polar orbit.

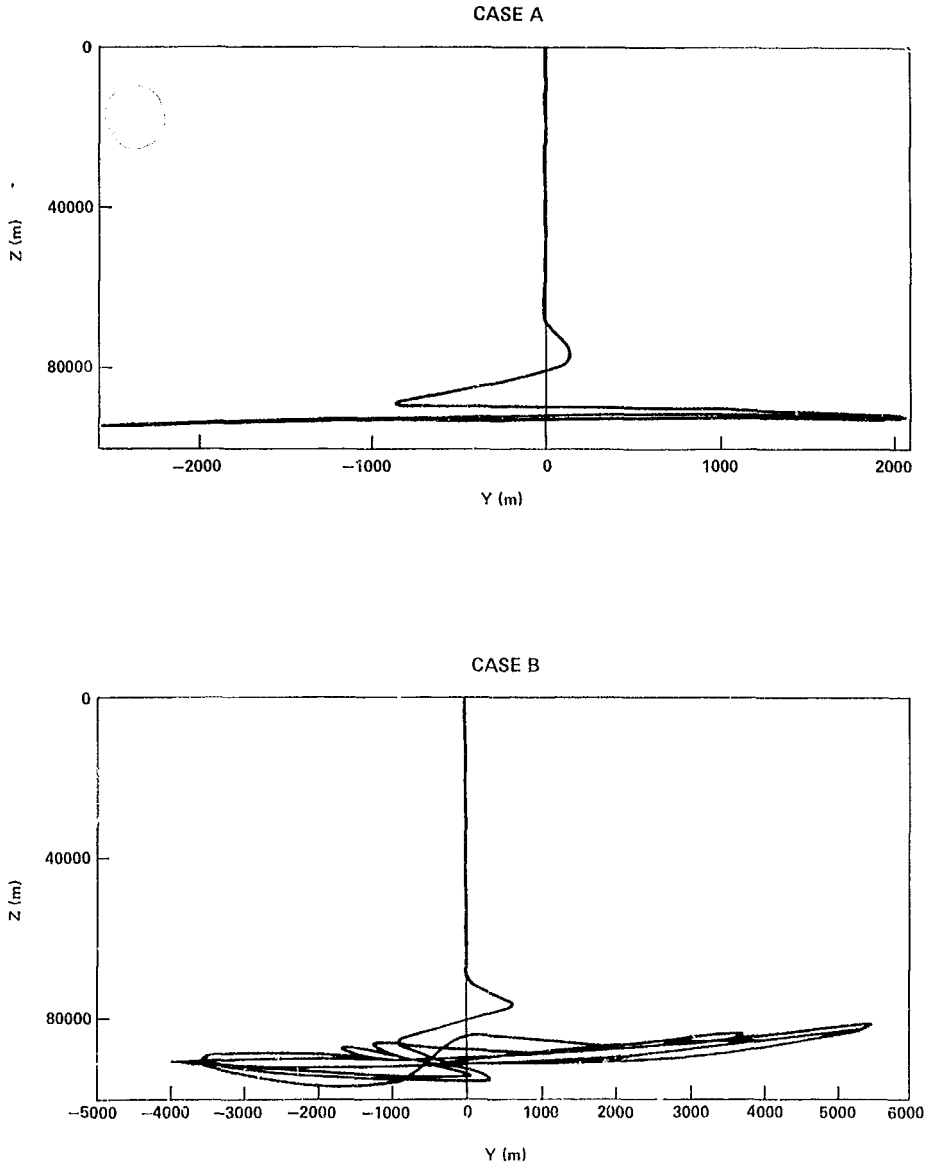

Figure II-17. Out-of-plane motion (y-z plot) — polar orbit.

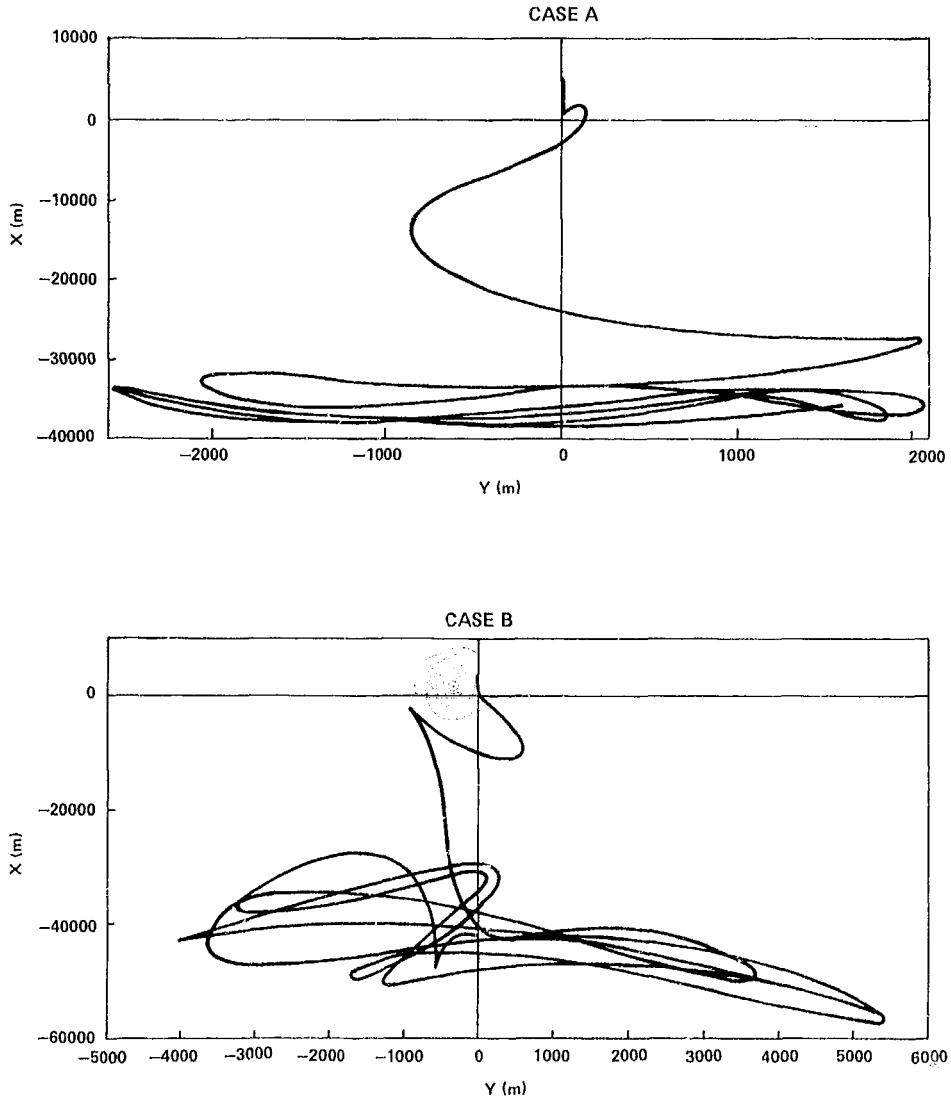

Figure II-18. Equatorial motion (x-y plot) — polar orbit.

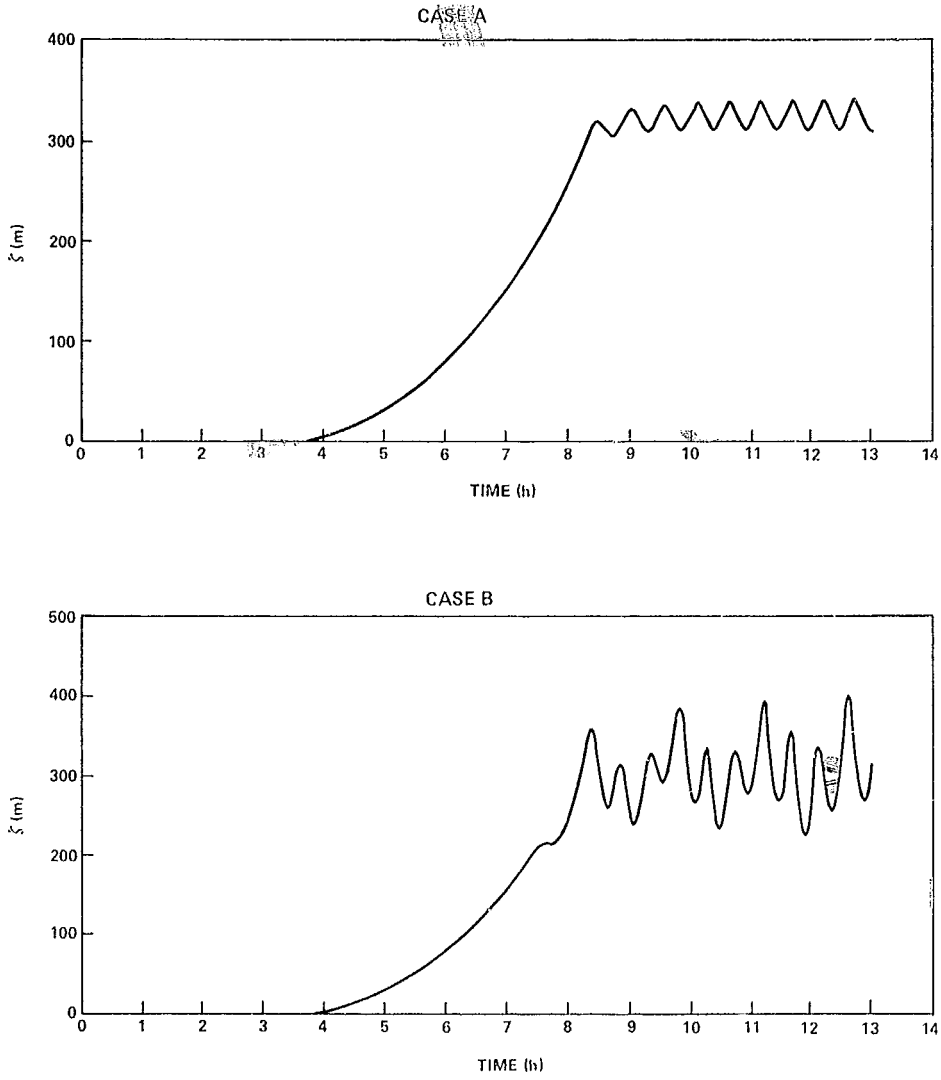

Figure II-19. Tether elongation versus time — polar orbit.

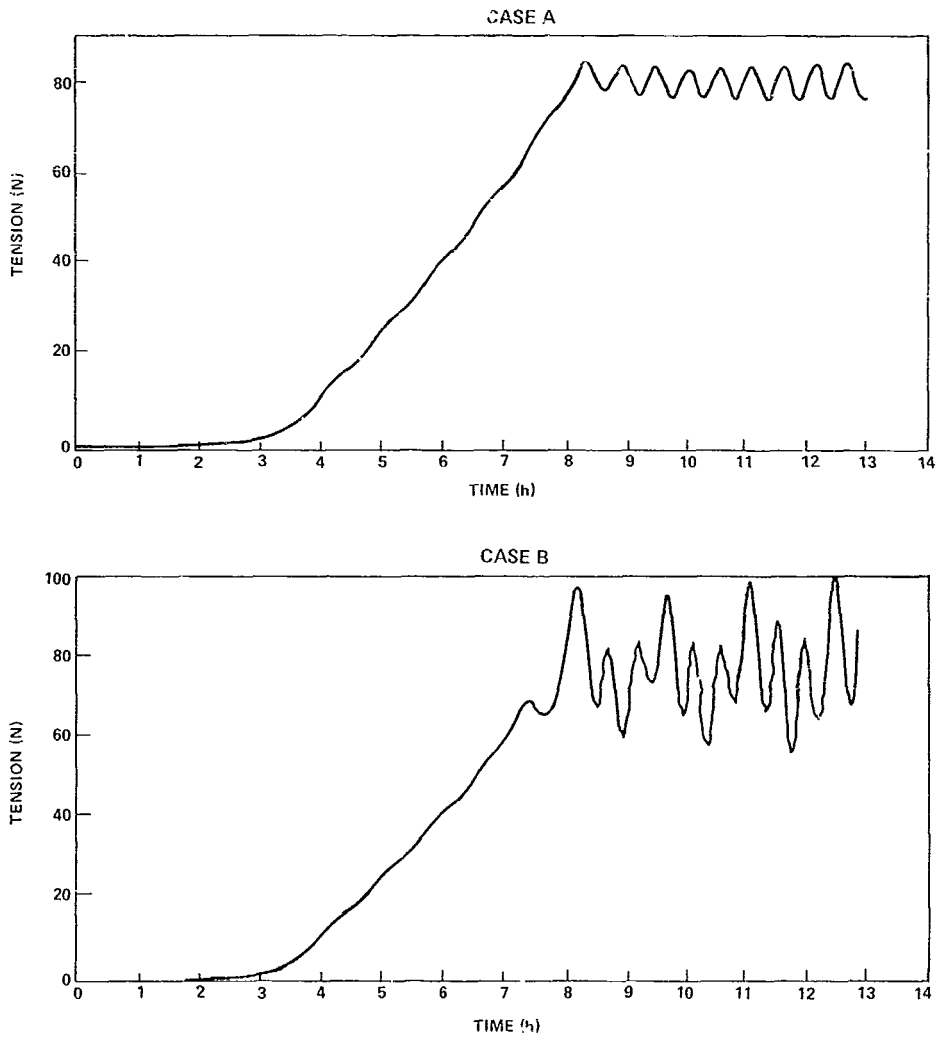

Figure II-20. Tether tension versus time — polar orbit.

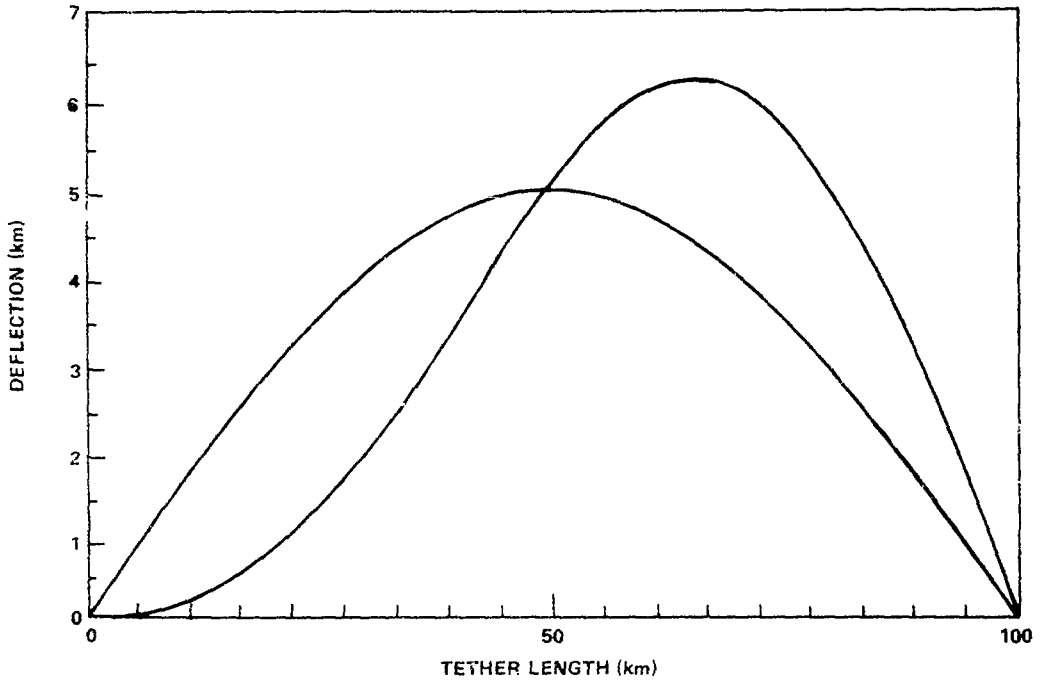

Figure II-21. Steady state modal deflections — 1 and 2 modes.

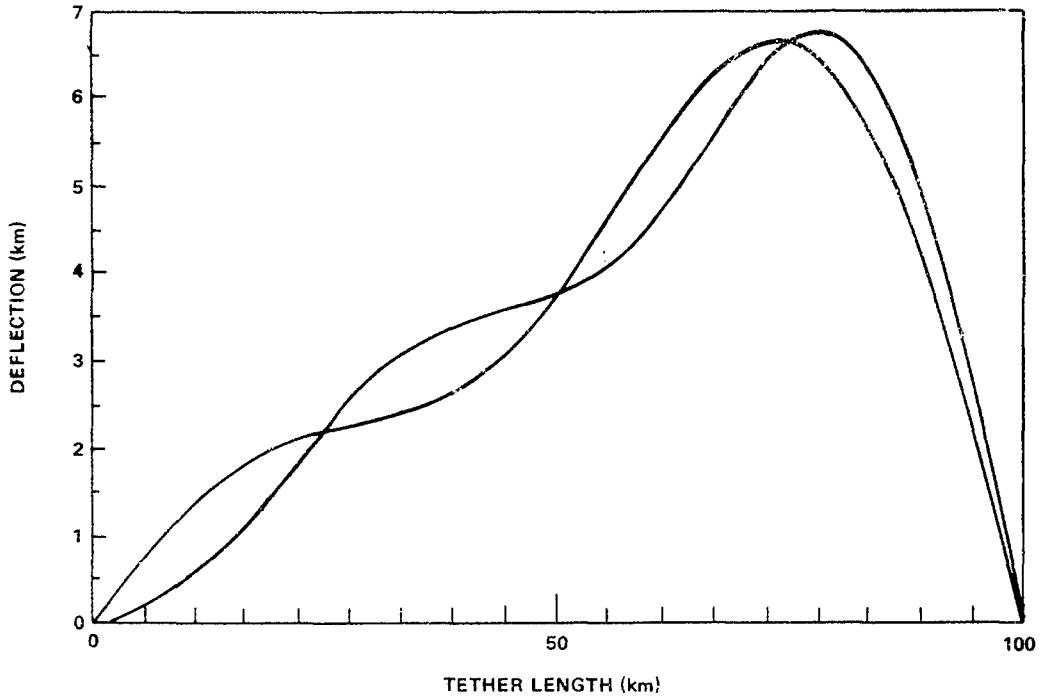

Figure II-22. Steady state modal deflections — 3 and 4 modes.

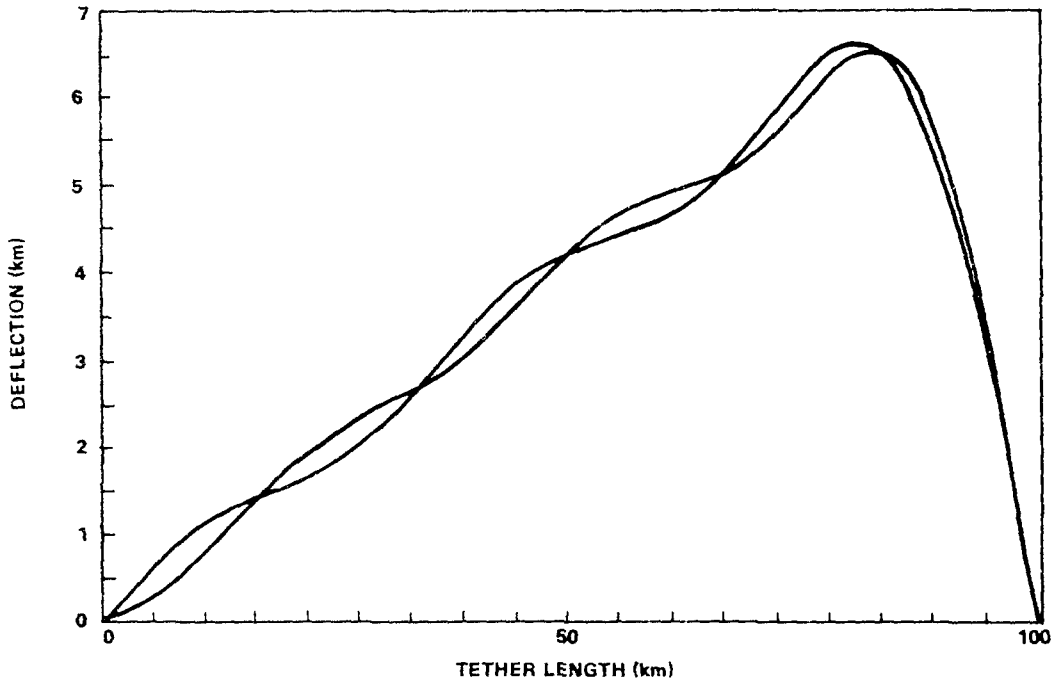

Figure II-23. Steady state modal deflections — 5 and 6 modes.

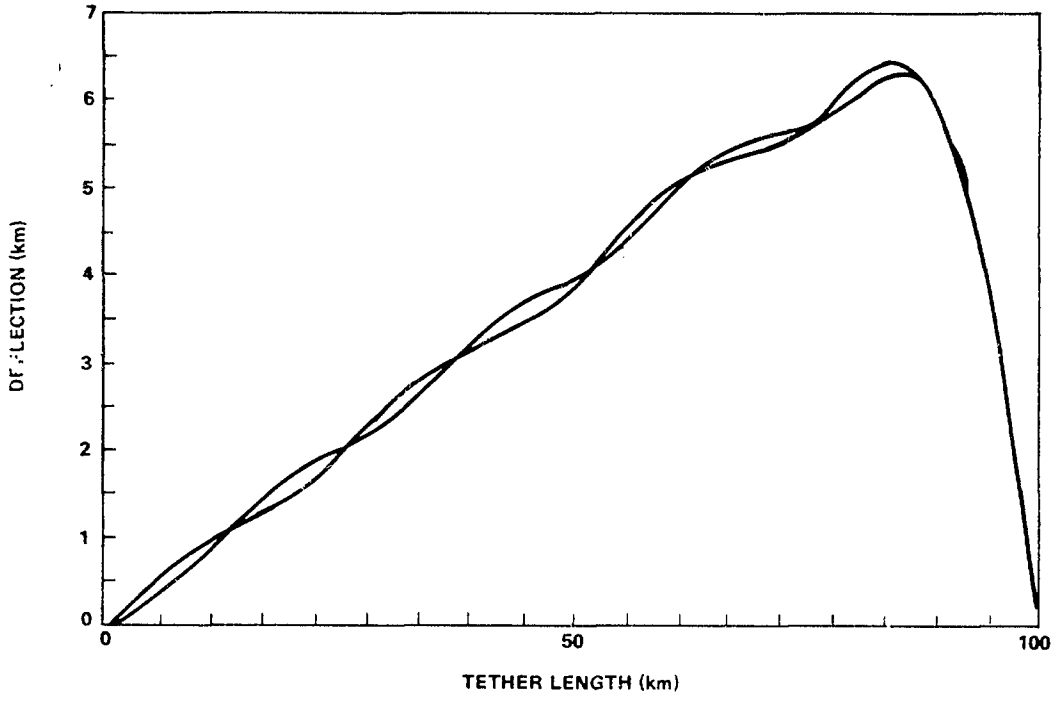

Figure II-24. Steady state modal deflections — 7 and 8 modes.

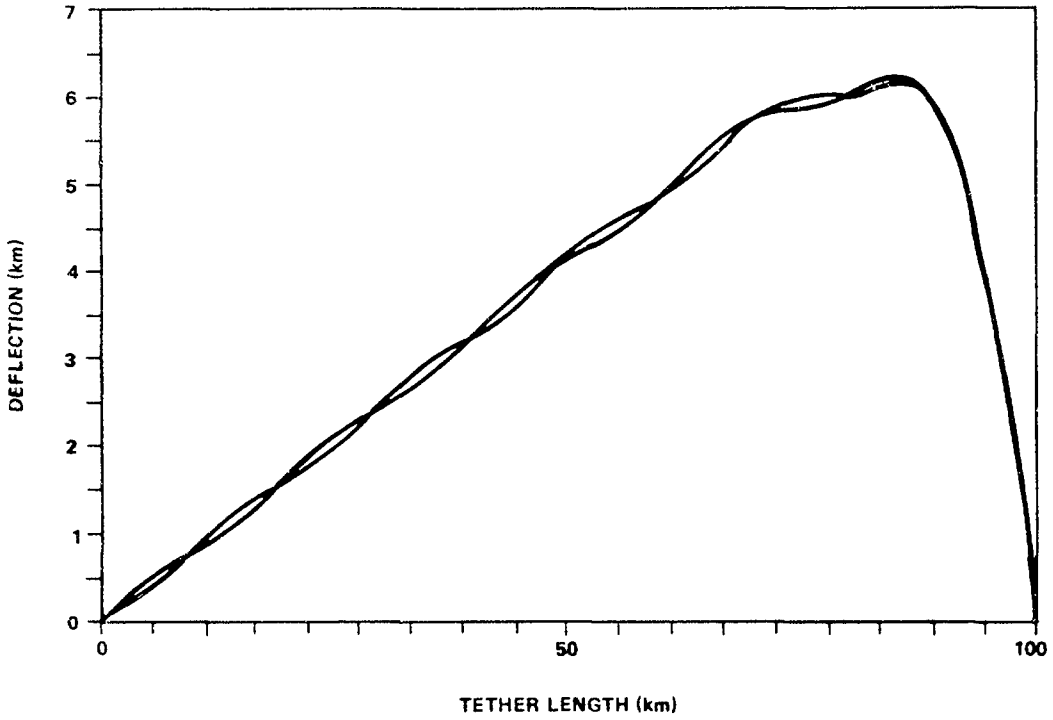

Figure II-25. Steady state modal deflections — 9 and 10 modes.

III. INVESTIGATION OF A TETHERED SUBSATELLITE CONTROL LAW

Ralph R. Kissel

A. Summary

A control law is presented which uses tension in the line, line velocity, and length to deploy and retrieve a subsatellite up to 100 km above or below the Shuttle or other space vehicle. The equations of motion used here are three-dimensional but include only the mass of the line and no other factors, i.e., tether dynamics, atmospheric forces, elliptical orbits, etc. These additional factors are covered in detail by M. Rheinfurth in Section II.

The results show that the subsatellite can be deployed in a stable manner in a few hours and can be retrieved in a stable manner if enough time is available. Approximately 19 h is the minimum time required for retrieval to 5 m from 100 km.

The subsatellite can be positioned to any distance from any other distance and stabilized at the new position in a few hours (107 up to 120 ± 0.5 km altitude required 1.5 h).

Feasibility of this technique will be governed by mechanical design limitations and time allowed to stabilize at a new position.

B. Introduction

Until the work presented in this report was done, no continuous control law was available to deploy, retrieve, or position a subsatellite suspended by a tether up to 100 km long. This law is an extension of one developed by C. Rupp and used by AMA in their work. The extension involves making the commanded length in that original control law a function of the actual length rather than an arbitrary set of commands. The particular function chosen is determined by the desired line velocity, position, damping, and retrieval time.

C. Method

The dynamic equations used here were derived by M. Rheinfurth and are presented elsewhere in this publication. The control law developed by Rupp is

$$\tau = 7\omega_0^2 \ell + 4\omega_0 \dot{\ell} - 4\omega_0^2 \ell_c \qquad \text{(III-1)}$$

where

ω_0 = orbital rate

ℓ = tether length

ℓ_c = is commanded length

τ = commanded tether acceleration.

The tension in the tether (at Shuttle) is given by

$$T = \tau\left(M_{sat} + \frac{M_{wire}}{2}\right) \qquad \text{(III-2)}$$

where M_{sat} is the subsatellite mass and M_{wire} is the mass of wire of length ℓ. For purposes of optimizing the tension, the control law was expanded to

$$\tau = (R^2 + 3)\,\omega_0^2 \ell + 2\zeta_c R\omega_0 \dot{\ell} - R^2\omega_0^2 \ell_c \qquad \text{(III-3)}$$

where R is the ω_c / ω_0, ω_c is the control law "stretch" frequency, and ζ_c is the control law damping.

The control law extension developed here sets

$$\ell_c = K_1\ell + K_3 \qquad \text{(III-4)}$$

where K_1 is chosen for performance and K_3 is chosen for the desired deployment velocity.

The idea for this extension was based on the old "carrot-and-stick" idea, i.e., command a length always ahead of the present length by an amount which will give the desired trajectory.

The values used for K_1 and K_3 are different for retrieval and deployment. During deployment, three sets of values are used depending on the relationship of the current length to either the phase 1-2 mode change length or the final length. During the initial phase, K_1 is given a value greater than one while K_3 is set to zero. The value of K_1 for this phase is chosen to minimize the time to the desired velocity. When the desired velocity is reached, the second phase begins and continues until the terminal phase begins. During the second phase, K_1 is set to one and K_3 is chosen to maintain the desired velocity. A smooth transition from the initial phase to the second phase requires that

$$K_3(\text{phase 2}) = L[K_1(\text{phase 1}) - 1] \qquad \text{(III-5)}$$

where L is the length for changing from phase one to phase two. The terminal phase has $K_1 = 0$ and K_3 equal to the desired final length. The terminal phase begins when the actual length is within K_3 (phase 2) units of the final length.

Retrieval works best when $K_3 = 0$ and $K_1 < 1$ for the entire retrieval time. If K_1 is too low, the subsatellite will go by the Shuttle; if K_1 approaches one then too much time is required to retrieve.

Other parameters which can be optimized together with K_1 and K_3 are ω_c and ζ_c. The ω_c and ζ_c are chosen primarily to minimize out-of-plane motion during retrieval. An ω_c of four ω_0 is theoretically optimum for best damping of out-of-plane motion.

Station keeping is dependent on ω_c and ζ_c, but not on K_1. The values for ω_c and ζ_c will need to be chosen based on desired response and may be different from values used during retrieval. The value for K_3 is similar to that used during the third phase of deployment, i.e., it is the desired length.

Implementing this control law may best be accomplished by a combination of digital and analog techniques. Equation (III-1) can probably best be implemented using analog techniques while the choosing of K_1 and K_3 appears simplest by digital methods.

Mechanizing the entire system has several difficulties, most of which must still be fully resolved. These will be briefly discussed in the conclusions.

All the simulations for this report were done on a desk-top HP-9830 calculator. All programs were either written especially for this problem or were adapted from an earlier project involving similar requirements.

D. Results

Figures III-1 through III-6 are illustrations of what could be expected. Obviously, a large number of simulations could be done depending on the control desired and the mission to be accomplished. Once these are specified a particular optimum solution could be worked out.

Table III-1 shows the parameter values used for the simulations in this report. Also used were

$$M_{sat} = 170 \text{ kg}$$

$$M_{wire} = 83 \text{ kg (100 km)}$$

$$\omega_c = 2\,\omega_0$$

$$\zeta_c = 1$$

with coordinates as defined in the list of symbols.

TABLE III-1. INITIAL CONDITIONS AND CONTROL VALUES

Units	m	m/s	deg	deg/s	deg	deg/s	None	m
Name	ℓ_0	$\dot{\ell}_0$	θ_0	$\dot{\theta}_0$	ψ_0	$\dot{\psi}_0$	K_1	K_3
Deploy	10	0.5	0	0	0	0	2	7 000
Retrieve	100 000	0	20	0	10	0	0.93	0
Station Keeping	100 000	0	20	0	10	0	0	100 000

Figure III-1 shows a side view of the deployment and retrieval trajectories. Deployment is smooth and relatively fast, with average tether velocity being purposely limited to approximately 8 m/s. This limit was deemed consistent with reel capability in steady state. The resultant time was 6.7 h to stabilize at ℓ = 100 km (atmosphere not considered). Setting the subsatellite out to 20 m with no initial velocity requires only 15 min more to go to 100 km. There was a 3 km overshoot but a change of parameters during the terminal phase could reduce this to almost any desired value.

Retrieval began with an extreme worst case, i.e., with the subsatellite in front of the Shuttle path and slightly off to the side. Atmosphere would tend to pull the subsatellite behind the path which other simulations show does not cause such a low altitude to be reached as shown here. Different parameters can minimize this effect to almost any point desired although somewhat more time would be required and parameters would need to be changed during retrieval. This particular retrieval required 26 h to reach 5 m below the Shuttle. The effect of out-of-plane motion is seen towards the end of the retrieval by the slight in-plane component.

Figure III-2 shows the same retrieval from the front. The out-of-plane motion is clearly seen. It can also be seen how this motion is damping out as the subsatellite approaches the Shuttle.

Figure III-3 shows the tether tension and velocity throughout deployment; both are relatively smooth. Maximum tension at the Shuttle is approximately 93 N and maximum velocity is approximately 9 m/s.

Figure III-4 shows tether tension and velocity during retrieval. Maximum tension at the Shuttle for this extreme case is about 123 N and maximum velocity is approximately 23 m/s. Velocities vary (plus and minus) and tension and velocity oscillate as a result of the control law trying to dampen the motion.

Table III-2 shows the best retrieval times to a given distance below the Shuttle that can be obtained with this control law.

TABLE III-2. BEST RETRIEVAL TIMES TO ℓ

ℓ (m)	5	10	50	100
t (h)	19.1	18.8	17.2	16.1

These times can be obtained with any ζ_c and ω_c but their choice is limited by the overshoot and maximum line velocity allowed. Times shorter than those in Table III-2 cause the subsatellite to miss the Shuttle.

The last part of retrieval requires precise knowledge of the control law parameters ℓ, $\dot{\ell}$, and τ. Table III-3 shows the resolutions required for automated retrieval to 50 m.

TABLE III-3. RESOLUTIONS FOR AUTOMATED RETRIEVAL TO 50 m

Parameter	Range	Resolution
Length	50 to 102000 m	±5 m
Velocity	-16 to 22 m/s	±0.005 m/s
Tension	0.001 to 130 N	±0.0025 N

Station keeping is illustrated by two very different cases in Figures III-5 and III-6. Figure III-5 uses the parameters given in Table III-1 and on page III-4, and Figure III-6 shows results by changing to $\omega_c = 4\,\omega_0$ and $\zeta_c = 10$. The standard parameters allow the tether length to approach 114 km and after 2 h is within 0.5 km of the desired 100 km length. This case clearly could not be tolerated. Figure III-6 shows the opposite situation in that the line length never exceeded 101 km, and since this length did not occur directly beneath the Shuttle, the subsatellite never even exceeded 100 km below the Shuttle. The actual parameters for station keeping would necessarily be between these two extremes.

Best station keeping values (for best damping) are $\omega_c = 4\,\omega_0$ and $\zeta_c = 0.5$. Approximately 8 h are needed to cut the out-of-plane amplitude in half after an initial disturbance. Velocity and tension are similar to that experienced during the initial part of retrieval.

Figure III-7 shows a possible analog diagram of the reel control system. The control law produces the desired torque and this is compared with the torque actually existing, measured in this case at the motor, to produce the error signal.

Figure III-8 shows the digital logic needed to implement the selection of K_1 and K_3 for each phase of the trajectory. The desired length is compared with the last commanded length and the current length to make the proper selection. Also needed is the predetermined value for changing from phase one to phase two in deployment.

Figure III-9 shows more detail on an actual mechanization. The torque motor uses tachometer feedback for stabilization. The length and velocity of the tether are measured by a pulley kept in frictional contact with the tether. The tension is measured by a spring damper arrangement on this same pulley. These signals are fed to the processor to produce a torque command.

Other ideas have been put forward as possible ways to deploy, retrieve, and control the subsatellite. Initial deployment methods include a spring release system, a gas jet driven system, and a rail or tube guided system. Retrieval ideas include using a boom and hook, a cushioned cone or catcher, or moving the Shuttle down to the subsatellite.

Length measurement could be done using magnetic pulses on the wire, paint, and photo-optics readout, counting turns of the wire reel or counting revolutions of a pulley held against the wire. An eccentric motor gear would give continuous measurement.

Direct position measurements may be possible by radar, laser, strobe light, received power, or measuring tether angle and length relative to the Shuttle. Some of these are discussed in other parts of this publication.

Wire velocity measurement could use the length measurement ideas and get a differential measurement per unit time.

Tension could be measured by the spring system already mentioned or by measuring motor current.

The required motor power has been estimated at approximately 900 W peak to develop about 9 N m at up to 600 rpm. Such a motor weighs approximately 50 N (10 lb). For a full 0.6 m diameter reel weighing about 5800 N (1300 lb) this motor could produce about 0.12 m/s^2 linear acceleration. This is adequate for all control requirements. It would also be adequate for initial deployment if 4 or 5 s is allowed for reel spin up or if a technique is used which does not require high reel acceleration.

E. Conclusions

Deployment and retrieval are theoretically feasible based on these control law studies. There are several potential problem areas, however.

First, the long retrieval time may limit the usefulness of the concept. Some time can be saved by retrieving the subsatellite at some distance from the Shuttle if a method is worked out to do this, such as a long boom or moving the Shuttle.

Second, retrieval measurements just before retrieval occurs require high resolution to guarantee success. A single device to measure tension, length, and velocity to the required resolution over their respective ranges could be difficult to build. However, a scheme to divide the range into two or more parts could reduce this difficulty.

The mechanics of actually deploying and retrieving the subsatellite could be quite involved. The subsatellite must be either given an initial velocity or displaced from the Shuttle for gravity gradient to become effective for further deployment and control; several ideas have been advanced to do this. Retrieval mechanisms must allow for a certain error in both velocity and position at retrieval time. They must also retrieve without damage and with guaranteed success; ideas have also been presented to do this.

Methods of measuring length, velocity, and tension have been advanced, but the merits of each must still be evaluated.

High velocities were usually seen at some time during retrieval, especially if minimum retrieval time was being sought. This places added requirements on the reel control mechanism and cable construction.

The trade-off for the best control law for a given mission must be done whenever the mission is specified. This may require, in the most complicated case, that all control parameters be functions of time. Station keeping, retrieval, and deployment would each have their own parameter set.

Operation above the Shuttle is the same as operation below. Missions being mentioned thus far require a different length and size cable for operation above than below. This could mean another control parameter set, at worst, but at least this would have to be investigated further.

Maximum tether acceleration has been less than 0.1 m/s^2 which is not a problem. However, initial deployment, if an initial velocity is required, could produce a far higher value. It is this high value that sizes the reel control motor if the entire reel must be accelerated; this must be further worked out.

The control law presented here allows freedom to stop and start from any tether length. This simply says that the control law is continuous rather than stepwise or arbitrary. Tension measurement is a requirement for successful retrieval. It is not a necessity for deployment.

Further work should be done to test this control law in the detailed simulation explained elsewhere in this publication. Also a hardware simulation could be of considerable value once a specific mission is defined.

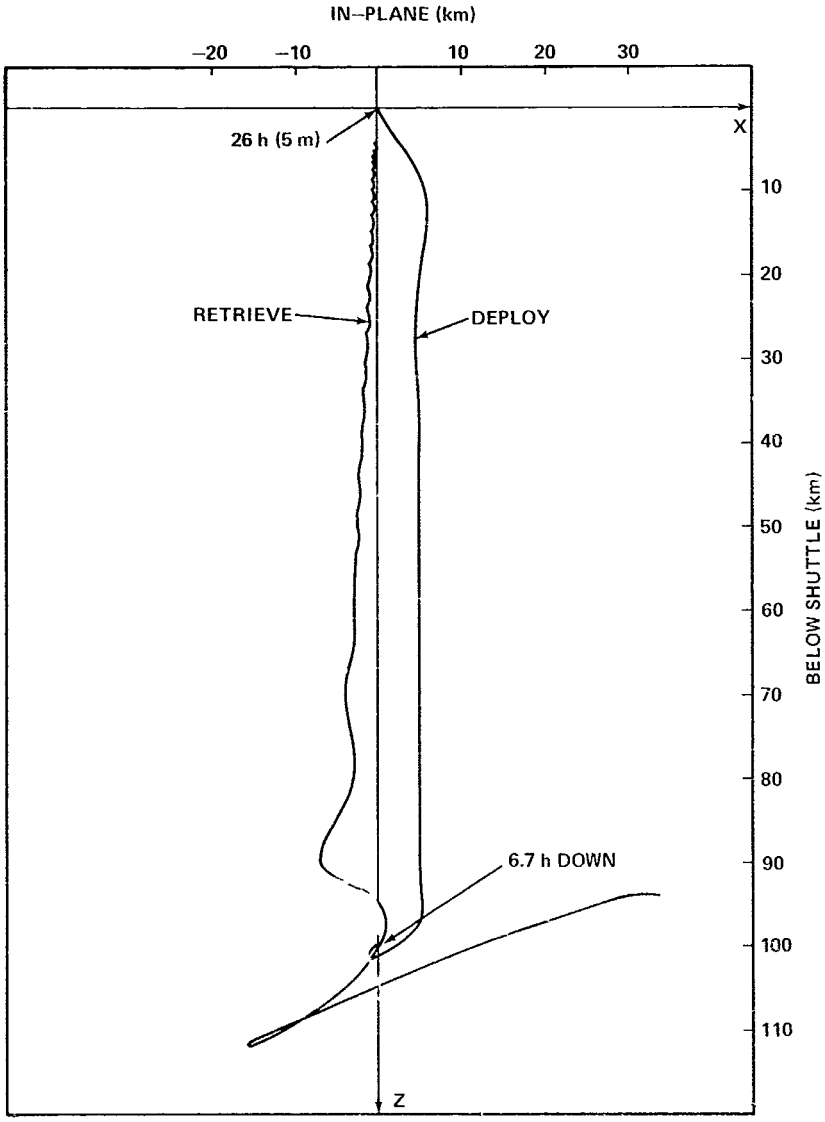

Figure III-1. Deployment and retrieval side view.

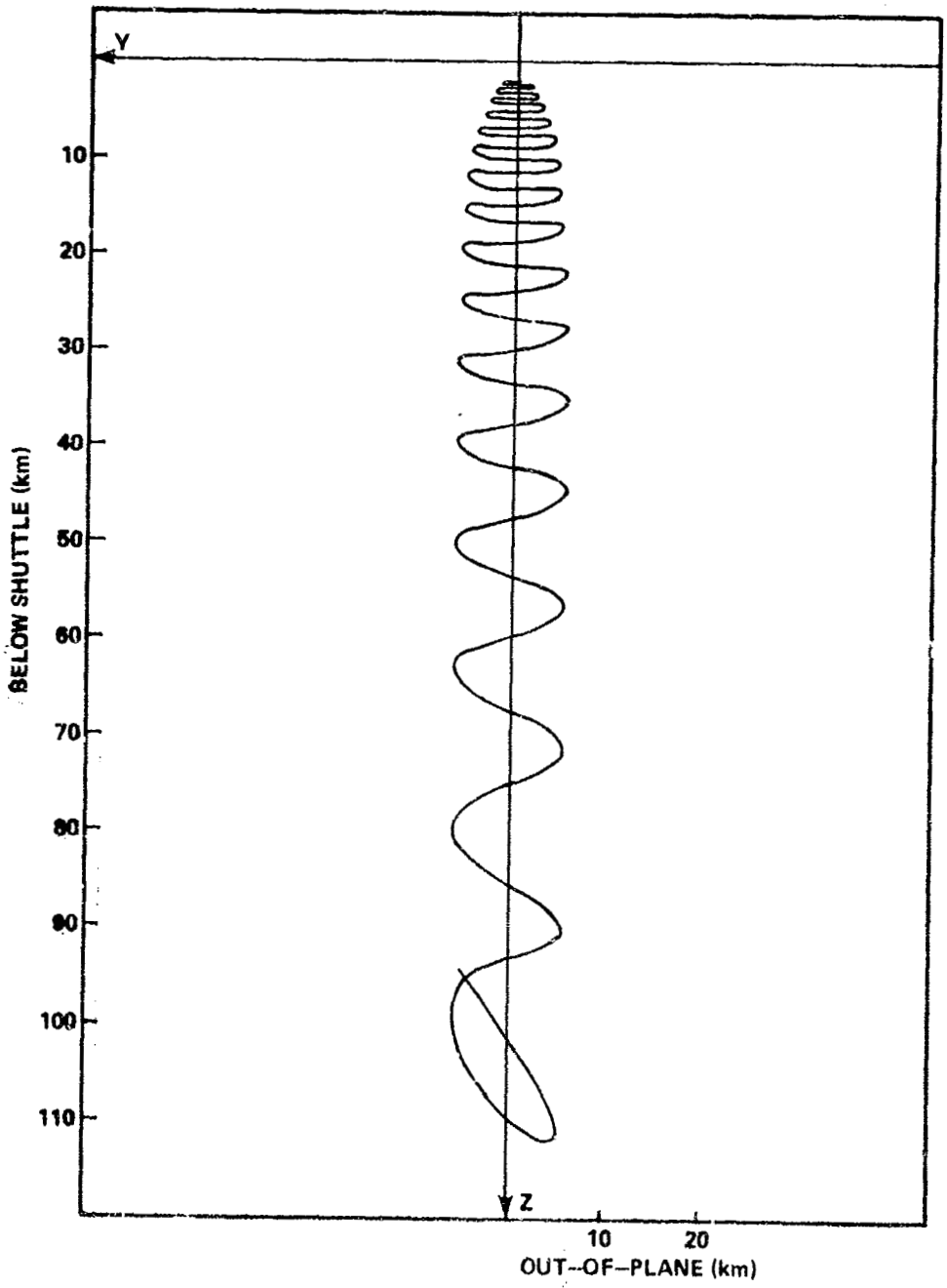

Figure III-2. Retrieval front view.

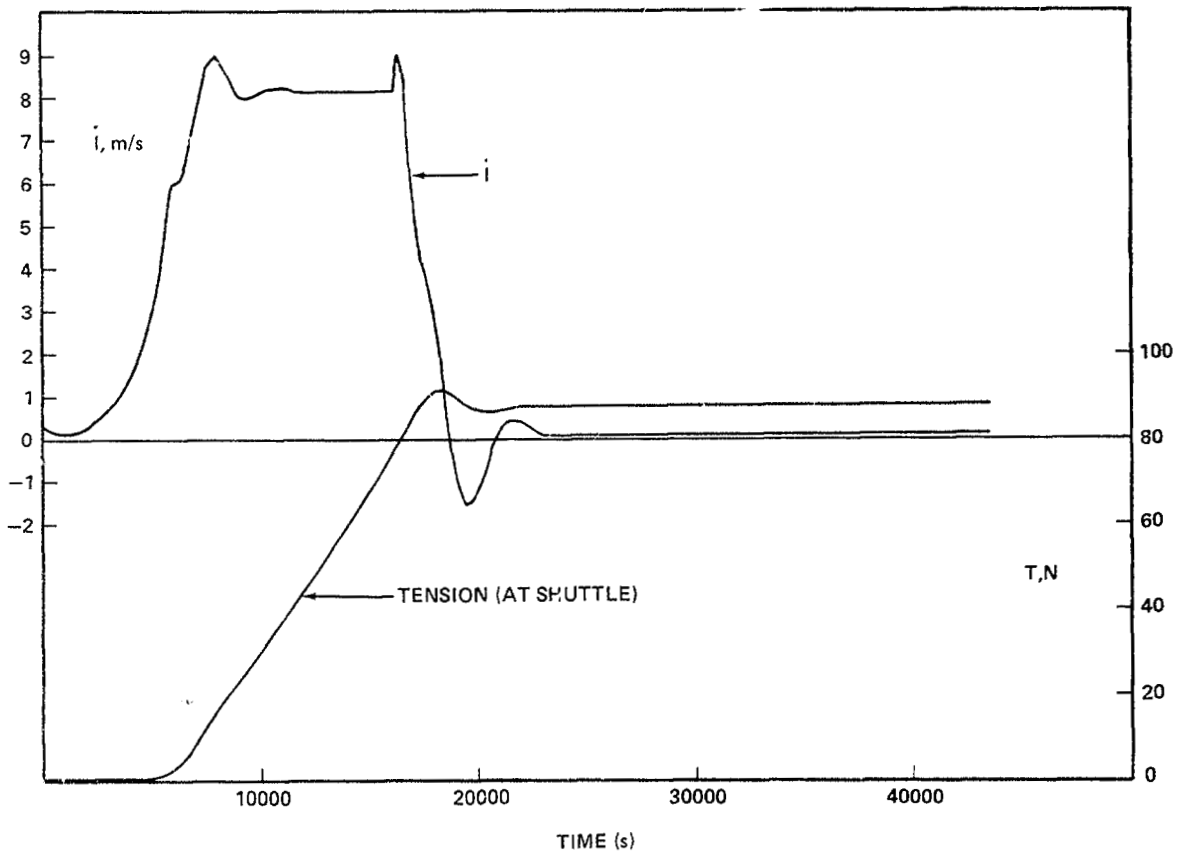

Figure III-3. Deployment (to 100 km).

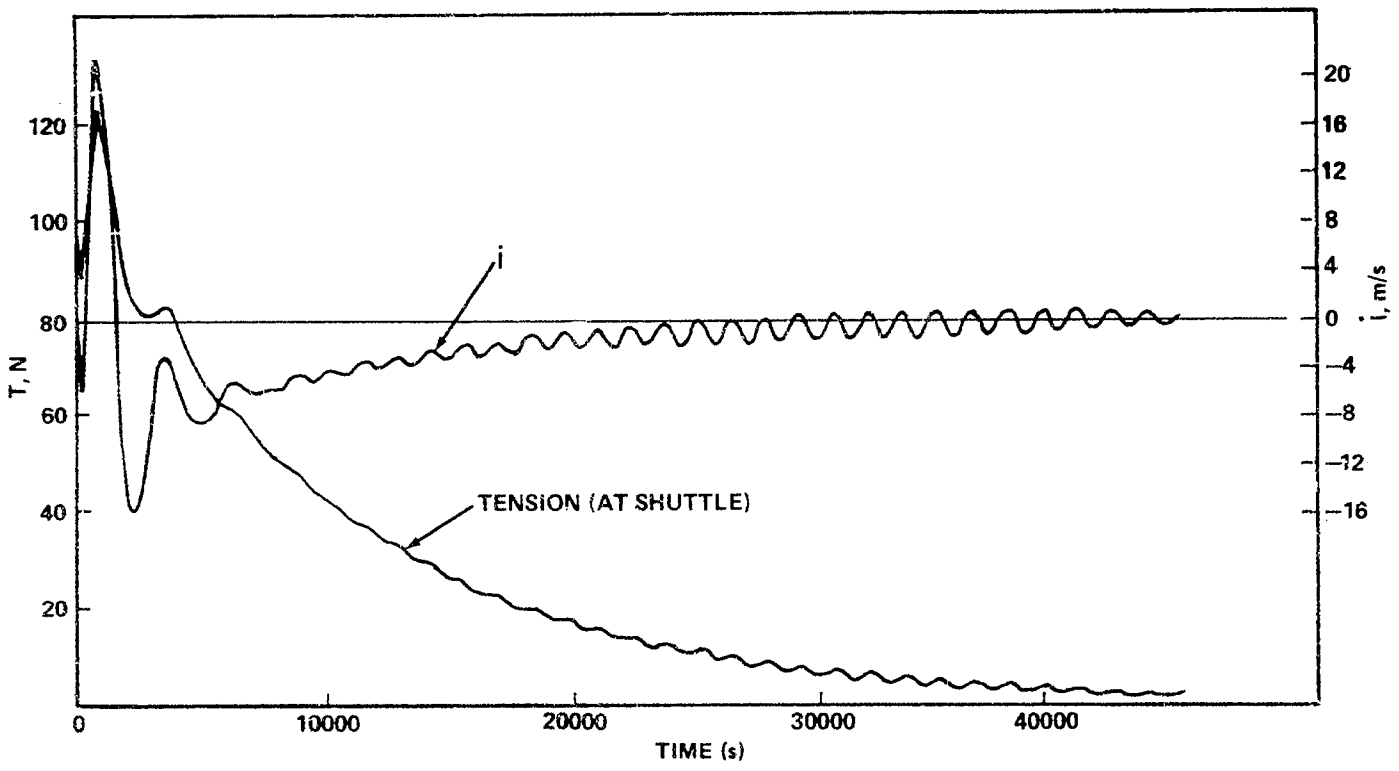

Figure III-4. Retrieval (from 100 km).

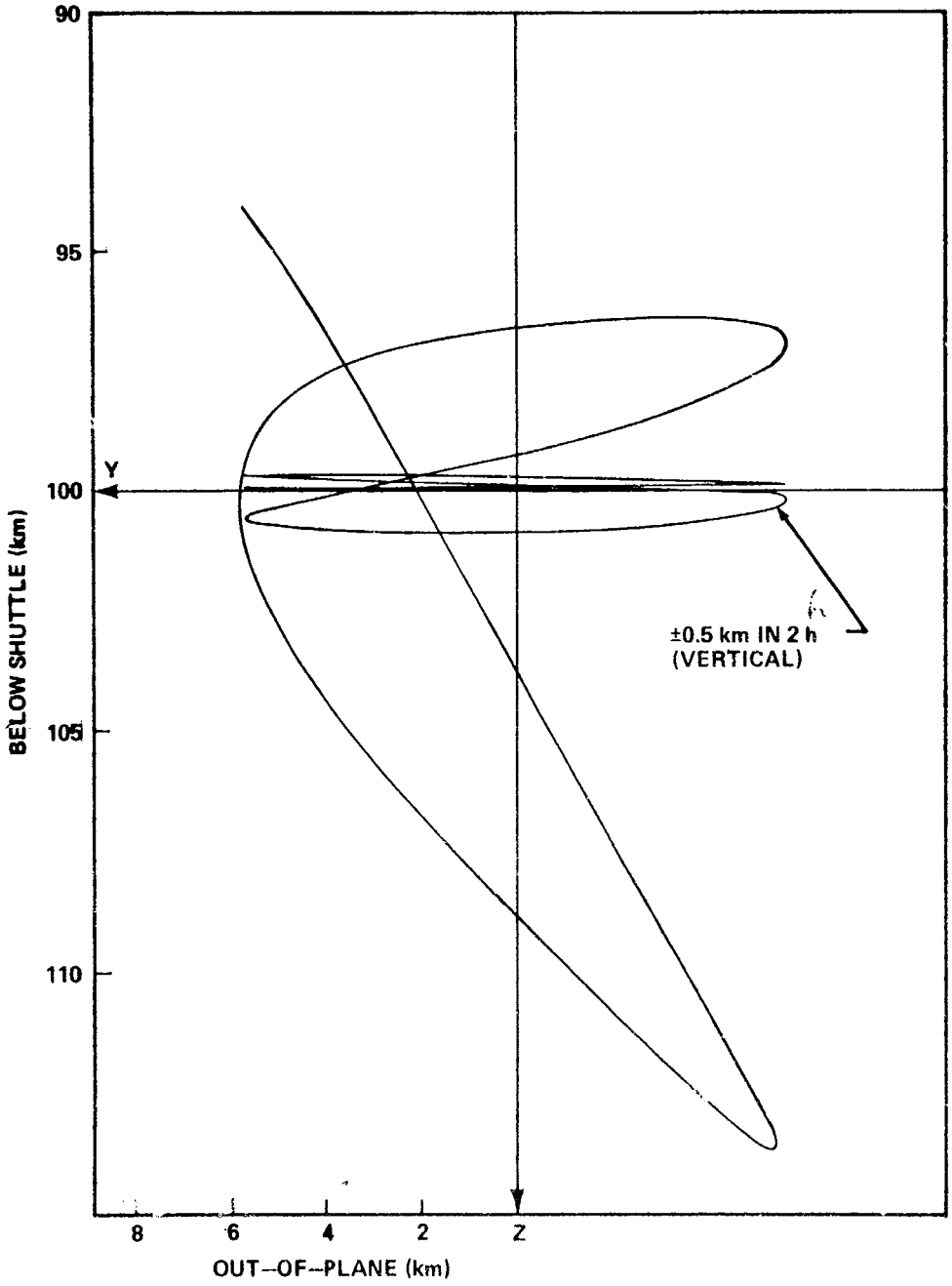

Figure III-5. Station keeping front view.

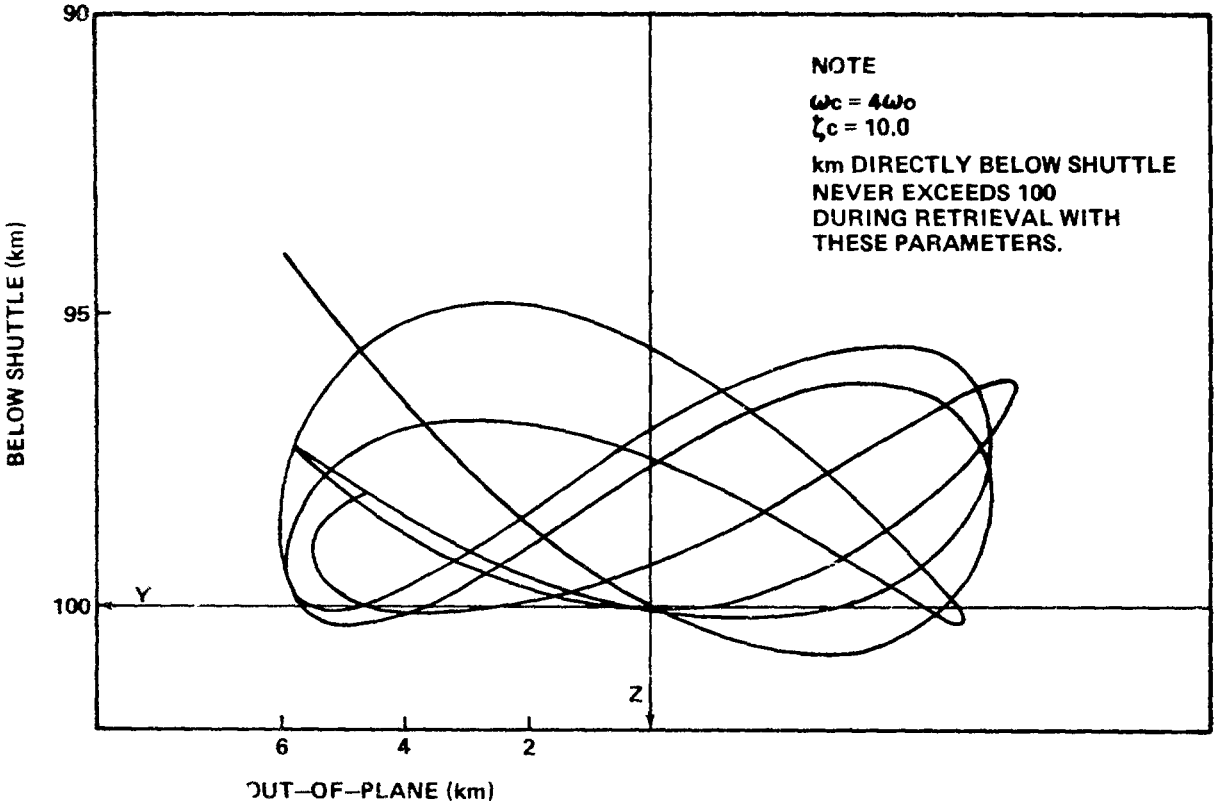

Figure III-6. Station keeping front view.

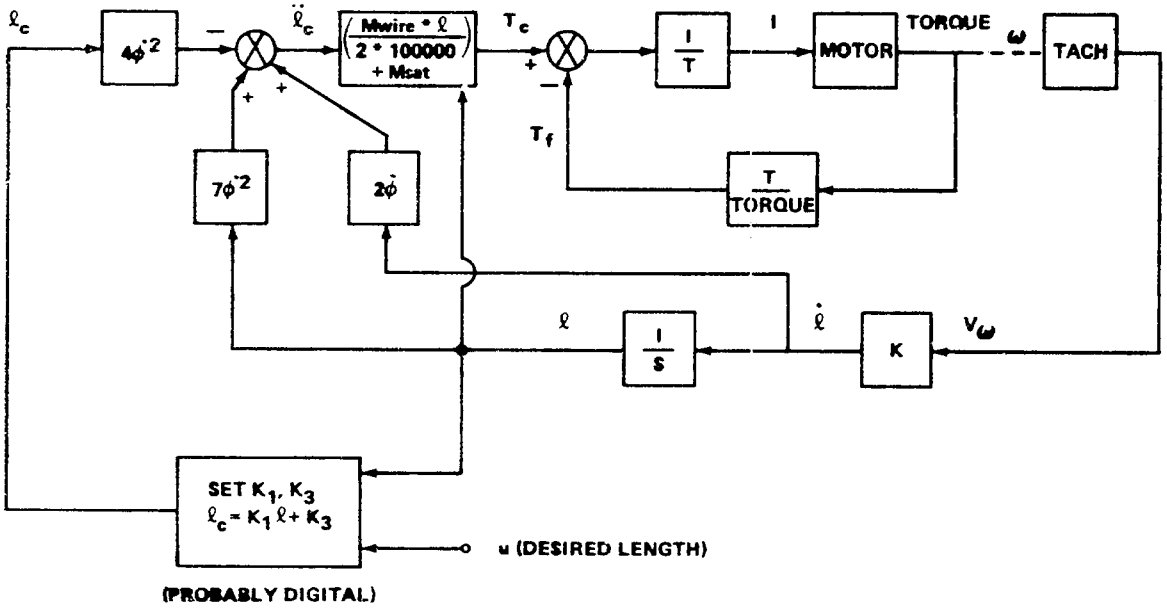

Figure III-7. Reel control system block diagram.

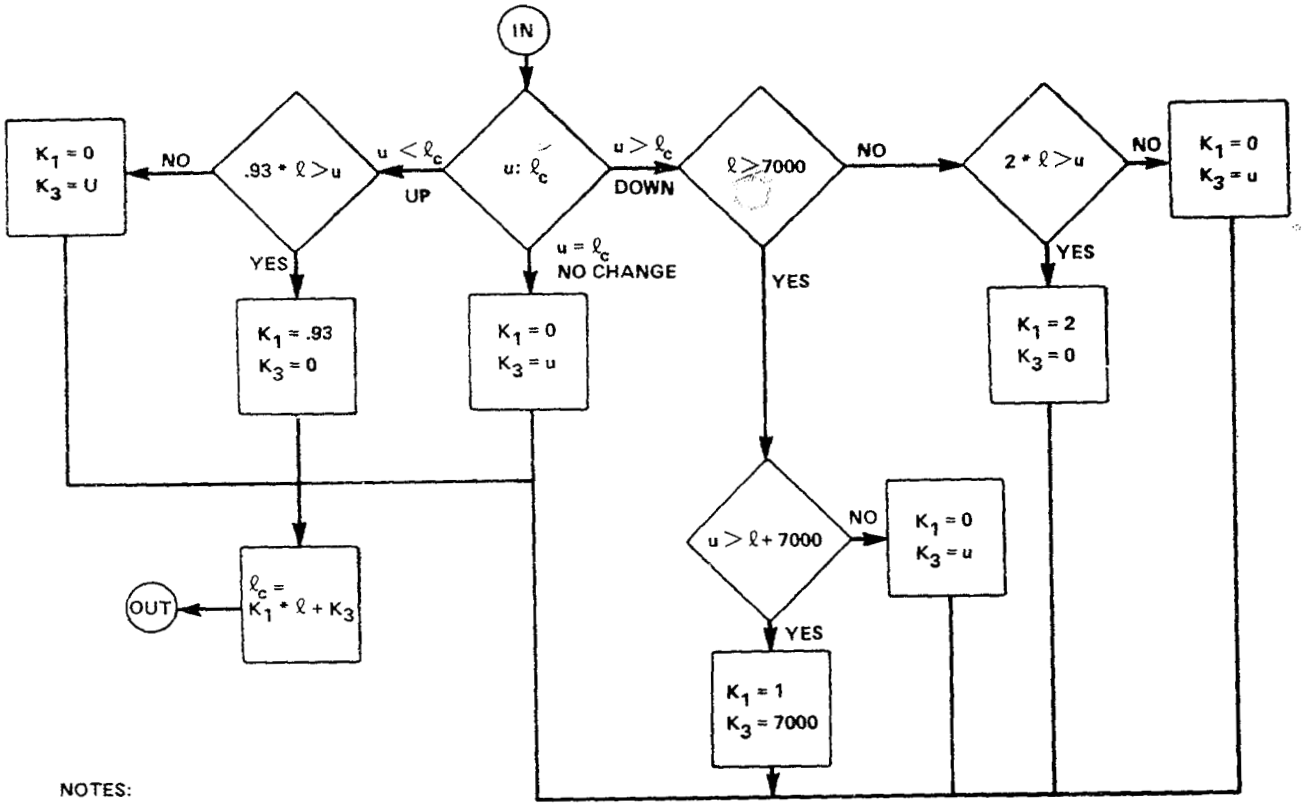

NOTES:

1. MUST REMEMBER LAST ℓ_c
2. ACCURACY REQUIREMENTS MAY IMPLY DIGITAL MECHANIZATION FOR RETRIEVAL
3. U = FINAL LENGTH

Figure III-8. Flow chart to find K_1, K_3 for $\ell_c = K_1 * \ell + K_3$.

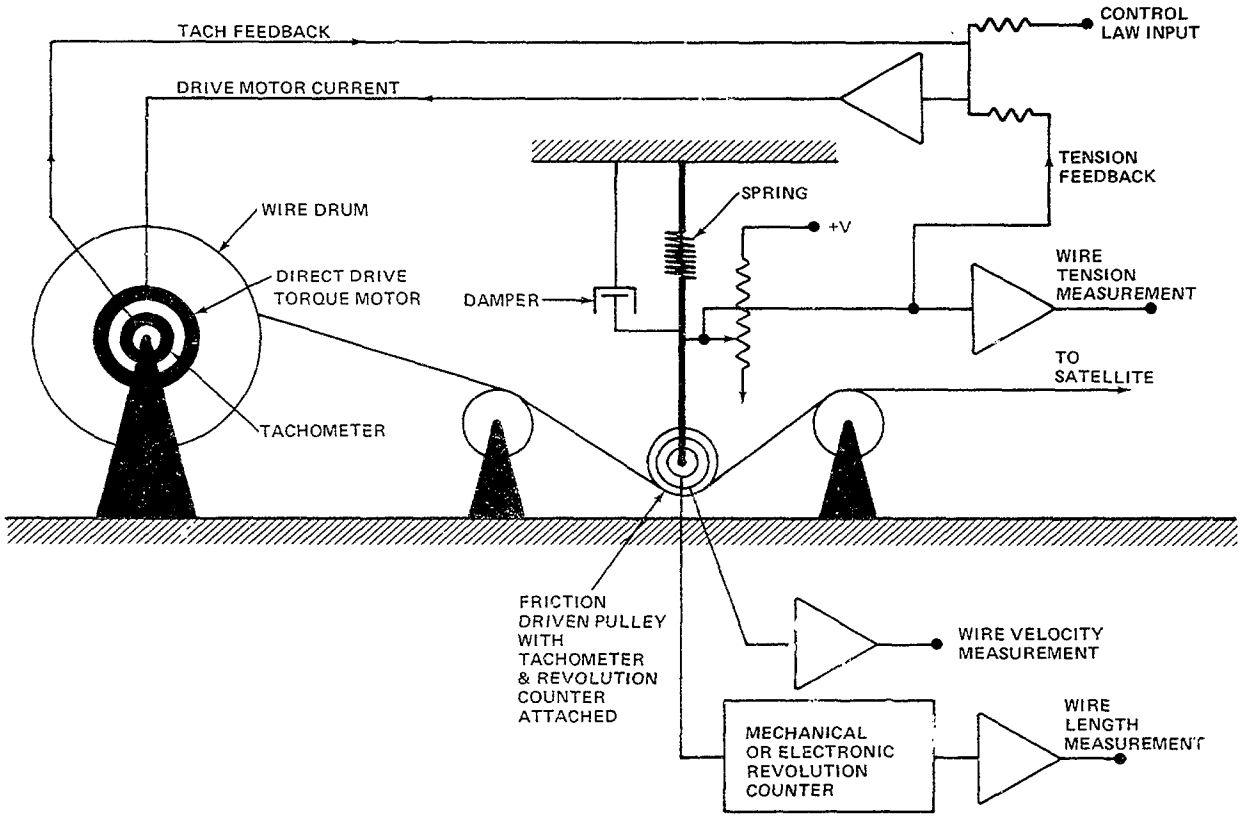

Figure III-9. Conceptual mechanization.

IV. AERODYNAMICS

Kenneth D. Johnston

The aerodynamic forces and heating on the satellite and tether wire are estimated and one possible design for aerodynamic attitude stabilization is examined in this section. The interference of the satellite with atmospheric probe measurements is also briefly discussed.

A. Tether Wire

The tether wire is so small ($D \leq 0.4$ mm) that the wire is in the free molecular flow regime over the entire altitude range (altitude $\geq$ 100 km). The Knudsen number (molecular mean free path/wire diameter) of the wire at 100 km altitude is approximately 400, and it increases at higher altitudes. A Knudsen number of 10 or greater is sufficient to guarantee free molecular flow.

The aerodynamic force coefficients were estimated using Reference IV-1. Although the free molecular force coefficients vary somewhat with wall temperature and speed ratio, the accuracy obtained by assuming these quantities to be constant over the altitude range is considered adequate for this study. Therefore, these quantities were taken to be constant at the values they assume at the midaltitude of 150 km. The normal force and axial force coefficients for the wire are given in Figure IV-1 as a function of the angle-of-attack of the wire.

Experimental data from Reference IV-2 were used to estimate the aerodynamic heat input to the wire. Figure IV-2 gives the total film coefficient, h_T (defined in the figure), as a function of altitude for free molecule flow at right angles to the wire. The equilibrium temperature of the wire was estimated by balancing the aerodynamic and solar heat input against the emitted radiant energy assuming that both the absorbtivity and emissivity are equal to 0.85. All other sources of energy input such as Earth radiation and electric current in the wire were ignored. Figure IV-3 gives the equilibrium wire temperature as a function of altitude with and without solar heating.

B. Nonaerodynamically Stabilized Satellites

If there is no requirement for aerodynamic attitude control, simple external shapes such as spheres or cylinders can be used. Only spheres and cylinders are considered here. Four sizes ranging from 0.5 to 2 m in diameter were chosen to bracket the probable size of the subsatellite. The speed of the subsatellite was obtained, whenever needed, by observing that the subsatellite and the orbiter travel at the same angular speed about the center of the Earth.

Figure IV-4 gives drag coefficients of spheres as a function of altitude. These curves were obtained from experimental data in Reference IV-3 for hypersonic, rarefied flow. A different curve is obtained for each diameter at the lower altitudes where the spheres are in the transitional flow regime, i.e., that flow regime between the continuum regime at low altitudes and the free molecular regime at high altitudes. Moderate changes in body size produce significant changes in force coefficients in the transitional flow regime.

The aerodynamic heat input to a 1 m diameter sphere was estimated using experimental data from Reference IV-2. The total film coefficient, h_T, is given in Figure IV-5. An energy balance similar to that for the tether wire was performed to find the equilibrium temperature of the sphere. This temperature is presented as a function of altitude in Figure IV-6.

Drag coefficients for cylinders at zero angle-of-attack and length-to-diameter ratio of 2 are given in Figure IV-7. Again, the separate curves for the different body sizes indicate the transitional flow regime. A "bridging formula" given in Reference IV-4 and modified in Reference IV-5 was used to estimate the coefficients in the transitional regime. The bridging formula bridges the gap between the continuum and free molecular regimes by supplying a curve shape based on experimental data for similar bodies. The free molecular coefficients were obtained from Reference IV-1.

C. Aerodynamically Stabilized Satellites

If aerodynamic attitude stability is desired, some system of vanes must be placed on the leeward end of the satellite to keep it pointing into the relative wind. The force exerted by the tether wire on the subsatellite could produce moments which might counteract the aerodynamic moments. This interference could be prevented if the wire were attached at the center of gravity of the subsatellite. This effect might also be minimized by locating the wire attachment

point judiciously. The tether wire would have much less effect in the yaw plane than in the pitch plane, so the tether wire might be ignored in a first approximation for yawing motion.

For a fin surface to be effective in high altitude, low density flight, it must be inclined at a large angle to the flow. This is because the lift curve slope, $\partial C_L / \partial \alpha$, of a fin surface is very small near zero angle-of-attack and becomes much larger at greater angles-of-attack. No attempt was made to find an optimum vane configuration since the present study is only to determine feasibility. Therefore, a simple configuration was chosen for convenience of computation. This configuration consists of a lightweight 45° half-angle cone frustum attached to a 1 m diameter spherical satellite with the apex of the cone coinciding with the center of the sphere. To estimate the moment of inertia of this configuration, it was assumed that the supporting structure and skin of the cone-frustum afterbody are equivalent in mass distribution to a 0.005 in. thick aluminum conical shell. Cone base diameters of 4, 6, and 8 m were chosen for the study. Some physical characteristics of these bodies are listed in Figure IV-8.

1. STATIC AERODYNAMICS

The drag coefficient of this configuration at zero angle-of-attack is given in Figure IV-9 as a function of altitude. These data were computed using Reference IV-4 and the modified bridging formula of Reference IV-5. The drag coefficients are converted to drag force in Figure IV-10 and compared with the sphere alone drag to illustrate the penalty in drag which results from attaching the afterbody. The drag force is rather large at the lower altitudes. This drag imposes a horizontal component of tension in the wire which might limit the size of afterbody which can be used. It would be useful to measure the tension in the wire at the satellite to provide an estimate of atmospheric density by assuming that the drag coefficient is known.

A "design altitude" of 107 km was selected for this study. The axial force coefficient is given as a function of angle-of-attack for this altitude in Figure IV-11. The normal force coefficient is given in Figure IV-12. The aerodynamic moment coefficient, C_M, about the center of the sphere is given as a function of angle-of-attack in Figure IV-13. As expected, this configuration is statically stable at $\alpha = 0$ since $C_M = 0$ and $\partial C_M / \partial \alpha < 0$ at $\alpha = 0$, i.e., if the body is disturbed from $\alpha = 0$, an aerodynamic moment is created which

tends to drive the body back towards $\alpha = 0$. However, it is not a sure thing that the body will come to rest again at $\alpha = 0$; it might oscillate with constant amplitude (zero dynamic stability) or with increasing amplitude (dynamic instability). Therefore, the dynamic stability of the configuration must be examined.

2. DYNAMIC STABILITY

Consider angular oscillations (about center of mass) in a plane (single degree of freedom motion) with only aerodynamic torques acting, except for the initial disturbance torque. The complicated dynamic interaction between the tether wire and the satellite is ignored. This idealized model might be useful for examining oscillatory motions in the yaw plane.

The one-dimensional equation of rotational motion is

$$I\ddot{\alpha} = \left(\frac{\partial M}{\partial \alpha}\right)_{\alpha=0} \alpha + \left(\frac{\partial M}{\partial \dot{\alpha}}\right)_{\dot{\alpha}=\alpha=0} \dot{\alpha} \qquad \text{(IV-1)}$$

where

$$\left(\frac{\partial M}{\partial \alpha}\right)_{\alpha=0} = \left(\frac{\partial C_M}{\partial \alpha}\right)_{\alpha=0} Q_\infty A_{REF} L_{REF} = -K$$

$$\left(\frac{\partial M}{\partial \dot{\alpha}}\right)_{\dot{\alpha}=\alpha=0} = \left(\frac{\partial C_M}{\partial\left(\frac{q L_{REF}}{U_\infty}\right)}\right)_{q=\alpha=0} \left(Q_\infty A_{REF} L_{REF}\right) \frac{L_{REF}}{U_\infty} = -C$$

or, in familiar form:

$$\ddot{\alpha} + \frac{C}{I}\dot{\alpha} + \frac{K}{I}\alpha = 0 \qquad \text{(IV-2)}$$

The quantity K is found by taking the slopes of the curves in Figure IV-13 at $\alpha = 0$. To keep K constant and equation (IV-2) linear, the maximum angle-of-attack must be limited to approximately 20°. The quantity

$$\left(\frac{\partial C_M}{\partial \frac{(q L_{REF})}{U_\infty}} \right)_{q=\alpha=0}$$

is the aerodynamic damping derivative. Its value was estimated at -2.0 from Reference IV-6 which uses the Newtonian impact theory that is valid for continuum flow. No attempt was made to modify the damping derivative to account for rarefied flow.

The solution to equation (IV-2) is

$$\alpha = \alpha_{MAX} e^{-\frac{C}{2I} t} \sin\left[\sqrt{\frac{K}{I} - \left(\frac{C}{2I}\right)^2}\, t + \phi \right] . \qquad \text{(IV-3)}$$

The damped natural frequency of oscillation is

$$f = \frac{1}{2\pi} \sqrt{\frac{K}{I} - \left(\frac{C}{2I}\right)^2} \text{ [CPS]} \qquad \text{(IV-4)}$$

and the undamped natural frequency is

$$f_N = \frac{1}{2\pi} \sqrt{\frac{K}{I}} \text{ [CPS]} \qquad \text{(IV-5)}$$

The aerodynamic damping was so small that there was no significant difference in natural frequency between the damped and undamped cases. The natural frequency is given as a function of altitude in Figure IV-14. The differences in frequency for the different sized bodies are small.

If it is assumed that at $t = 0$ and $\alpha = 0$, the satellite is given an impulsive angular speed, $\dot{\alpha}_0$, the maximum angular deflection is given by

$$\alpha_{MAX} = \frac{\dot{\alpha}_0}{\sqrt{\frac{K}{I} - \left(\frac{C}{2I}\right)^2}} \quad . \tag{IV-6}$$

The maximum angle is given as a function of the initial angular speed disturbance in Figure IV-15 for 107 km altitude. For a given $\dot{\alpha}_0$, increasing the size of the afterbody has an adverse effect in limiting the maximum angle; this is due to the increase in moment of inertia. However, for a given angular impulse disturbance, Figure IV-16 shows that increasing the size of the afterbody is very effective in limiting α_{MAX}.

To evaluate the effectiveness of aerodynamic damping, we find the time required, t_D, for the amplitude of the oscillations to decay to 1/e of α_{MAX}. From equation (IV-3),

$$t_D = \frac{2I}{C} \quad . \tag{IV-7}$$

The decay time is given as a function of altitude in Figure IV-17. This time increases rapidly with altitude, and for altitudes greater than 110 to 115 km the aerodynamic damping is practically ineffective. Some form of internal damping might be required for the higher altitudes.

The selection of the afterbody size will depend on the disturbances expected, e.g., wind profiles or jerks from the tether wire, and on the maximum allowable amplitude of oscillation and decay time. No attempt was made to estimate the disturbances to be expected.

The aerodynamic heating and equilibrium surface temperature of the spherical satellite was given in Figures IV-5 and IV-6. The aerodynamic heating of the conical afterbody was obtained in a similar way from experimental data in Reference IV-2 and presented in Figure IV-18. The data in Reference IV-2 are for complete cones; however, these data were used unchanged to estimate the convective heat transfer to the cone frustums. Performing an

energy balance as before yields the equilibrium temperatures in Figure IV-19. Separate curves were obtained for the different sized bodies at the lower altitudes in the transitional flow regime.

D. Satellite Interference with Atmospheric Measurements

If an attempt is made to measure atmospheric properties, such as density, by means of an instrument mounted at the surface of the satellite, the measurements are likely to be far different from the values in the undisturbed atmosphere that one would like to record. The air molecules pile up on the front of the satellite in a shock layer as illustrated in Figure IV-20. The density, temperature, and pressure are greatly increased above their undisturbed values, and the air molecules are partially dissociated and ionized. One might attempt to overcome this satellite interference by extending a probe through the shock layer into the undisturbed freestream. The scope of this preliminary study is limited to estimating the shock layer thickness and, therefore, the length of probe required.

A computation method for the ideal gas flow field in the stagnation region of a spherical body was developed by Jain and Adimurthy [IV-7] and extended by Jain and Kumar [IV-8] to real gas and further modified by Hendricks [IV-9]. The flow field along the stagnation streamline of a 1 m diameter sphere at 107 km altitude was computed using this program. The ideal gas version of this program gave reasonable agreement with experimental temperature and density profiles [IV-7] and the real gas version gave fairly good agreement with other theoretical solutions [IV-8 and IV-9], so these data can be treated with a reasonable degree of confidence, although a thorough comparison with experimental data is not available. Figure IV-21 gives the nondimensional density, temperature, and atomic oxygen (mass fraction) profiles along the stagnation streamline as a function of nondimensional distance from the surface of the sphere for the case of a noncatalytic wall. From this figure the shock layer extends approximately 1.1 radii ahead of the sphere at this altitude. Therefore, a probe longer than 55 cm would be required to protrude into the undisturbed freestream at 107 km; longer probes would be required at higher altitudes. The complicated problem of the interference of the probe with the flow field about the satellite was not considered. The probe system will undoubtedly require much more study in the future.

E. References

IV-1. Sentman, Lee H.: Free Molecule Flow Theory and Its Application to the Determination of Aerodynamic Forces. Lockheed Report LMSC 448514, Appendix C, October 1968.

IV-2. Kienappel, K.; Koppenwallner, G.; and Legge H.: Force and Heat Transfer Measurements on Inclined Cones in the Hypersonic Range from Continuum to Free Molecular Flow. Eighth International Symposium on Rarefied Gas Dynamics, Stanford University, July 1972, Academic Press, 1974.

IV-3. Bailey, Allan B.: High Speed Sphere Drag in the Transition Flow Regime in an Aeroballistic Range. Rarefied Gas Dynamics, Supplement 4, vol. 2, Academic Press, 1967, pp. 1127-1144.

IV-4. Warr, John W.: An Orbital Aerodynamics Computer Program to Calculate Force and Moment Coefficients on Complex Vehicle Configurations. LMSC-HREC D162498, Lockheed Missiles and Space Company, Huntsville, Alabama, August 1970.

IV-5. Johnston, K. D.: A Comparison of the Lockheed Transitional Flow Bridging Formula with Experimental Data. S&E-AERO-AA-73-69, Marshall Space Flight Center, October 1973.

IV-6. Tobak, Murray and Wehrend, William: NACA TN3788, 1956.

IV-7. Jain, A. C. and Adimurthy, V.: Hypersonic Merged Stagnation Shock Layers, Part II: Cold Wall Case. AIAA Journal, vol. 12, no. 3, 1974.

IV-8. Kumar, Ajay, and Jain, A. C.: Nonequilibrium Merged Stagnation Shock Layers at Hypersonic Speeds. Int. J. Heat and Mass Transfer, vol. 18, 1975, pp. 1113-1118.

IV-9. Hendricks, William L.: A Similarity Solution of the Navier-Stokes Equations with Wall Catalysis and Slip for Hypersonic, Low Reynolds Number Flow over Spheres. AIAA Paper no. 75-675, May 1975.

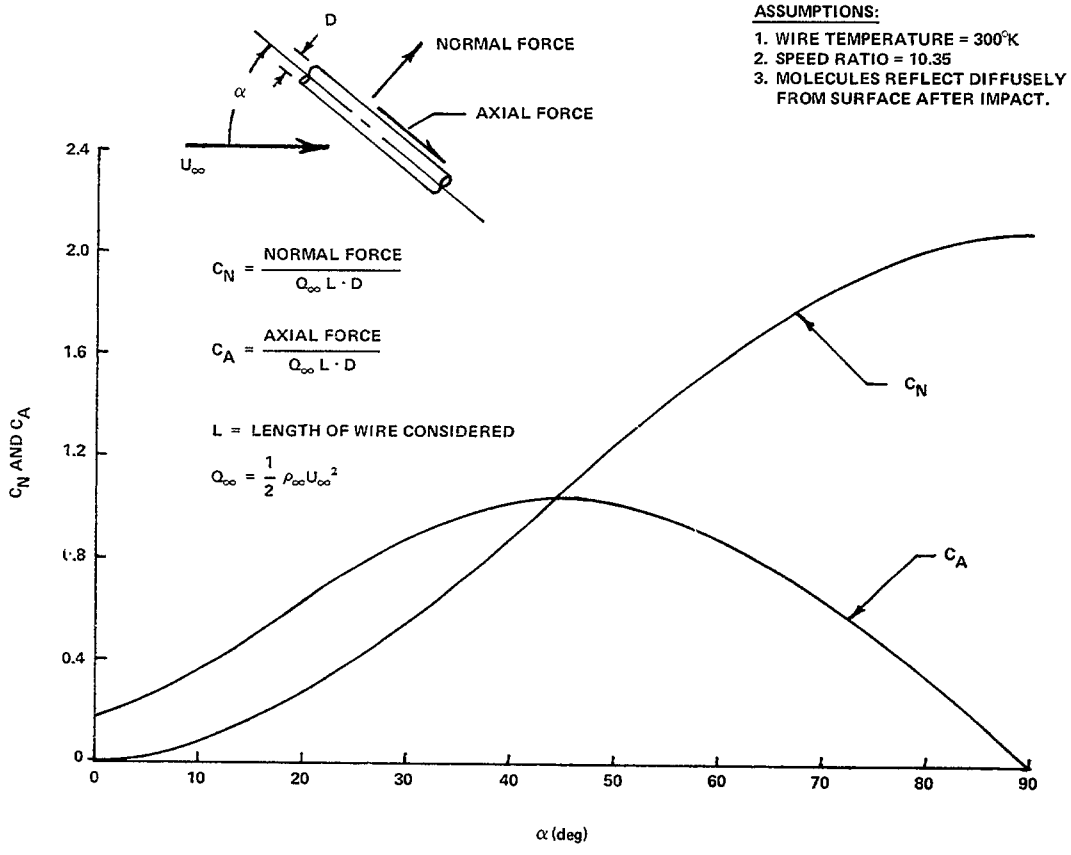

Figure IV-1. Aerodynamic force components on tether wire in hypervelocity, free molecular flow.

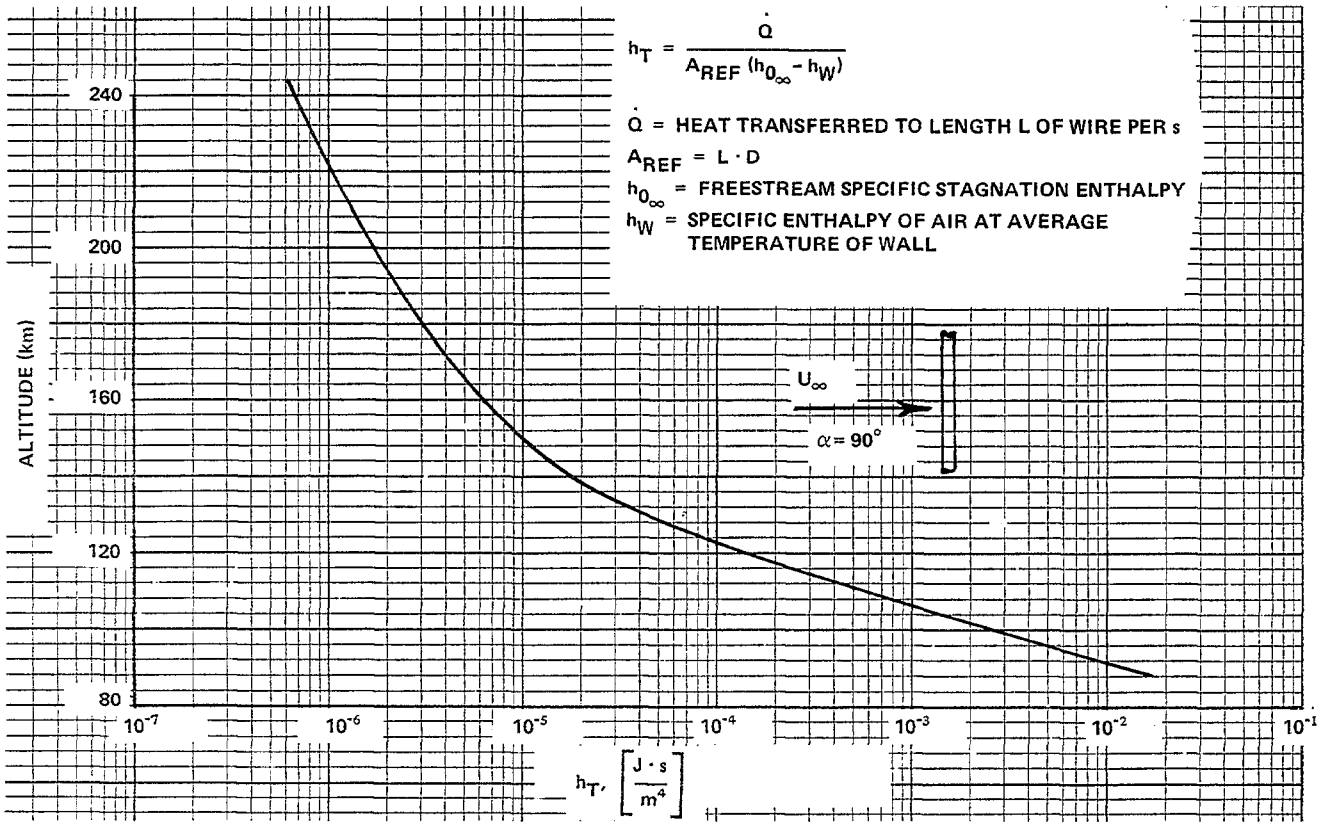

Figure IV-2. Aerodynamic heating of tether wire at $\alpha = 90°$.

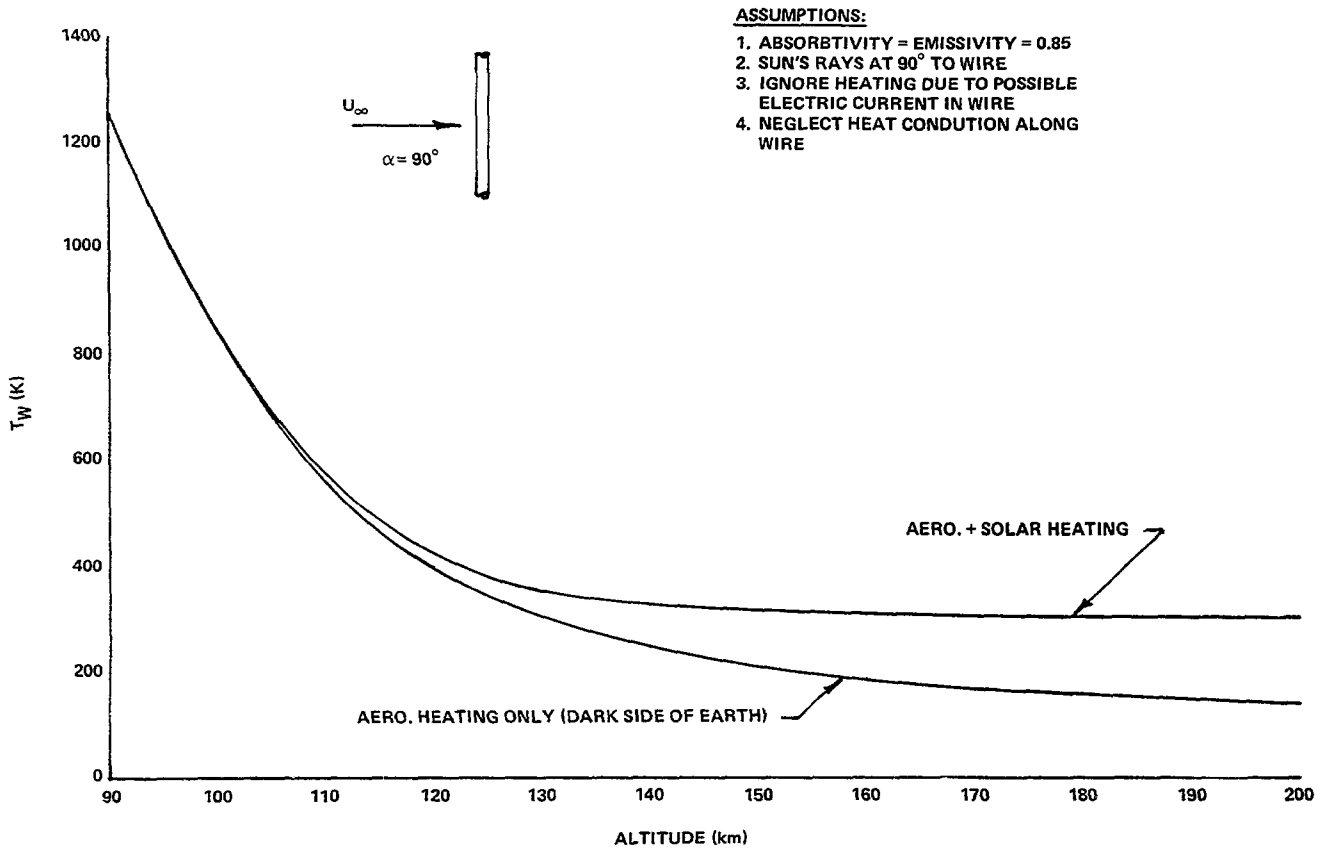

Figure IV-3. Equilibrium temperature of tether wire at $\alpha = 90°$.

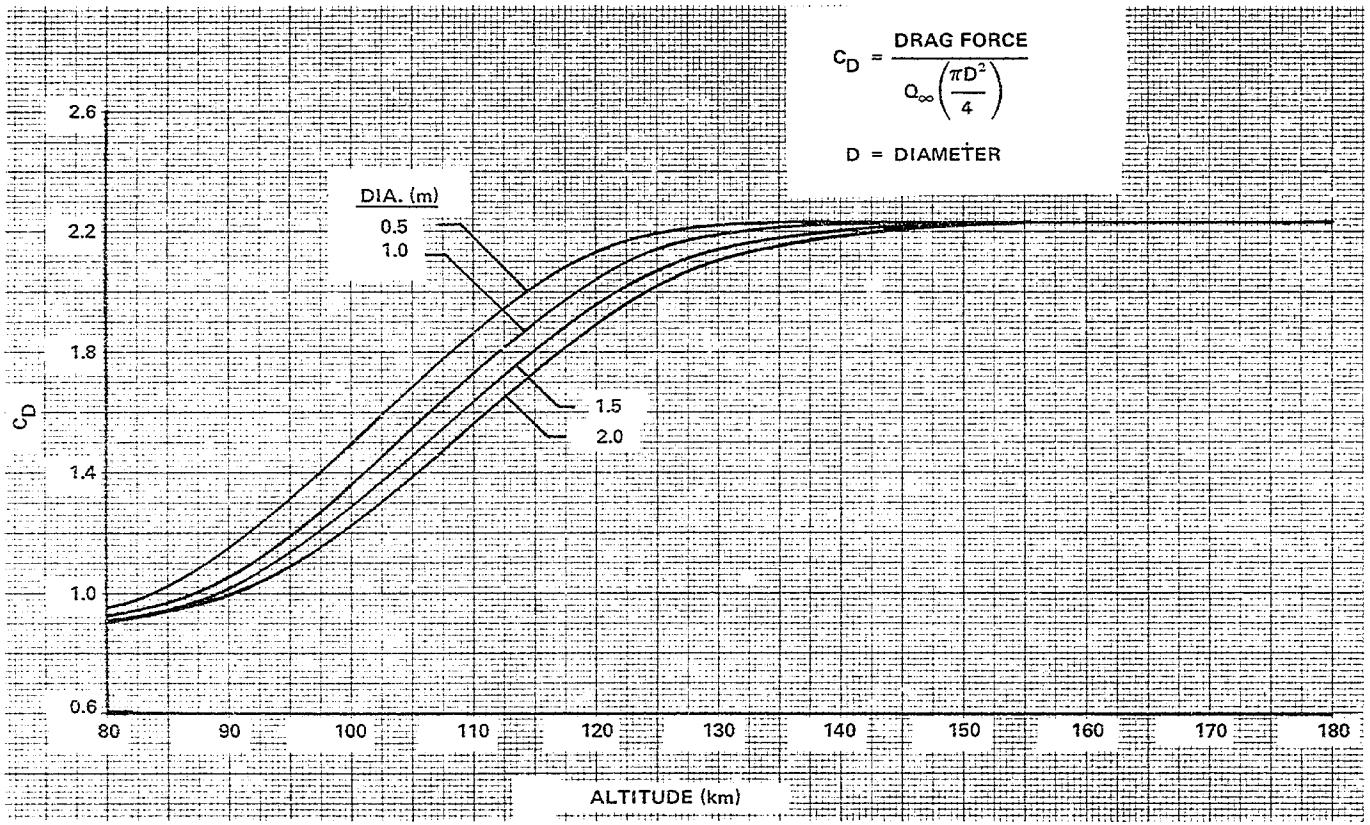

Figure IV-4. Drag coefficient of spheres in orbit.

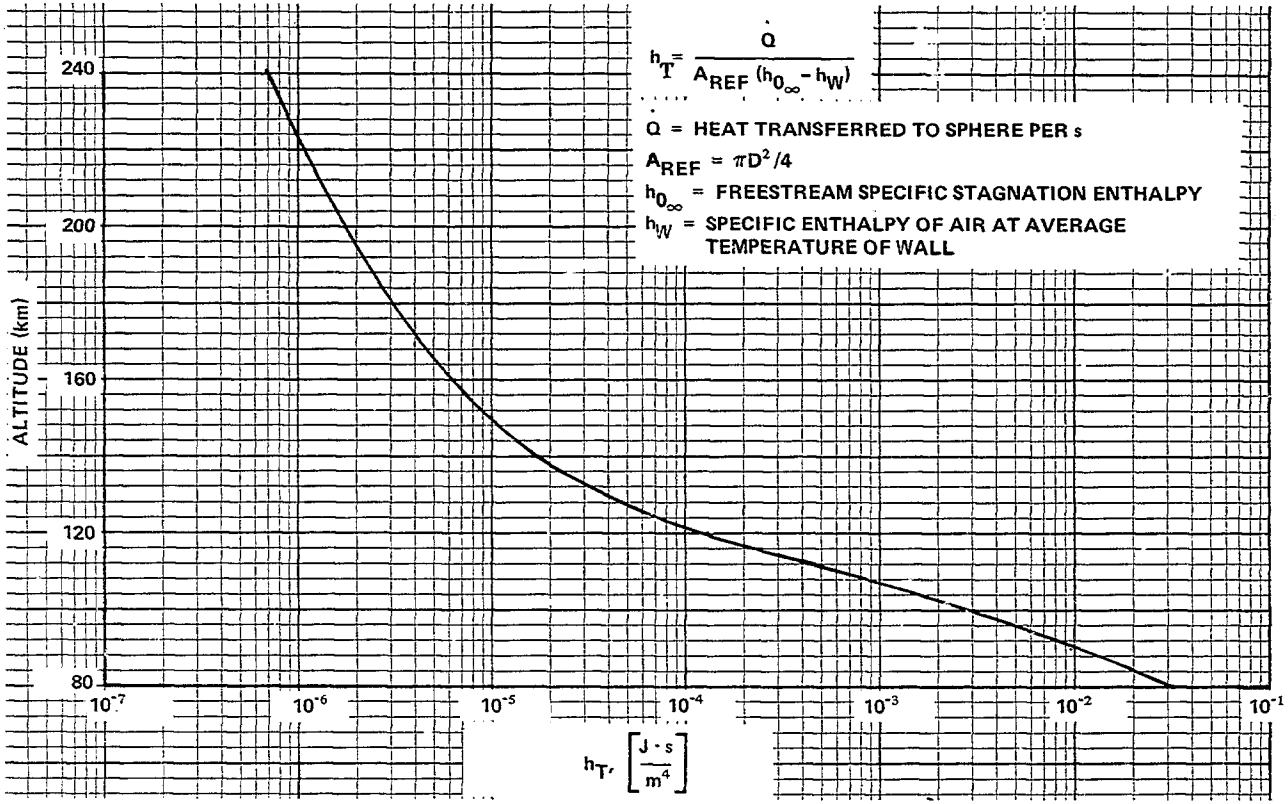

Figure IV-5. Aerodynamic heating for sphere (D = 1 m).

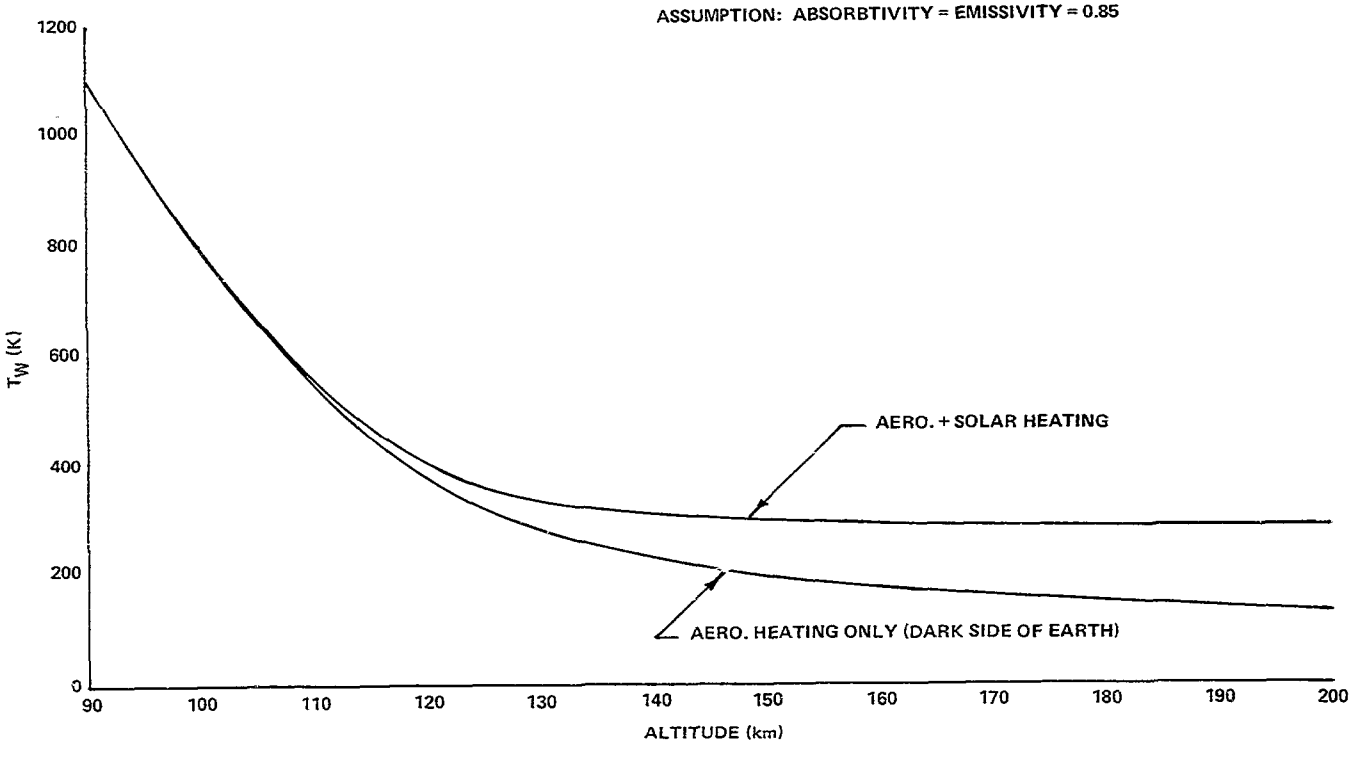

Figure IV-6. Equilibrium surface temperature for spherical satellite (D = 1 m).

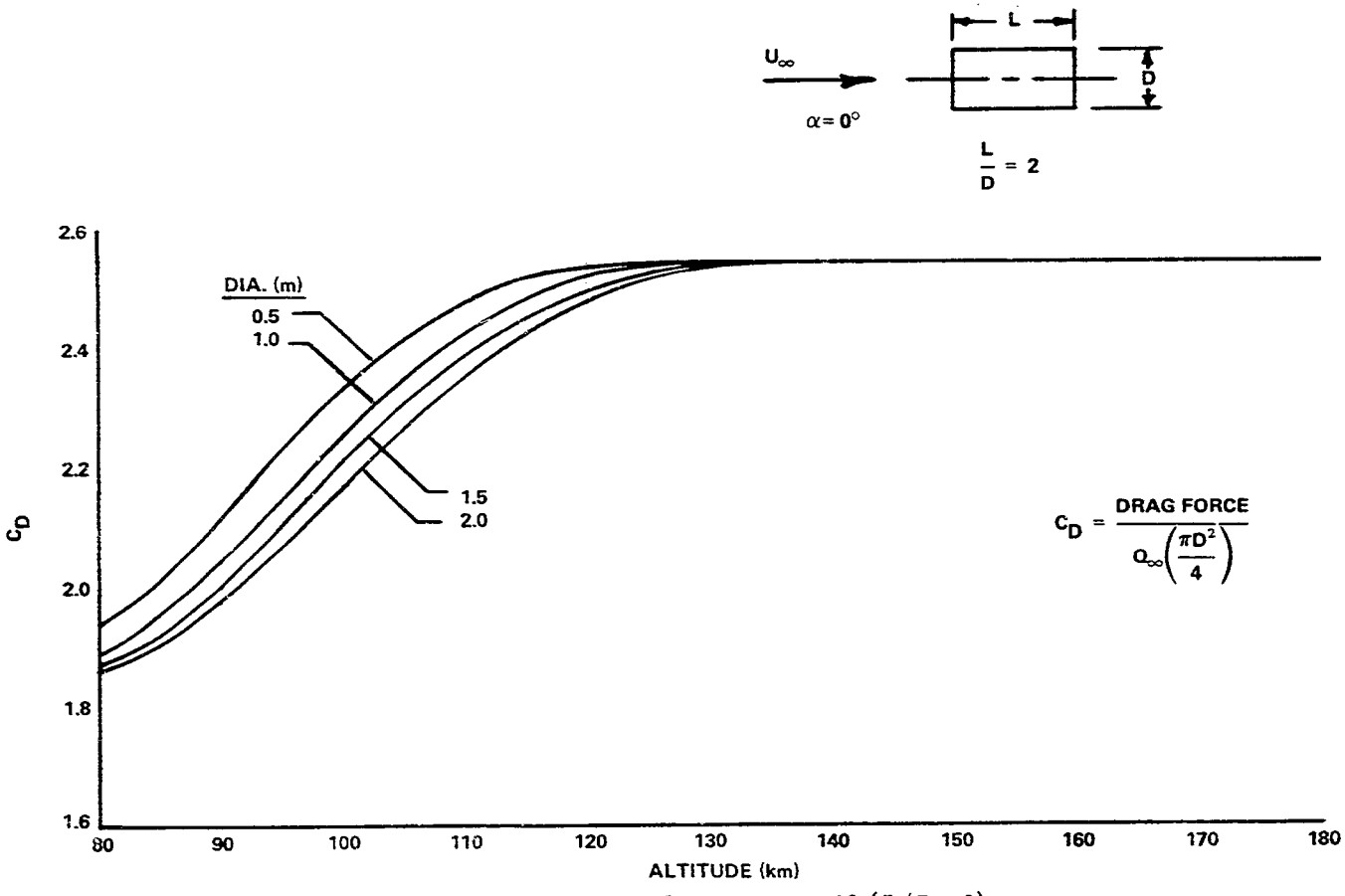

Figure IV-7. Drag coefficient of cylinders at $\alpha = 0°$ $(L/D = 2)$.

ASSUMPTIONS:

1. CENTER OF MASS OF BODY AT CENTER OF SPHERE
2. MASS OF SPHERICAL BODY = 100 kg
   $I_c = 10\ kg \cdot m^2$
3. STRUCTURE AND SKIN OF CONE-FRUSTUM AFTERBODY ARE EQUIVALENT IN MASS DISTRIBUTION TO A 0.005 in. THICK ALUMINUM CONICAL SHELL
   ($\rho = 0.3515\ kg/m^2$ OF SURFACE AREA)

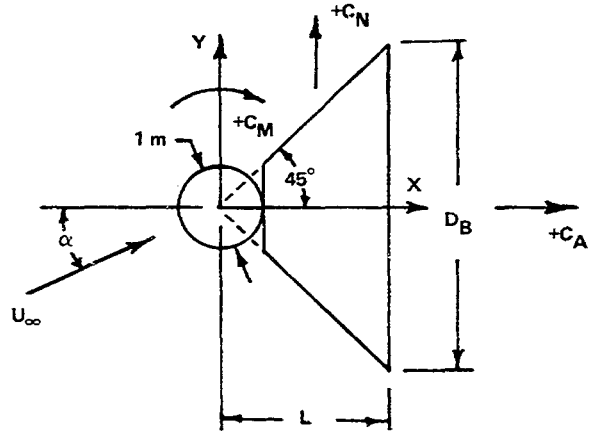

D_B (m)	L (m)	$\frac{A_{REF}}{\frac{\pi D_B^2}{4}}$ (m^2)	L_{REF} (m)	SURFACE AREA OF CONE-FRUSTUM (m^2)	MASS OF CONE-FRUSTUM (kg)	I_Y, I_Z ($kg \cdot m^2$) CONE-FRUSTUM	I_Y, I_Z ($kg \cdot m^2$) COMPOSITE BODY
4	2	12.566	2	16.655	5.854	18.658	28.658
6	3	28.274	3	38.874	13.664	94.807	104.81
8	4	50.265	4	69.979	24.598	299.81	309.81

Figure IV-8. A subsatellite shape for aerodynamic stability (sphere-cone-frustum).

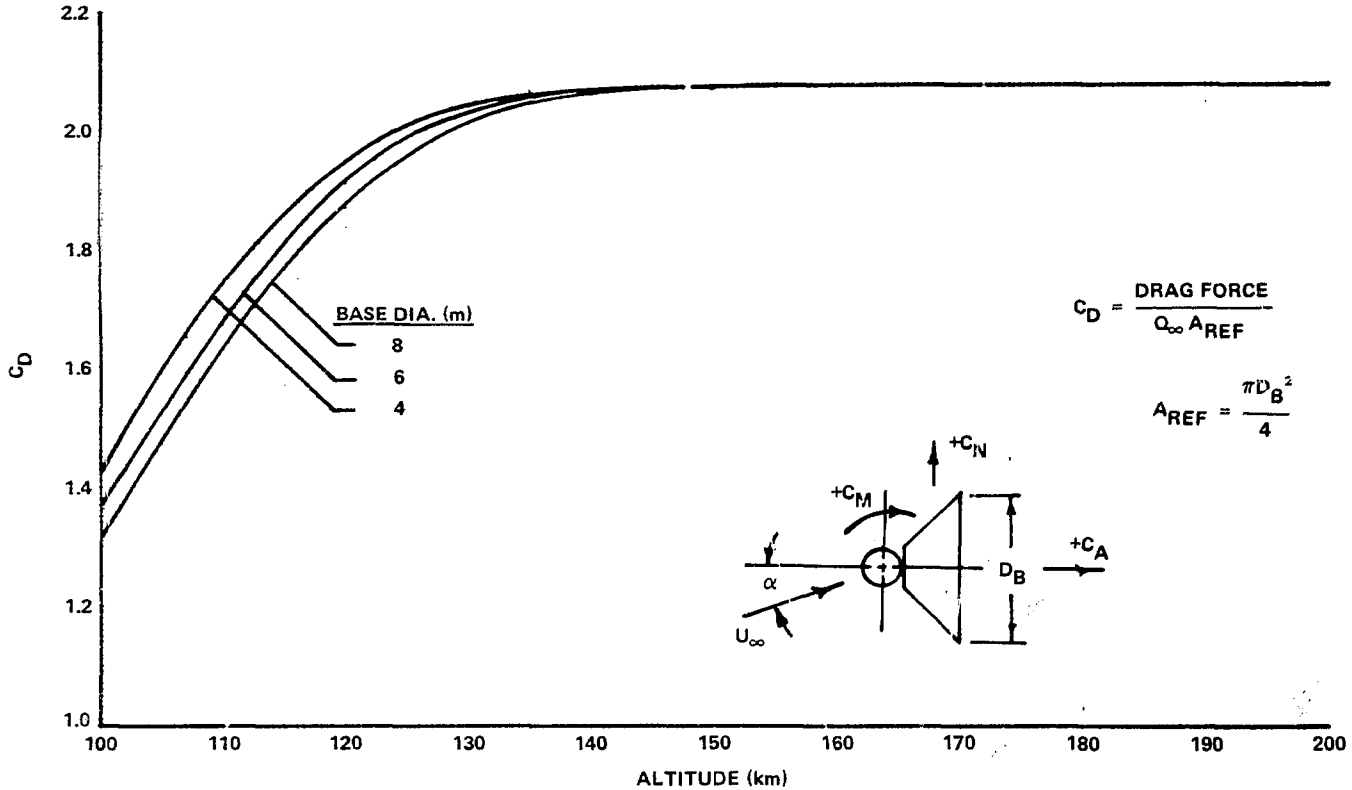

Figure IV-9. Drag coefficient of sphere with cone-frustum afterbody in orbit at zero angle of attack.

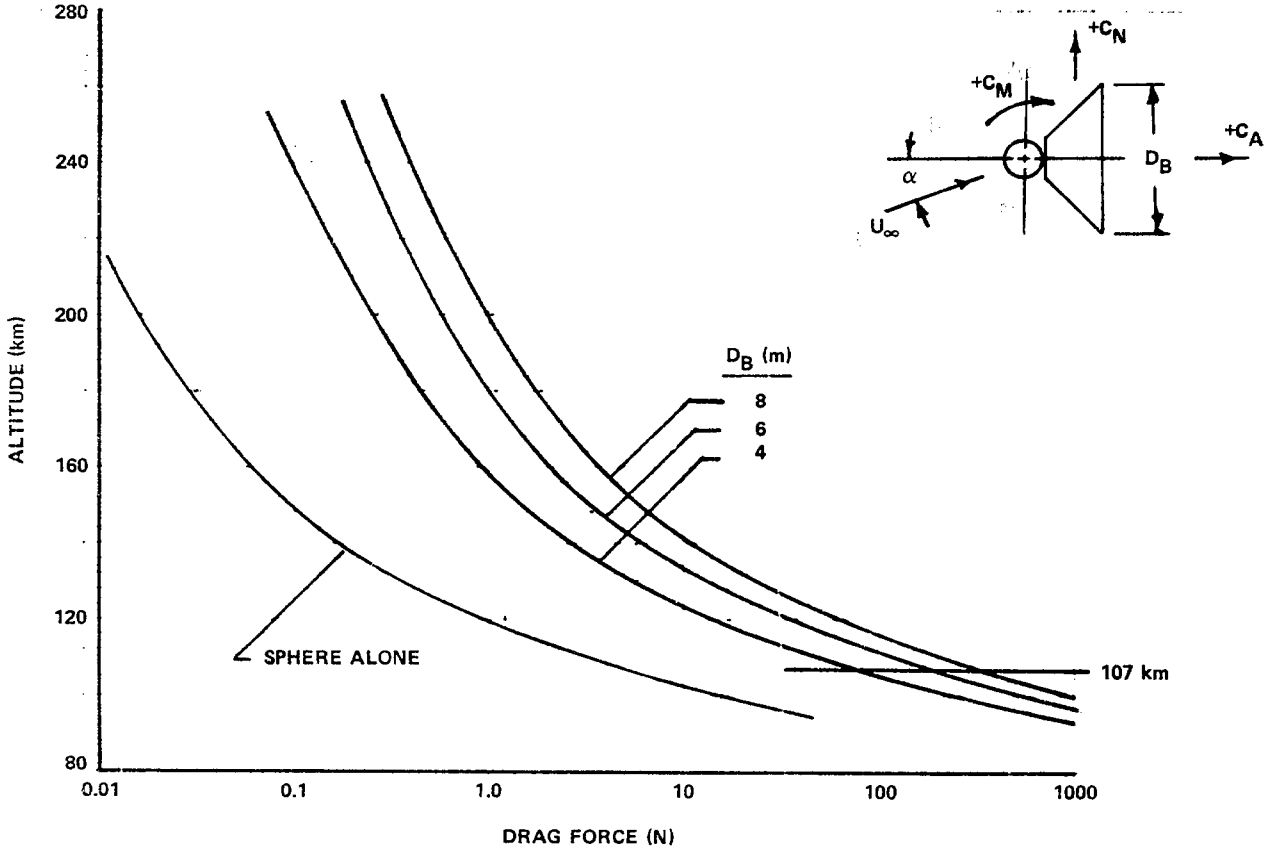

Figure IV-10. Drag force on sphere with cone-frustum afterbody at $\alpha = 0°$.

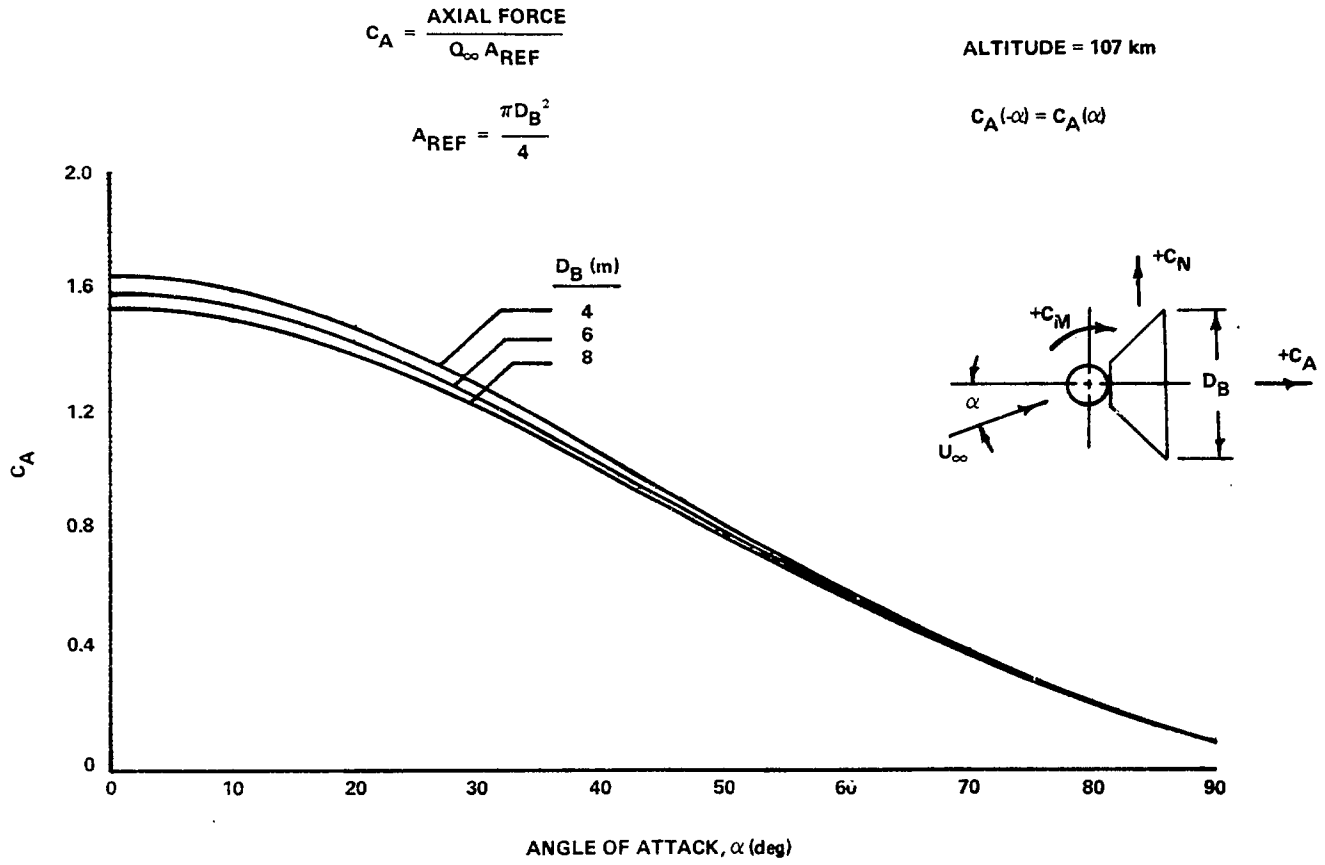

Figure IV-11. Axial force coefficient of sphere with cone-frustum afterbody.

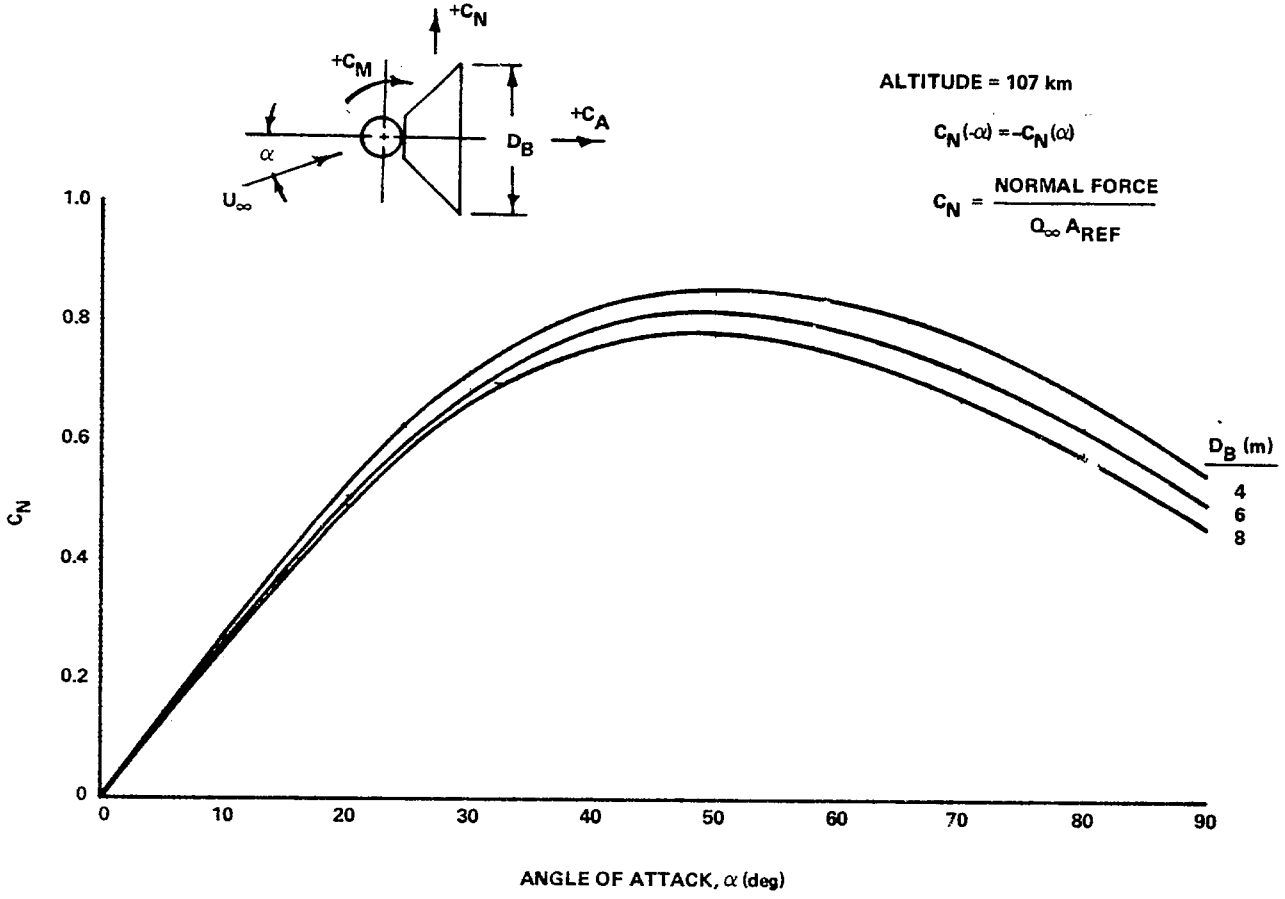

Figure IV-12. Normal force coefficient of sphere with cone-frustum afterbody.

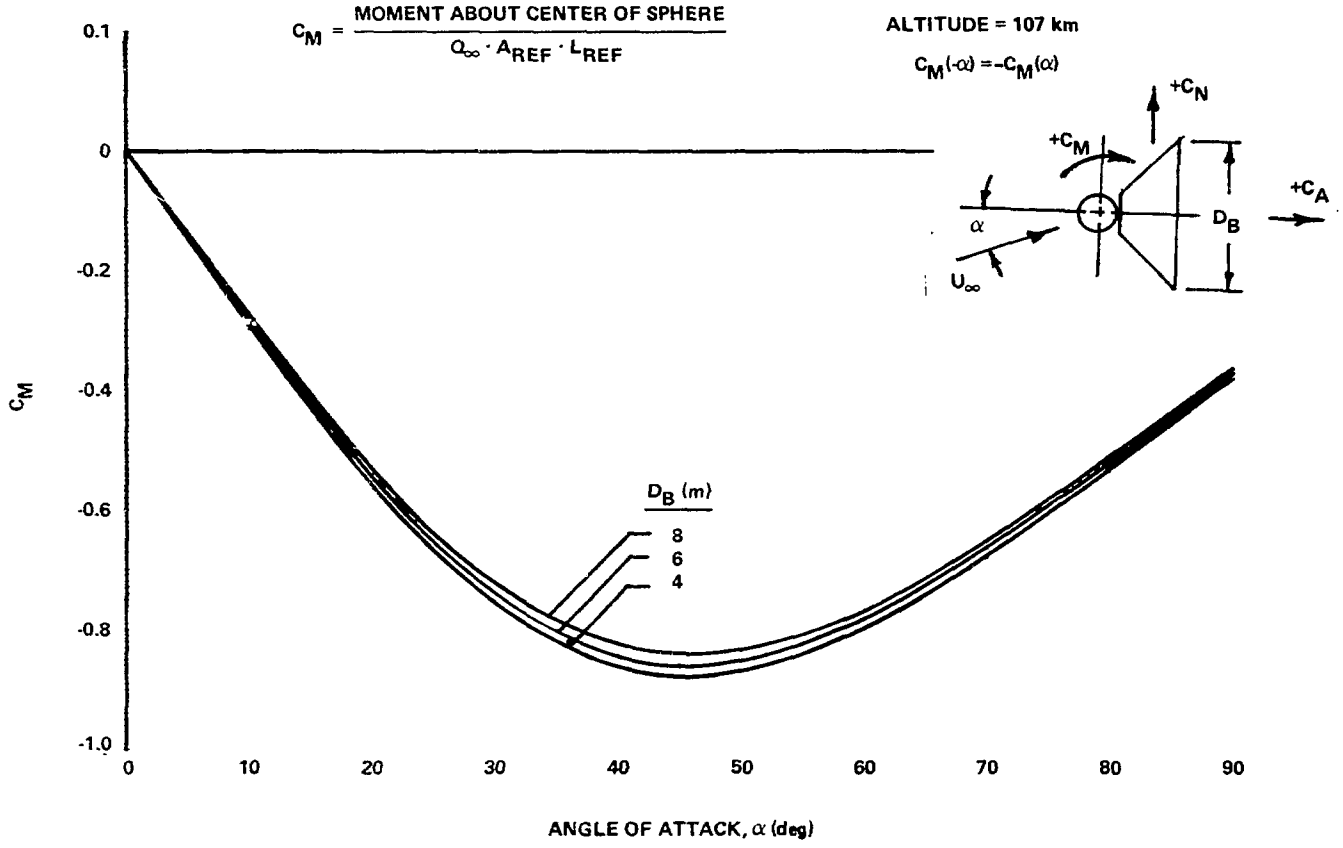

Figure IV-13. Moment coefficient of sphere with cone-frustum afterbody.

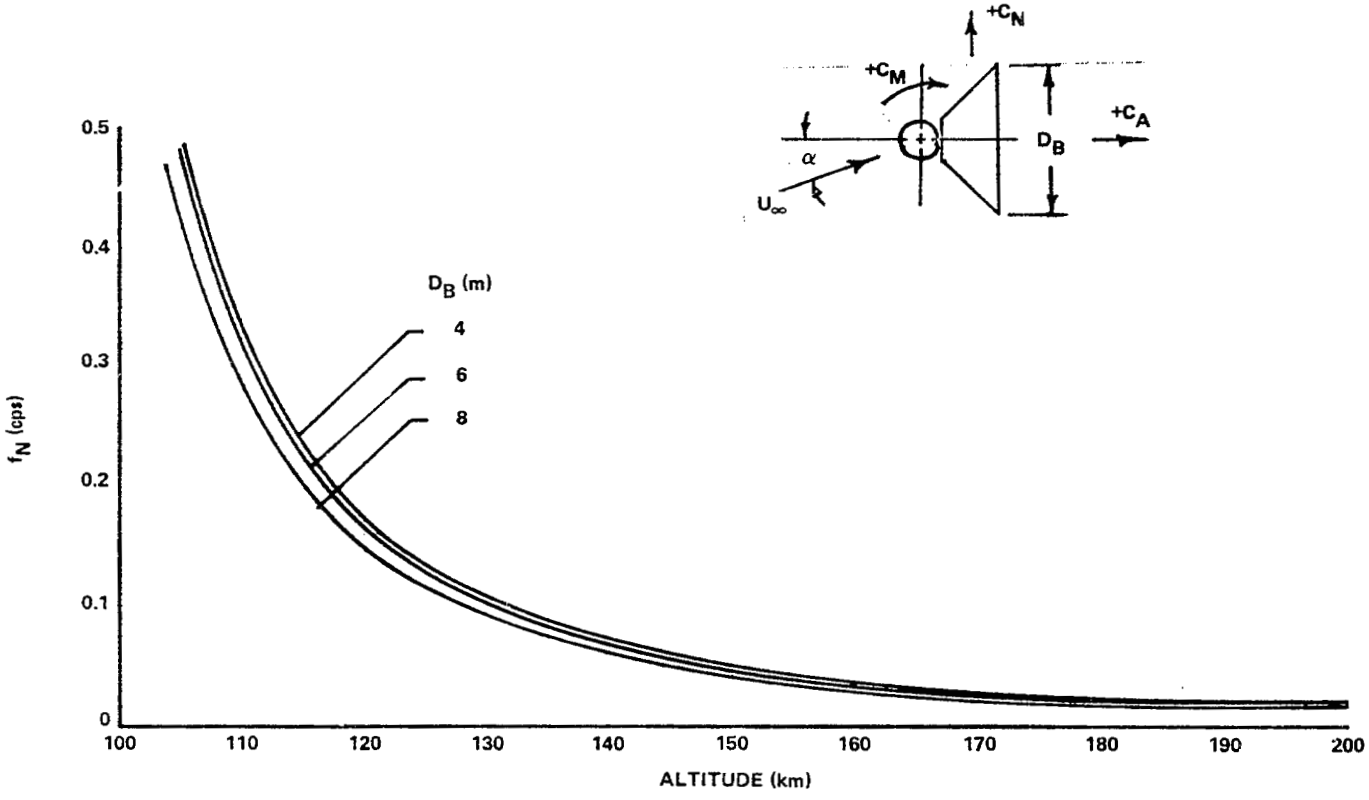

Figure IV-14. Natural frequency of oscillation of sphere-cone-frustum subsatellite as function of altitude.

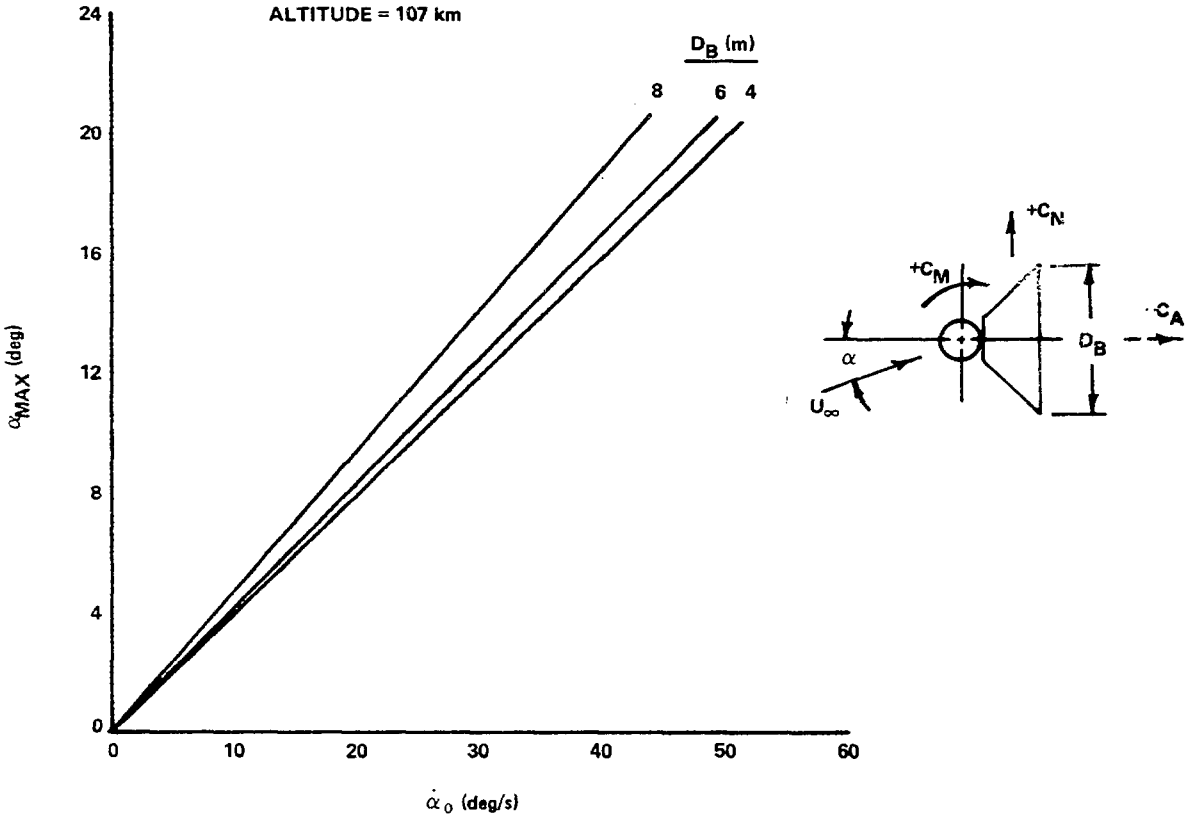

Figure IV-15. Maximum amplitude of sphere-cone-frustum subsatellite oscillation as function of initial angular speed disturbance at $\alpha = 0°$.

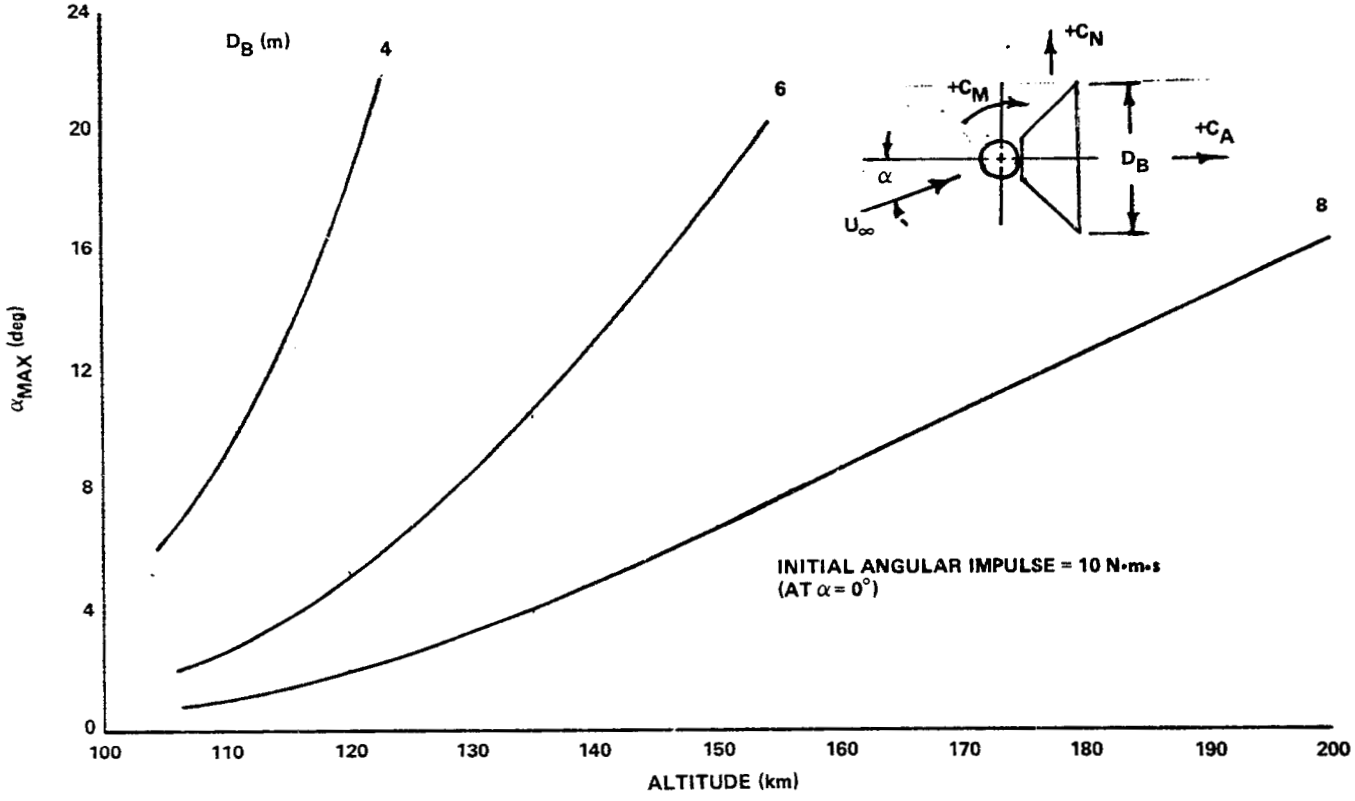

Figure IV-16. Maximum amplitude of oscillation of sphere-cone-frustum subsatellite as function of altitude.

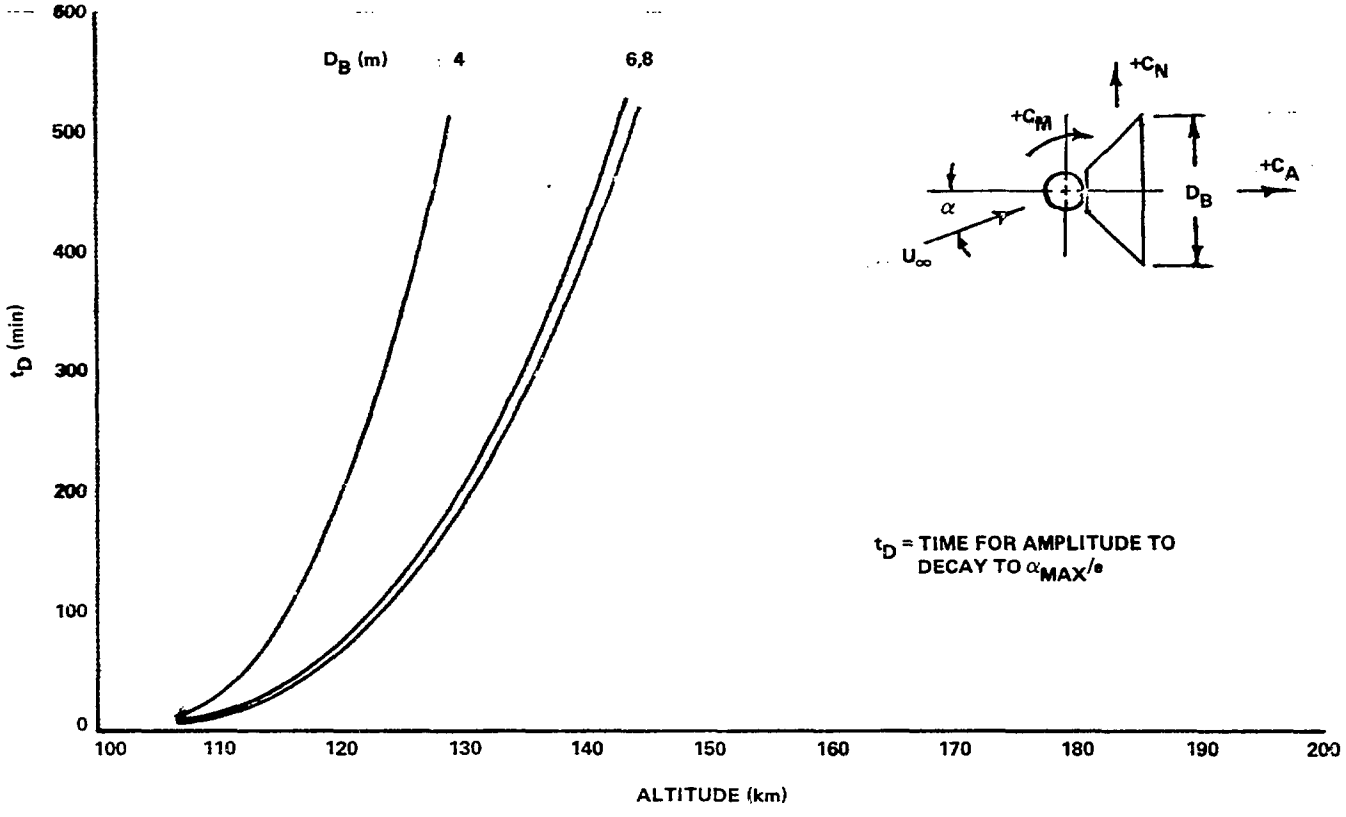

Figure IV-17. Decay time for amplitude of oscillation of sphere-cone-frustum subsatellite as function of altitude.

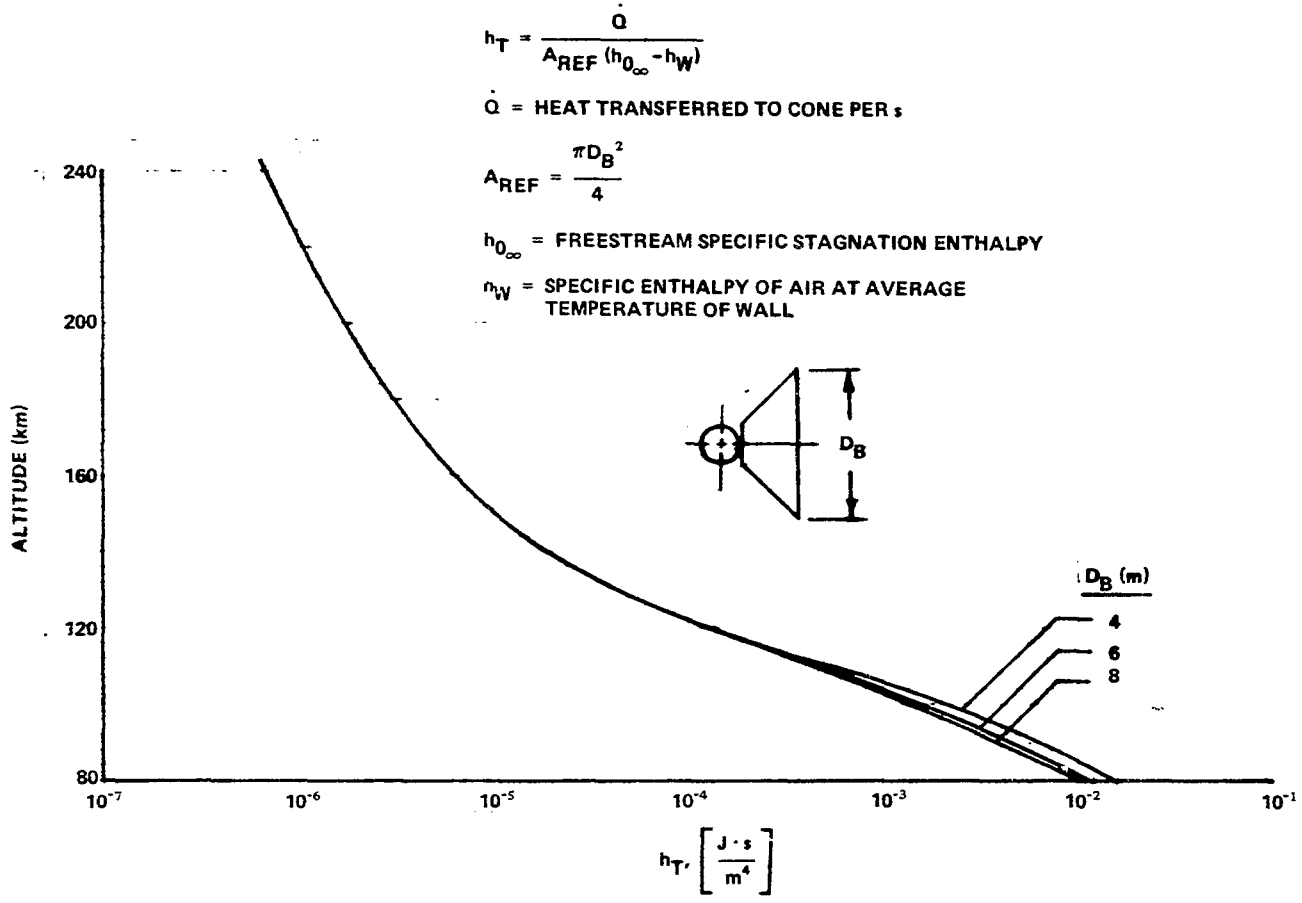

Figure IV-18. Aerodynamic heating for cones.

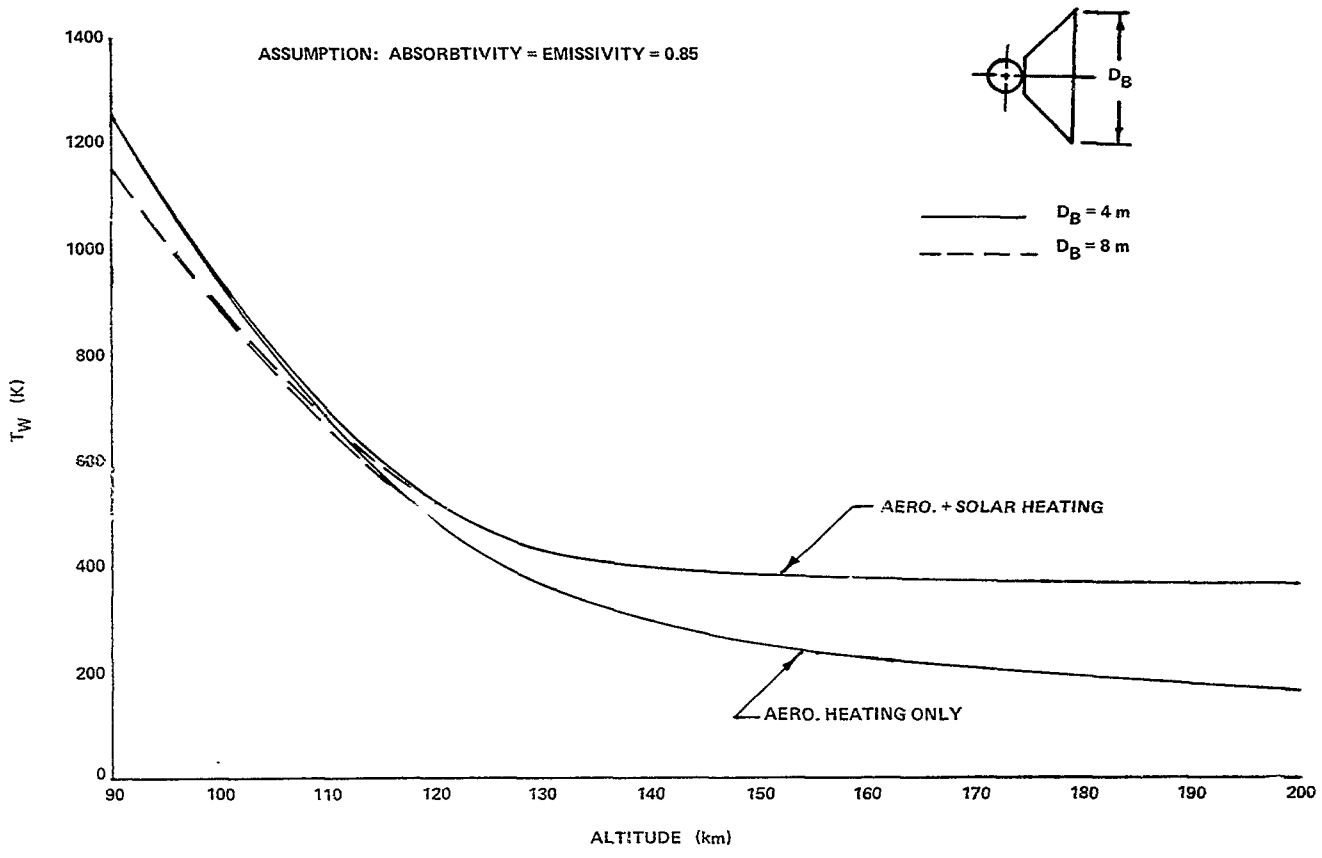

Figure IV-19. Equilibrium temperature of conical afterbody at $\alpha = 0°$.

Figure IV-20. Interference of satellite with atmospheric measurements.

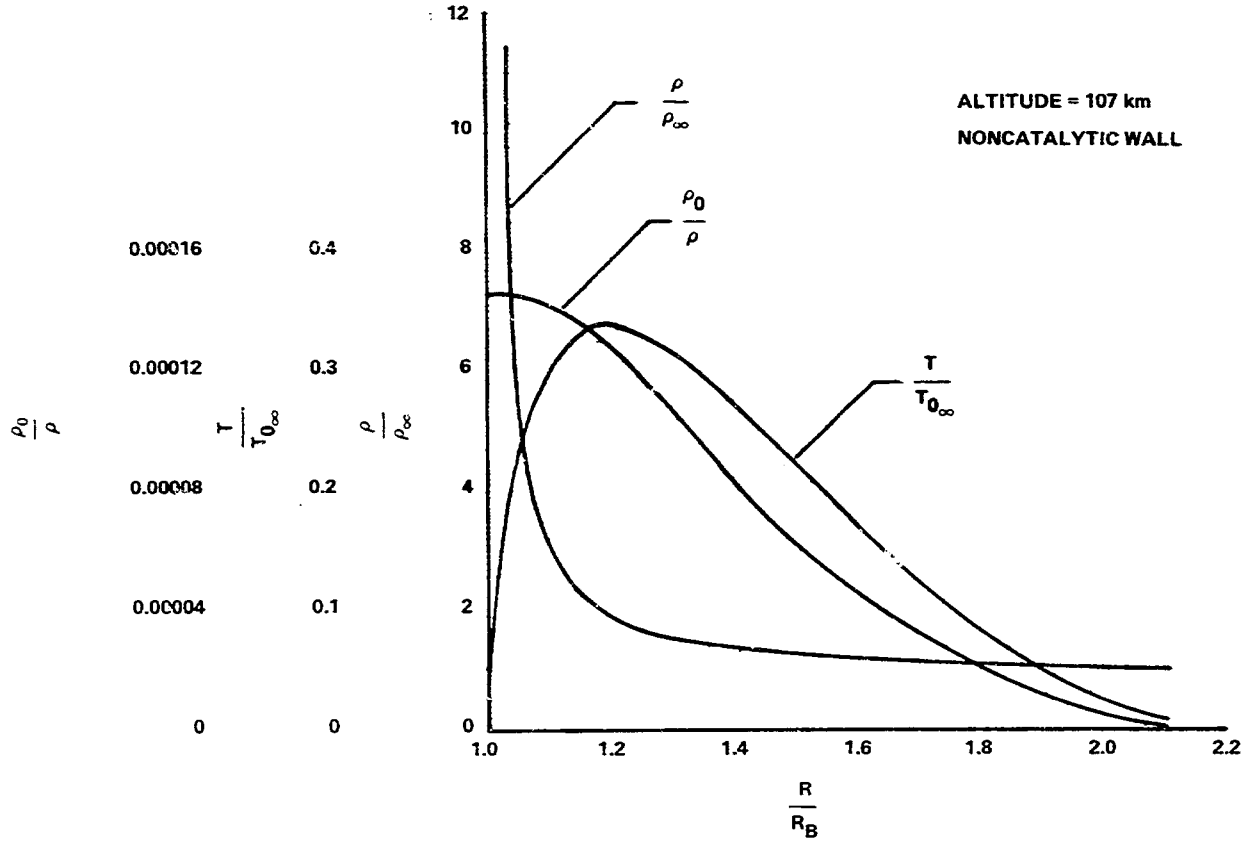

Figure IV-21. Density, temperature, and atomic oxygen (mass fraction) profiles on stagnation streamline ahead of 1 m diameter sphere.

V. THERMAL STUDIES

William P. Baker

A. Summary

A preliminary thermal assessment was made to determine the external heating rates and the resulting temperatures of a low orbit spherical satellite and its tether wire, and to assess the thermal protection requirements to effectively maintain the temperatures of the electronic packages and the antenna within acceptable limits.

The resulting recommendations are to apply: (1) 3.81 cm (1.5 in.) of high performance insulation (HPI) to the external surface of the satellite shell, and (2) 2.54 cm (1 in.) of high temperature reusable surface insulation (HRSI-LI900) external to the satellite's antenna.

B. Introduction

The objectives were (1) to determine the thermal effects of aerodynamic, solar, Earth radiation and albedo, and internal heat upon an Atmospheric Magnetospheric Plasma in Space (AMPS) tethered subsatellite and its tether wire and (2) to study passive thermal control techniques toward maintaining acceptable temperature limits.

Other sources [V-1 through V-6] were used for information and calculation techniques.

C. Analysis

The approximate aerodynamic heating rate versus altitude was determined and plotted in Figure V-1. Figure V-2 presents a plot of aerodynamic and solar heat as percentiles of the total external heating versus altitude. At the design altitude (107 km), the satellite's external heat input percentages are approximately 97 percent aerodynamic, 2 percent solar, 0.4 percent Earth radiation, and 0.6 percent albedo. These approximate percentages at 130 km are 62 percent aerodynamic, 27 percent solar, 5 percent Earth radiation, and 6 percent albedo.

These assumptions were made in computing the nominal external temperature of a spherical uncooled steel shell satellite versus orbital altitude (Fig. V-3).

1. Oxidized spherical steel shell satellite

   a. Mass — 100 kg

   b. Diameter — 1.12 m

2. Negligible convective cooling and no radiating fins — radiation from external surface to space.

3. Random rotation of sphere; i.e., no stabilizing fins for velocity vector control.

4. 107 km (350 kft) nominal orbital altitude of satellite; 90 min orbital time, 7450 m/s orbital velocity.

5. 50°C maximum internal temperature limit.

6. Transitional to free molecular flow at 90 to 110 km altitude. Free molecular flow at altitudes over 110 km.

7. Equilibrium or steady state conditions.

8. Circular orbit.

D. Results and Graphs

An optimum thickness 3.81 cm (1.5 in.) of high performance insulation could be applied external to the subsatellite shell to reduce the heat flow from outside to inside.

High temperature reusable surface insulation (HRSI-LI900) can be applied external to the subsatellite's antenna for effective temperature control. A 2.54 cm (1 in.) thickness will maintain the antenna temperature below 150°C at altitudes down to < 107 km.

The greatest increase of the tether wire temperature occurs at altitudes below approximately 120 km. For example, if the subsatellite is deployed to 107 km, the tether cable material must withstand temperatures up to 495°C, but only 395°C at 114 km.

Assuming a 50°C operational limit internal to the satellite (experiment/instrument package), an active and/or semi-passive thermal control system appears to be required at the lower altitudes (130 km or less). The thermal control system heat load may be minimized by applying passive high performance insulation external to the experiment/instrument package. Figures V-3 and V-4 show typical calculated temperatures for the external surface and the results of reducing the internal heating load by applying HPI to the satellite shell. The HPI retards the heating rate to give long thermal transients to the internal portions of the satellite. Figure V-5 shows the results of applying 3.8 cm (1.5 in.) of HPI (optimum thickness) on the transient heat up of the experiment/instrument package. The results indicate 30 hr to achieve a 50°C temperature rise at the design altitude of 107 km. Therefore, for short experiment times the transient nature of the passive HPI may be adequate for thermal control.

Calculations were made to determine if high temperature reusable surface insulation (HRSI-L1900) can be used to limit the satellite antenna's temperature to its maximum allowable value (150°C) and to define an optimum HRSI thickness.

Figure V-6 indicates steady state antenna temperatures for different thicknesses of the HRSI at the design altitude (107 km) and also for 100 km. The antenna temperature buildup at 100 km and 107 km altitudes using 2.54 cm (1 in.) optimum HRSI thickness is shown on Figure V-7. Figure V-8 indicates the basic construction of a HRSI tile.

A temperature profile of the tether wire was calculated for 100 to 220 km altitude (Fig. V-9), making these assumptions:

1. Wire's cylindrical axis at 90° to line of flight.
2. Solar angle of incidence = 90°.
3. No heat conduction along the wire.
4. No electrical current flow in wire.
5. Steady state condition.
6. Absorptance (α) = 0.9 and emittance (ϵ) = 0.8 for the wire surface.
7. Aerodynamic and solar heat input to the projected area ($2r\ell$) and heat output by radiation from the entire cylindrical area ($2\pi r\ell$) to deep dark space.

E. Conclusions

At some flight conditions, it appears that passive thermal control methods will suffice to successfully maintain the temperatures of the subsatellite instruments within acceptable limits. A more indepth study must be made to determine applicable ranges of altitude and/or internal heat loads.

Active cooling will be required at the design altitude, 107 km, with the expected orbital and instrument heat loads.

Additional work is needed to refine the thermal analysis for uncontrolled satellites. The altitudes should be determined where passive thermal control is adequate to limit the internal temperature $\leq 50°C$. Active cooling methods also should be investigated.

Passive thermal control schemes should be evaluated for velocity vector controlled satellites, e.g., finned areas for thermal radiation, heat pipe application, and external coatings.

F. References

V-1. Frank Kreith, Principles of Heat Transfer. Pennsylvania: International Textbook Co., 1965.

V-2. Jackson R. Stalder and David Jukoff, "Heat Transfer to Bodies Traveling at High Speed in the Upper Atmosphere," NACA Report No. 944; Ames Aeronautical Laboratory, 1948.

V-3. A. W. Ratliff, "Aerodynamic Heating in a Free Molecular Flow," Internal Note P& VE-P-65-4; Marshall Space Flight Center, 1965.

V-4. N. H. Kemp and F. R. Ridell, "Heat Transfer to Satellite Vehicles Reentering the Atmosphere," Jet Propulsion, Vol. 27, 1957, pp. 132-139.

V-5. Robert W. Truitt, Fundamentals of Aerodynamic Heating. New York: The Ronald Press Co., 1960.

V-6. Robert M. Van Vliet, Passive Temperature Control in the Space Environment. New York: The MacMillan Co., 1965.

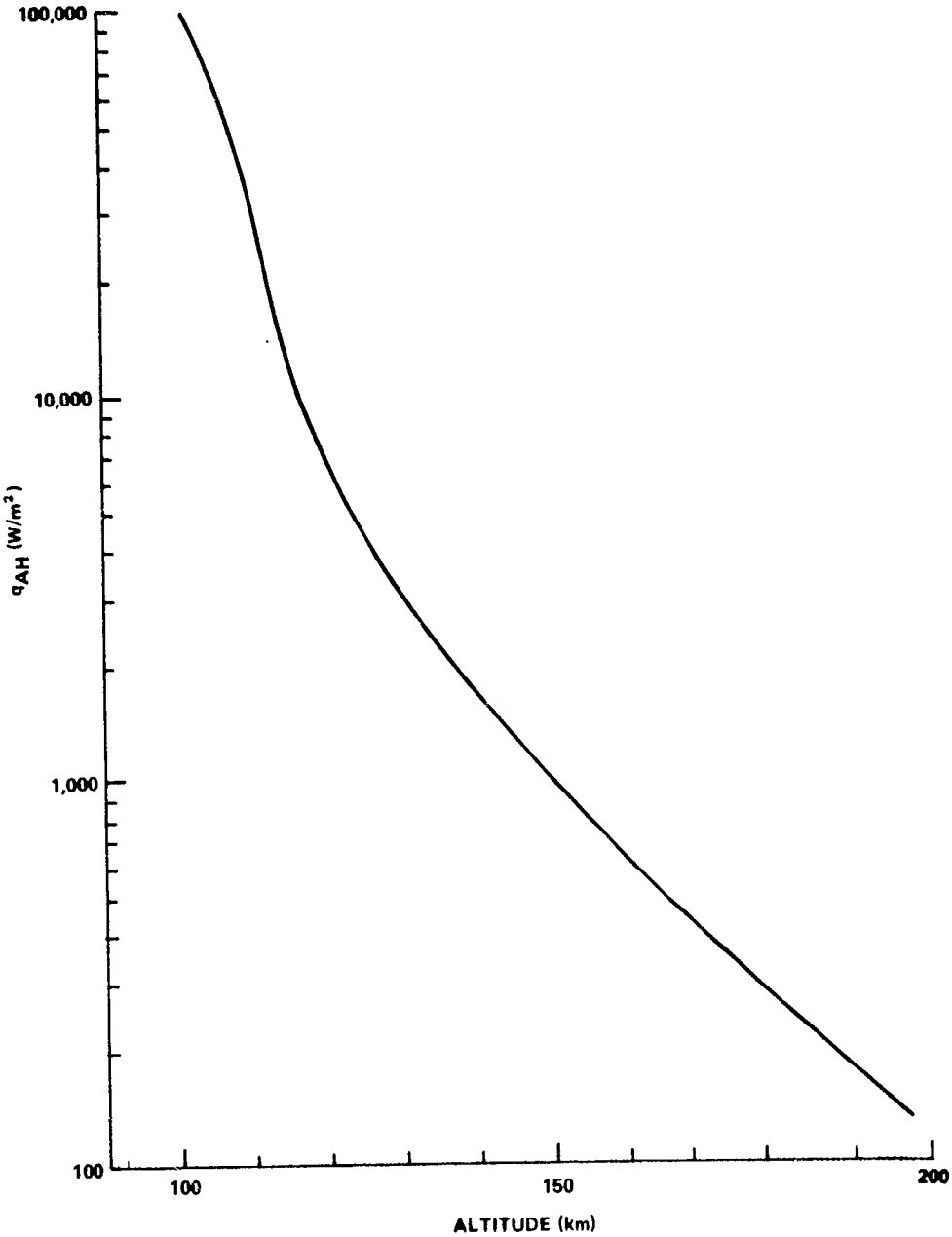

Figure V-1. Aerodynamic heating rate versus altitude.

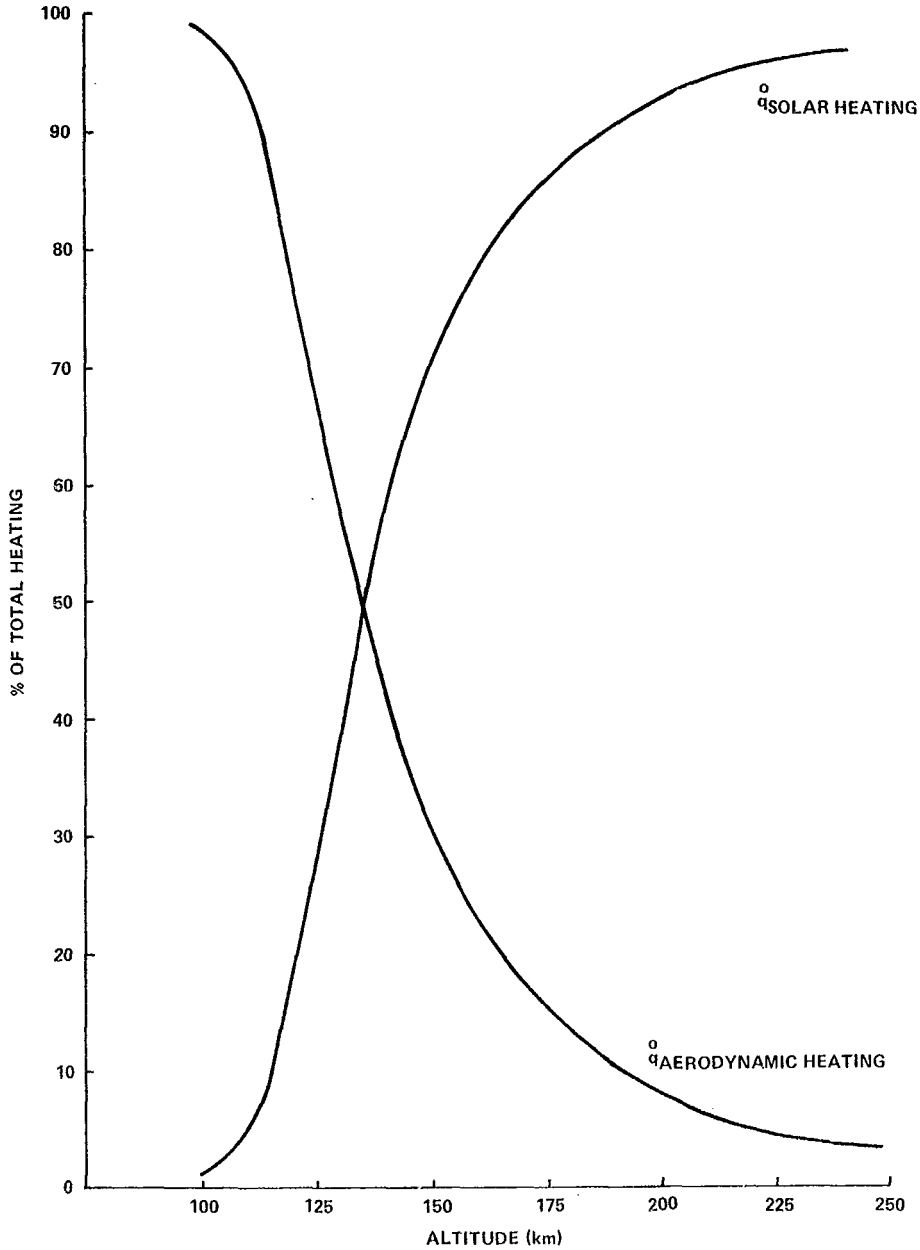

Figure V-2. Aerodynamic and solar heat as percentiles of total external heat.

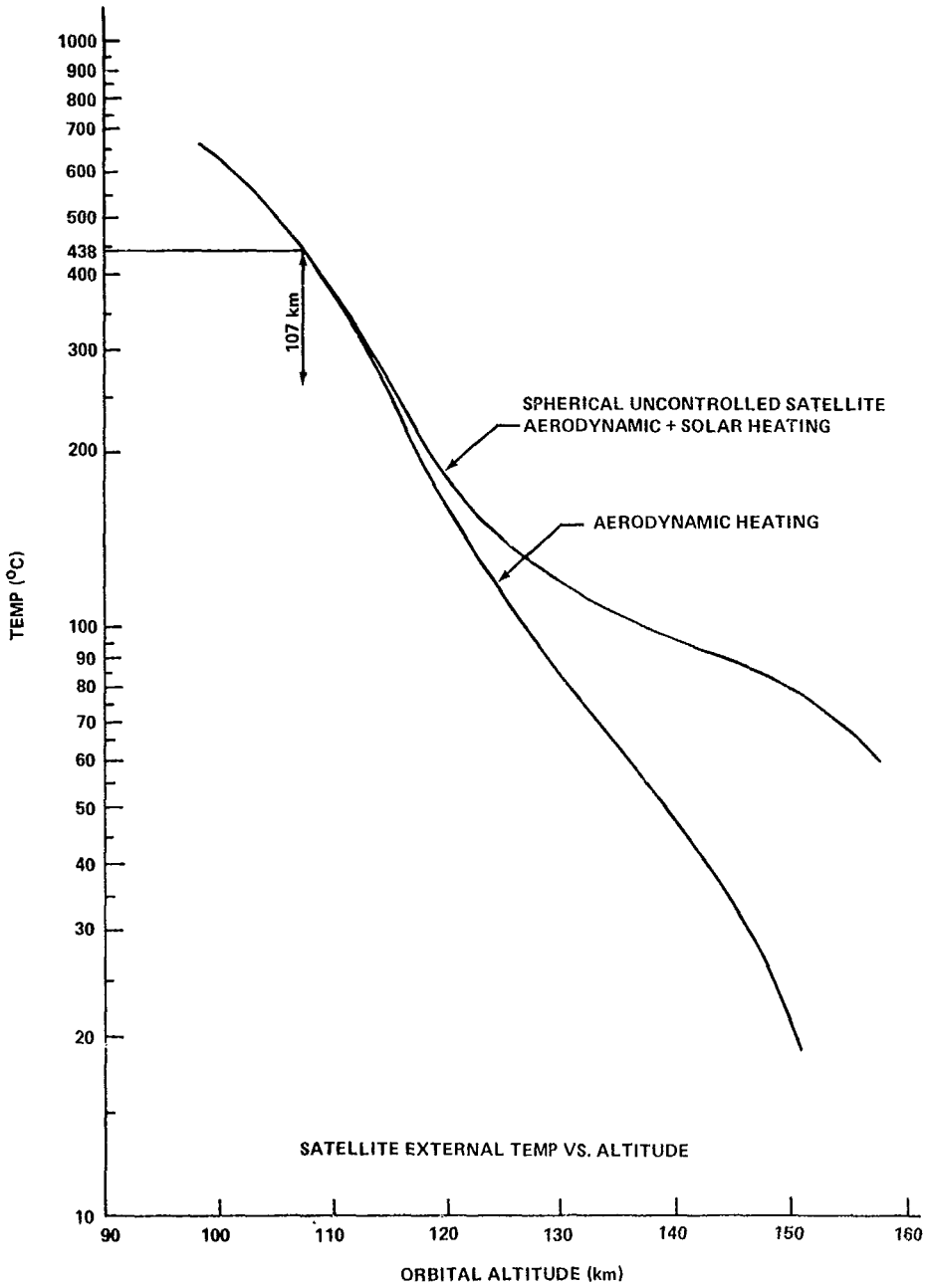

Figure V-3. Satellite external temperature versus altitude.

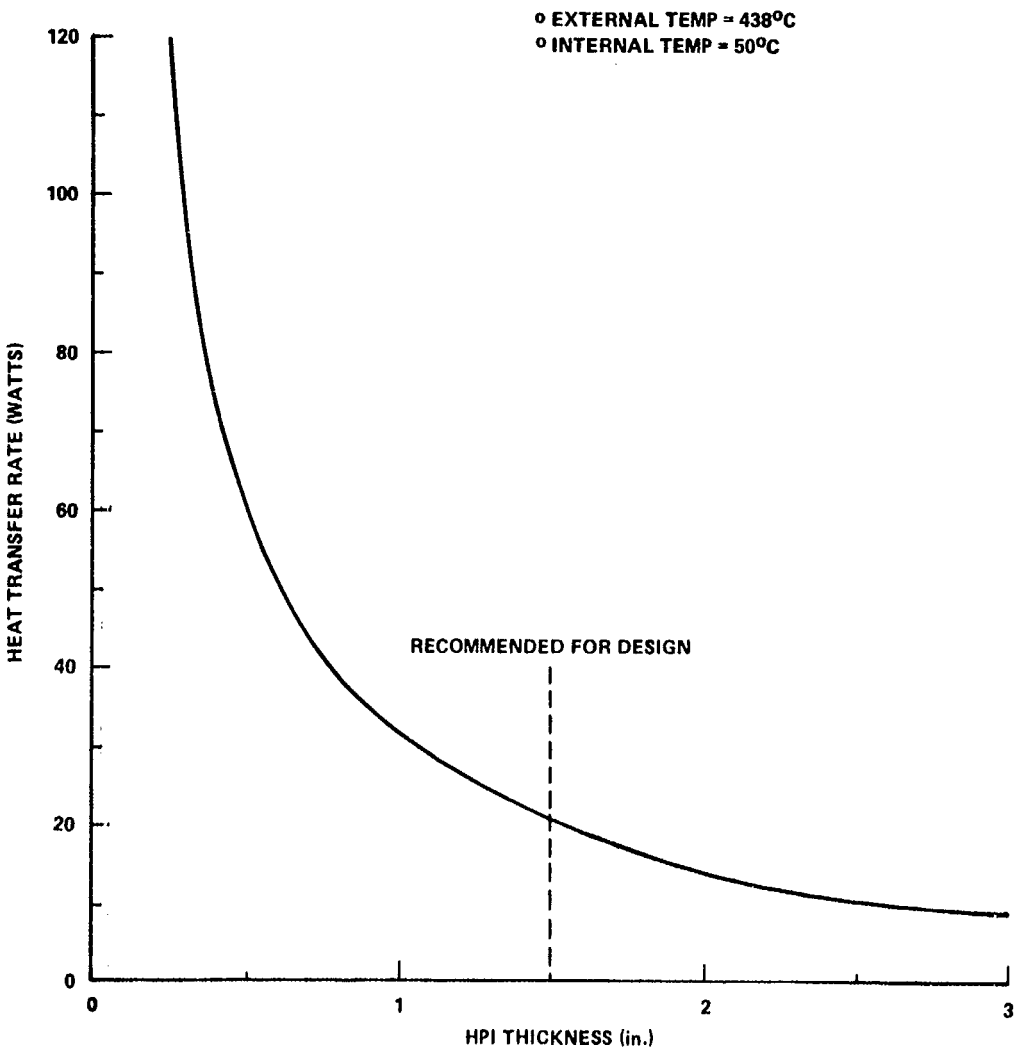

Figure V-4. High performance insulation thickness versus heat transfer rate for spherical tethered satellite.

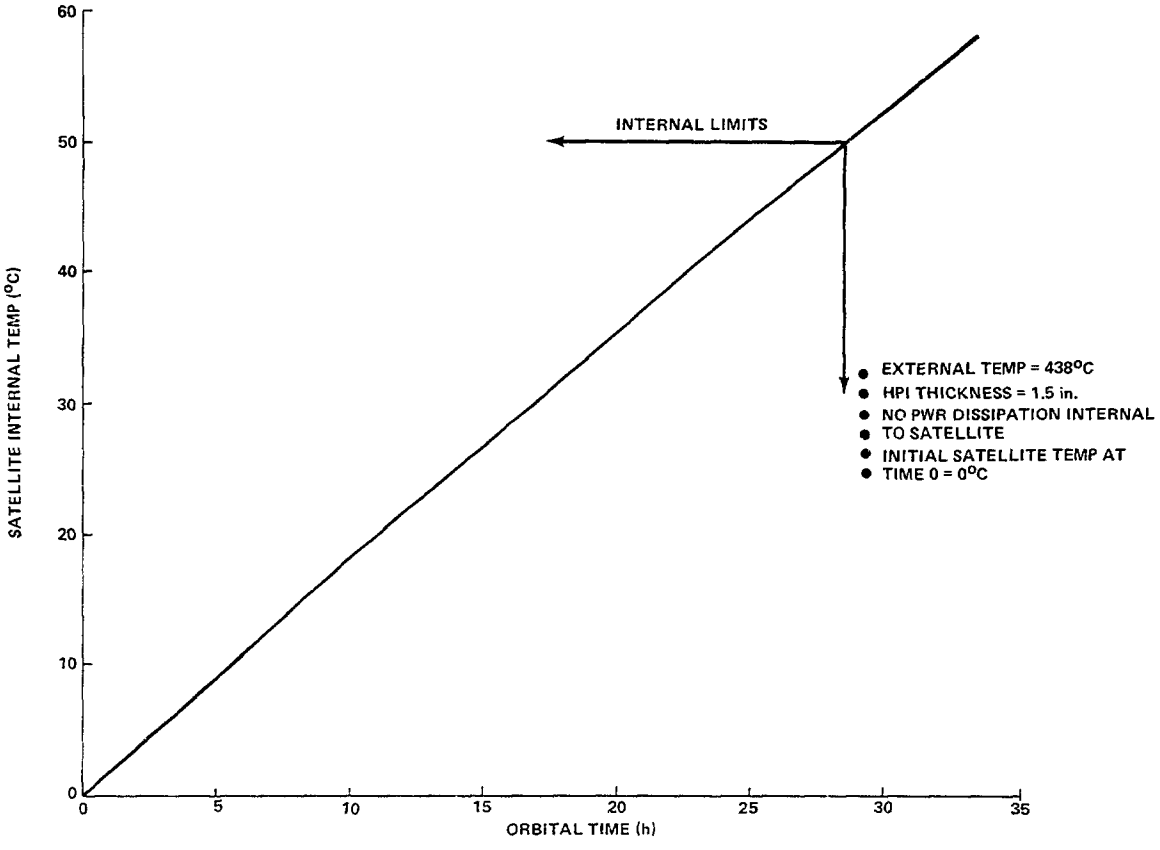

Figure V-5. Internal heat-up rate versus orbital duration at 107 km altitude for tethered satellite.

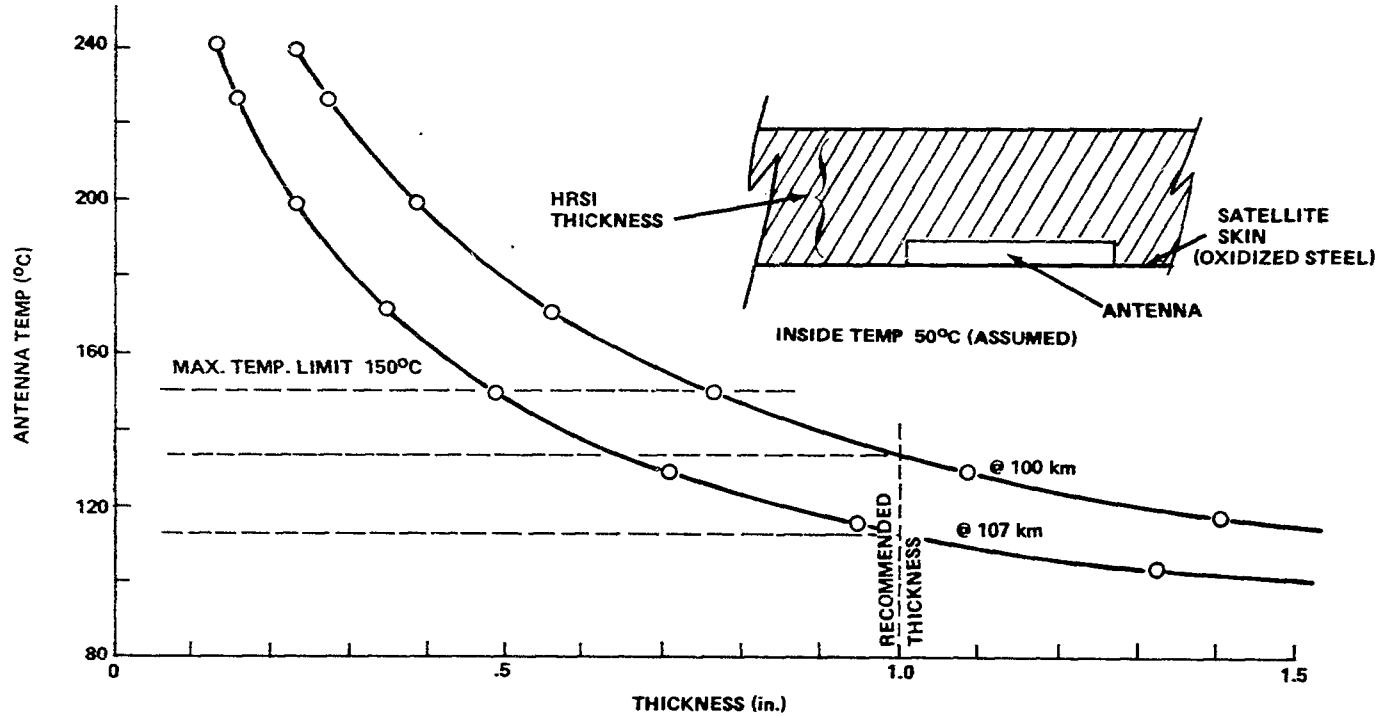

Figure V-6. High temperature reusable surface insulation (HRSI-LI900) on AMPS subsatellite antenna.

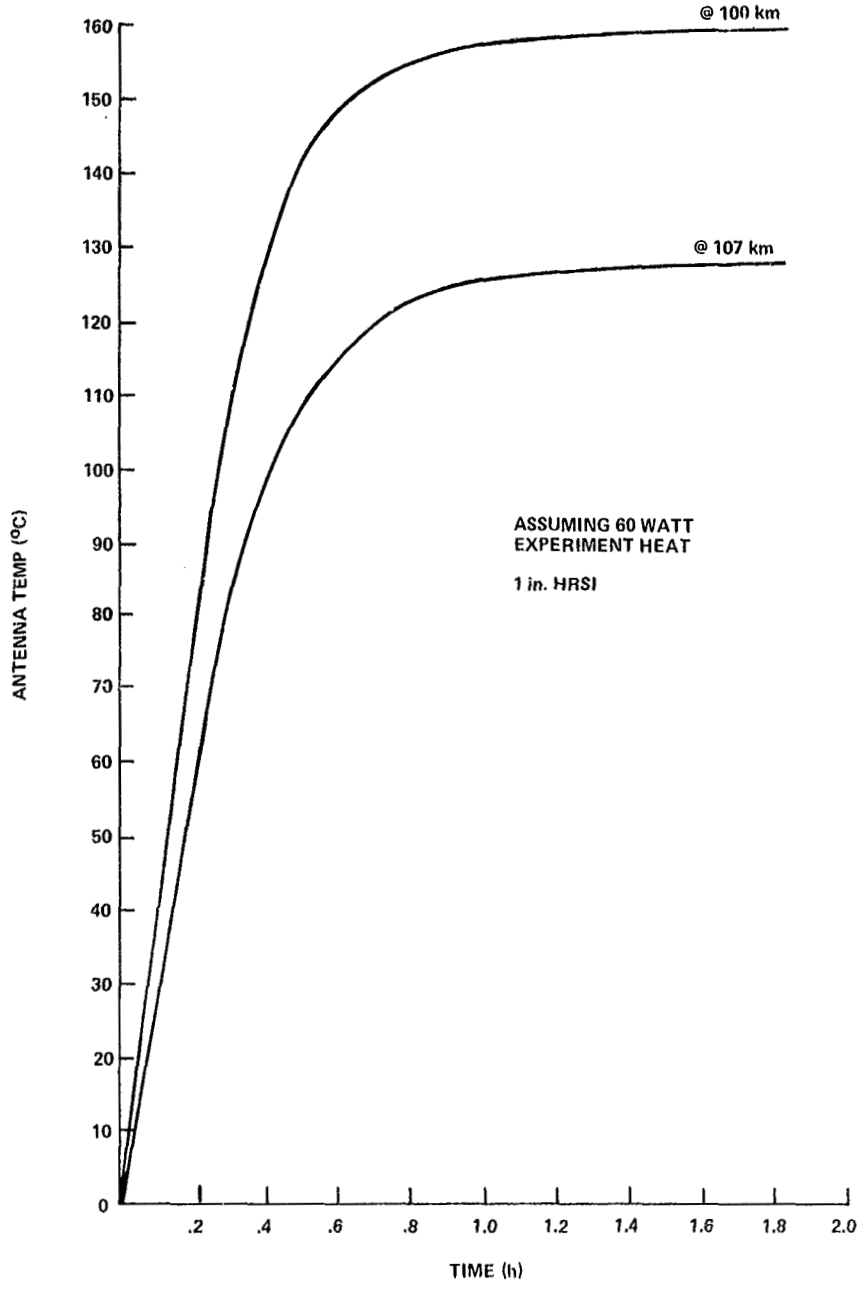

Figure V-7. Antenna temperature versus time.

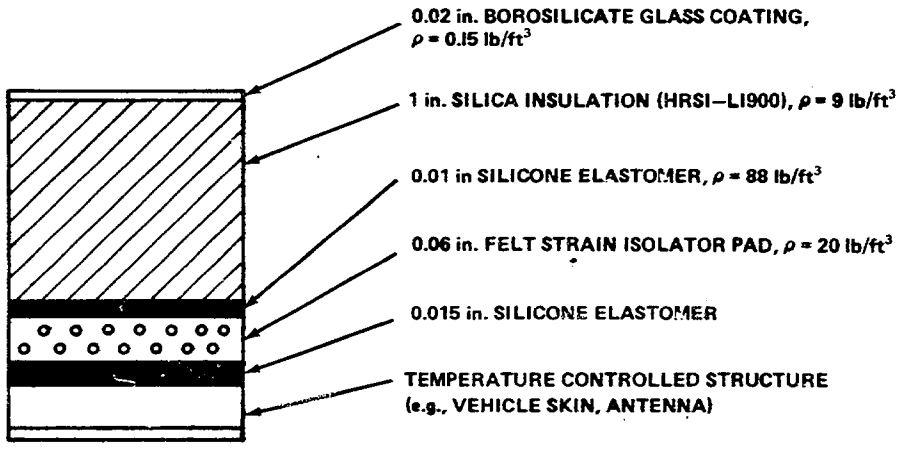

Figure V-8. HRSI (LI900) tile — basic construction.

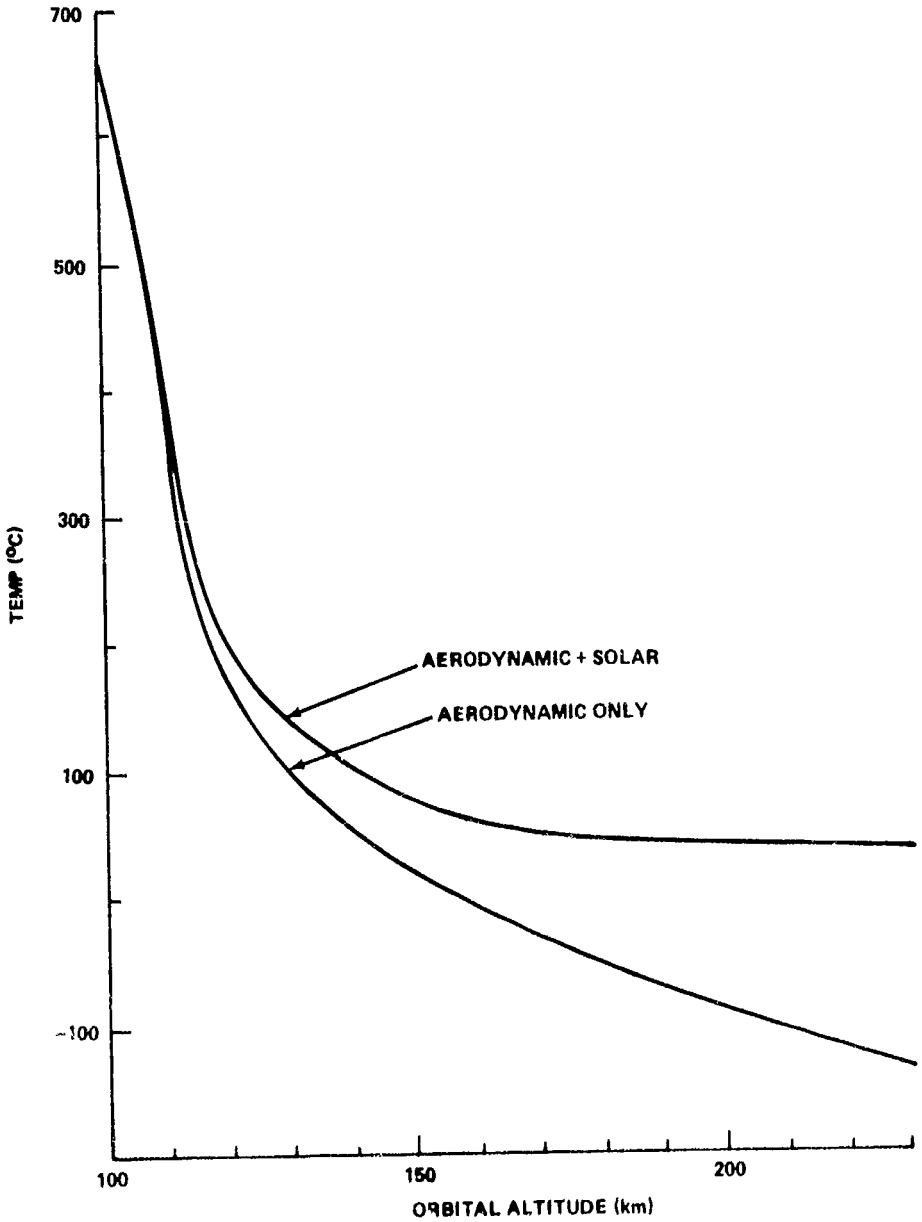

Figure V-9. Wire temperature versus altitude.

VI. TETHERED SUBSATELLITE COMMUNICATIONS SYSTEM DESIGN

J. A. Dunkin

A. Summary

1. Antenna pattern distortions due to the tether do not appear to be a problem if the distance between the antenna and the tether is greater than two wavelengths.

2. Antennas suitable for the Atmospheric Magnetospheric Plasma in Space (AMPS) tethered subsatellite have been identified which can withstand 180°C, a temperature higher than the predicted temperature of the antenna when covered with LI-900 insulation.

3. The plasma cutoff frequency may preclude the use of S-band communications at altitudes below 110 km.

4. Most equipment for S-band operation could be off-the-shelf hardware with a minimum of modification.

5. Communications at frequencies above S-band will require extra support equipment on the AMPS facility.

B. Introduction

The primary communication problem, which was addressed during the AMPS tethered subsatellite feasibility study, was to determine if a communication link could be established from the tethered subsatellite to the Orbiter using low cost, off-the-shelf hardware. Some associated problems which were addressed during the study were the effect of the tether on the antenna pattern, the temperature of the subsatellite antenna, and the effect of the plasma generated by the subsatellite on the communication link.

RF tracking of the subsatellite was not considered as a part of this study; however, use of a scanning laser radar which is currently under development is suggested for missions which have critical tracking requirements.

C. Method

The communication requirement of the tethered subsatellite are very similar to the communication requirements of sounding rocket programs; therefore, a good selection of flight proven, off-the-shelf communications hardware is available, especially in the S-band. Since the proposed AMPS facility will have S-band communications equipment available, a subsatellite to Orbiter communications link margin calculation was performed for a typical S-band system made up of off-the-shelf sounding rocket type components. The calculations were based upon the following key assumptions:

1. Subsatellite antenna gain — -2 dB
2. Receive antenna gain — +24 dB
3. Data rate — 200 kbps
4. Subsatellite transmitter power — 1 W
5. Bit error rate — 10^{-5}
6. Receive system noise figure — 7 dB
7. Plasma cutoff is not a problem
8. Maximum range from Orbiter to subsatellite — 120 km

Assuming the above, the system will have a +7.7 dB margin which is adequate.

The effect of the plasma generated by the subsatellite was evaluated by the method outlined by Mitchell in an article entitled, "Communications-System Black-Out During Reentry of Large Vehicles," Proc. IEEE, Volume 55, No. 5, pp. 619-626, May 1967. It was found that the S-band communications system would be blacked out at an altitude just below 105 km. Until better data are available on the plasma generation characteristics of the subsatellite, a conservative estimate is that the S-band system will operate down to an altitude of 110 km. A graph of plasma cutoff frequency versus altitude in kilometers is given in Figure VI-1.

Selection of a specific antenna for the subsatellite cannot be made until the shape and size of the subsatellite are well defined, since the antenna and outer skin of the subsatellite are integral parts of each other. However, several types of antennas such as planer spirals and flush mounted wrap-around antennas, which are well suited to this application, are available commercially. Because of the surface heating encountered by the subsatellite, the antenna must be covered with a thermal protective shield. An excellent material for such a shield is LI-900. LI-900 combines low dielectric constant and low loss tangent with good thermal insulating properties. The use of LI-900 may require a slight retuning of the antenna, which will not be a major problem.

The MSFC antenna group was consulted on the effect of the tether on the antenna pattern. It is their best judgment based on past experience, that antenna pattern distortions due to the tether will not be a problem if the distance between the antenna and the tether is greater than 2 wavelengths.

D. Conclusion

Communications from the tethered subsatellite to the Orbiter using off-the-shelf equipment is feasible at altitudes above 110 km. At altitudes below 110 km, the plasma cutoff frequency will force the use of C-band for communications, thereby, limiting the available equipment.

Additional work should be done to refine the data on the RF losses due to the plasma generated by the subsatellite, and additional work should be done to define a communication system operating at C-band or higher for operation below 110 km. Also additional work needs to be done to define systems to meet the tracking requirement of specific missions.

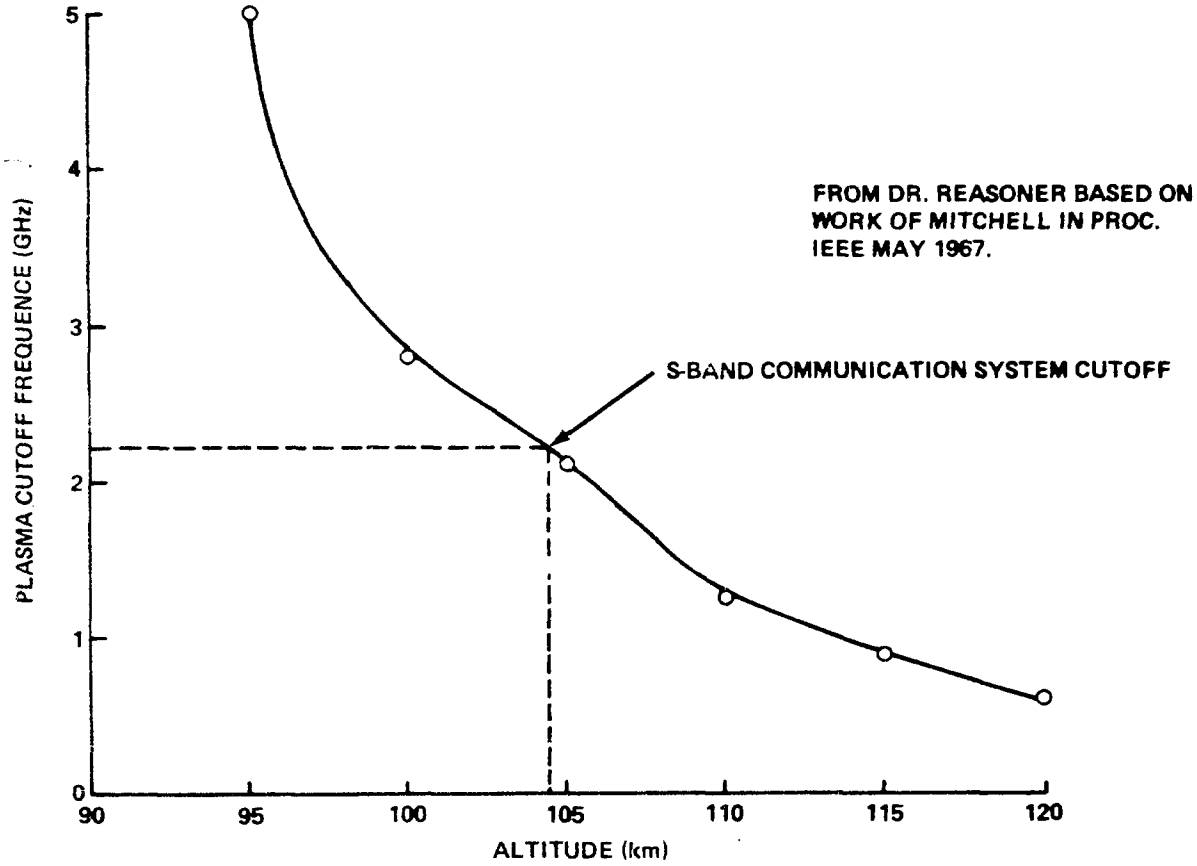

Figure VI-1. Plasma cutoff frequency.

APPENDIX

COMPUTATIONAL ROUTINE FOR ELIMINATING UNKNOWN LAGRANGE MULTIPLIERS

The purpose of this appendix is to present an algorithm that eliminates the unknown Lagrange multipliers. These multipliers enter Lagrange's equations of motion by the introduction of extraneous coordinates. As a result, the dynamic analysis contains more coordinates than there are degrees of freedom of the dynamical system. This mode of operation may not seem like progress because it increases the number of equations to be solved, however, the ensuing equations are of greater simplicity and symmetry. In addition, it enables one to calculate internal forces and dynamic loads of interest.

To eliminate the Lagrange multipliers, the equations of motion are written in state space form. Thus, they make up a set of ordinary nonlinear differential equations of first order as

$$D\dot{\underline{x}} = \underline{F}_E + \underline{F}_I - B^T \underline{\lambda} \quad , \tag{A-1}$$

where $\underline{F}_E$ represents the external forces acting on the system and $\underline{F}_I$ the inertial forces. The internal reaction forces are calculated from the relationship:

$$\underline{F}_R = -B^T \underline{\lambda} \tag{A-2}$$

The constraint matrix B is defined by the constraint equation as

$$\Phi = B\underline{x} - \underline{b} = 0 \tag{A-3}$$

The Lagrange multipliers can now be eliminated by carrying out the following steps. First, the equations of motion, equation (A-1), are premultiplied by the inverse of the coefficient matrix D, which yields

$$\dot{\underline{x}} = D^{-1} (\underline{F}_E + \underline{F}_I - B^T \underline{\lambda}) \tag{A-4}$$

Secondly, the equations of constraint, equation (A-3), are differentiated with respect to time, which yields

$$B \dot{\underline{x}} + \dot{B} \underline{x} - \dot{\underline{b}} = 0 \tag{A-5}$$

Inserting equation (A-4) into equation (A-5) results in

$$BD^{-1}(\underline{F}_E + \underline{F}_I - B^T \underline{\lambda}) + B \dot{\underline{x}} - \dot{\underline{b}} = 0 \tag{A-6}$$

or

$$-BD^{-1} B^T \underline{\lambda} = \dot{\underline{b}} - \dot{B} \underline{x} - BD^{-1} (\underline{F}_E + \underline{F}_I) \tag{A-7}$$

and finally

$$\underline{\lambda} = -(BD^{-1} B^T)^{-1} [\dot{\underline{b}} - \dot{B} \underline{x} - BD^{-1} (\underline{F}_E + \underline{F}_I)] \tag{A-8}$$

The reaction forces themselves can be readily obtained from equation (A-2) as

$$\underline{F}_R = +B^T (BD^{-1} B^T)^{-1} [\dot{\underline{b}} - \dot{B} \underline{x} - BD^{-1} (\underline{F}_E + \underline{F}_I)] \tag{A-9}$$

The mathematical analysis of the tethered subsatellite does not make use of this algorithm because the unknown constraint force, which is the tension in the tether, can be directly obtained from the tether control law and the viscoelastic forces of the tether.

BIBLIOGRAPHY

Colombo, G., et al.: Shuttle-Borne "Skyhook": A New Tool for Low-Orbital-Altitude Research. Smithsonian Astrophysical Observatory Report, September 1974.

Eades, J. B.: Tethered Body Problems and Relative Motion Determination. Analytical Mechanics Associates Contract NAS5-21453, Final Report, August 1972.

Grossi, M. D. and Colombo, G.: Interaction of Tethered Subsatellites and the Magnetic Field of the Earth. Smithsonian Astrophysical Observatory, November 1974.

Isaacs, J. D., et al.: Satellite Elongation into a True "Skyhook." Science, vol. 151, February 11, 1966, p. 682.

Rupp, C. C.: A Tether Tension Control Law for Tethered Subsatellites Deployed along the Local Vertical. NASA TM X-64963, September 1975.

Siebel, M. P.: AMPS Tethered Satellite Working Meetings. Minutes of Meetings, Marshall Space Flight Center, Alabama, February-July 1975.

Weiffenbach, G. C.: A Study of the Electrodynamics of Long Conducting Tethers in the Near Earth Environment. Smithsonian Institution Contract NAS8-31678 (in progress).

Worley, H. E., et al.: Preliminary Analysis of Cable Retrieval Technique for the Tethered ATM Workshop.

APPROVAL

TETHERED SUBSATELLITE STUDY

By William P. Baker, J. A. Dunkin, Zachary J. Galaboff, Kenneth D. Johnston, Ralph R. Kissel, Mario H. Rheinfurth, and Mathias P. L. Siebel

The information in this report has been reviewed for security classification. Review of any information concerning Department of Defense or Atomic Energy Commission programs has been made by the MSFC Security Classification Officer. This report, in its entirety, has been determined to be unclassified.

This document has also been reviewed and approved for technical accuracy.

William R. Marshall

WILLIAM R. MARSHALL
Associate Director for Engineering
Science and Engineering

☆ U.S. GOVERNMENT PRINTING OFFICE 1976-641-255/456 REGION NO. 4